Delays and the control of movement in legged animals

by

Sayed Naseel Mohamed Thangal

M.S., Drexel University, 2011

B.Tech., SASTRA University, 2007

Thesis Submitted in Partial Fulfillment of the

Requirements for the Degree of

Doctor of Philosophy

in the

Department of Biomedical Physiology and Kinesiology

Faculty of Science

SIMON FRASER UNIVERSITY

Summer 2022

Declaration of Committee

Name:	**Sayed Naseel Mohamed Thangal**
Degree:	**Doctor of Philosophy**
Title:	**Delays and the control of movement in legged animals**
Committee:	**Chair:** **Dawn Mackey** Associate Professor, Biomedical Physiology and Kinesiology
	Max Donelan Supervisor Professor, Biomedical Physiology and Kinesiology
	James Wakeling Committee Member Professor, Biomedical Physiology and Kinesiology
	C. David Remy Committee Member Professor, Institute for Nonlinear Mechanics University of Stuttgart
	Jeremy Wong Committee Member Research Associate, Kinesiology University of Calgary
	Stephen Robinovitch Examiner Professor, Biomedical Physiology and Kinesiology
	Monica Daley External Examiner Associate Professor, Ecology & Evolutionary Biology University of California, Irvine

Abstract

The ability to respond quickly to a perturbation is essential to the survival of an animal. As animal size increases, several features that influence response time also change—larger animals suffer from longer sensorimotor delays, proportionally weaker muscles, and heavier body segments. Larger animals also have more time available to react due to longer characteristic movement times. I studied how these features affect neural control of the fastest perturbation responses, and I used simple neuromechanical models to estimate how response time changes with animal size. In chapters 2 and 3, I quantified the scaling of inertial delays—the time required to physically reposition body segments and regain stability after a perturbation. In chapters 4 and 5, I quantified the scaling of the fastest response times to a perturbation under two control configurations—feedforward vs. feedback control. I tested whether they are affected more by the force generation capacity of muscles or by sensorimotor delays. I developed two tasks representing common perturbation response scenarios in animal locomotion: a distributed mass pendulum approximating swing limb repositioning (swing task), and an inverted pendulum approximating whole body posture recovery (posture task). I parameterized the anatomical, muscular, and inertial properties of these models using literature scaling relationships. I found that inertial delays depended both on movement task and movement size. Inertial delays got longer with larger movements, and scaled faster in the posture task than the swing task. As movement size increased, inertial delays exceeded sensorimotor delays, and this occurred for smaller movements in larger animals. Across animal size and task, force capacity of muscles limited feedforward control response times, while sensorimotor delays limited feedback control response times and forced the use of lower controller gains to prevent instability. Feedback control response times also exceeded available movement times in animals of all sizes, while feedforward control did so only for the largest animals. Feedback control was about four times slower than feedforward control in the smallest animals, but only around two times slower in the largest animals. Thus, both small and large animals are more likely to use feedforward control to react quickly against perturbations.

Keywords: Biomechanics, scaling, response time, perturbation, control theory, time delays

Dedication

To my family:

Ippa, Imma and Nazeeh

Acknowledgements

I am deeply indebted to Max for his guidance and mentorship during my doctoral studies. Apart from training in research work, I also relearned how to learn, enhanced my scientific writing and presenting skills, and developed a deeper understanding on topics of ethics and equity. I appreciate the well-rounded training that I got during my time in the Locomotion Lab, and for Max's patience as I struggled with the challenges of the program.

I feel privileged to have Dr. David C. Remy, Dr. James Wakeling, and Dr. Jeremy Wong on my supervisory committee. They dedicated their time and resources to teach me the topics that they have expertise in, and I could not have completed my research projects without their significant input.

I am grateful to my family for giving me the strength to face the difficulties of graduate school, and for having faith in me as I pursue my career aspirations. I feel very lucky to have made several great friends during my time in Vancouver. They have taught me how to live and laugh in this unfamiliar land, and supported me when I was down. I am especially grateful to all my friends in the Locomotion Lab; having a friendly and supportive group of lab mates has made my PhD a fulfilling experience. Thank you everyone, for being there when I need you.

The pandemic has been very difficult on me and my family, and I feel fortunate to have been in Vancouver during this challenging time. I am thankful to SFU and the BC health system for its COVID-19 response which kept me safe, and helped me to continue my research work during the lockdowns and restrictions.

Contents

List of Tables

List of Figures

Chapter 1. Introduction

Animals come in a wide range of sizes and locomote in many different ways, and we can take advantage of this diversity to gain a deeper understanding of the neural control of locomotion. Terrestrial mammals range in size from the two gram Etruscan pygmy shrew to the twelve ton African bush elephant (Jürgens, 2002; Larramendi, 2015). Yet they share the same materials and structure in the design of their neuro-musculoskeletal system. For example, all mammals have skeletal systems composed of calcium phosphates and can tolerate limited stresses (bending stress limits ~200 Mpa (Norberg and Aldrin, 2010)), similarly organized nervous systems with limited signal conduction velocities (nerve conduction velocities ~60 m/s (More, 2013)), and similar muscle architecture with limited force production capacity (maximum isometric stress ~20 N/cm^2 (Medler, 2002)). Studying how animals of different sizes are able to locomote effectively, and the challenges that they face due to physiological limitations, can give us insights that we would miss if we studied only one species. The findings would have several applications—it could help us better understand motor control in humans and help us develop better therapeutic interventions, help us develop better robots and exoskeletons, and further our understanding of animal biology and evolution.

We can probe how the neural control of locomotion works in animals by quantifying its performance limits. For example, we could quantify how fast animals could run, how heavy a weight they could lift, or how far they could jump. Here, I chose to quantify the fastest response times to a perturbation in animals. To respond as quickly as possible to a perturbation, all the relevant components of an animal's neuro-musculoskeletal system would have to perform at their limits. It would have to sense the perturbation quickly and accurately, transmit the signals and compute the correct responses as fast as possible, and then activate its muscles to produce the strongest forces that can reposition the body while maintaining posture and balance. Thus, I can study how physiological limits of the neuro-musculoskeletal system affect neural control. Measuring perturbation response times in-vivo in different sized animals in a standardized and comparable manner would be difficult, and would face ethical issues, as failure to respond

effectively can result in falls and injury. Therefore, I use computational modeling, where I can individually vary the features of the neuro-musculoskeletal system that contribute to the perturbation response, and study its effect on response time. Computational modeling also allows me to integrate information from disparate fields in the literature, and study combinations of parameters that don't exist in nature.

In this thesis, I use simple neuromechanical computational models to study how the fastest perturbation responses scale with animal size, and how physiological limitations affect response time. This thesis combines techniques and knowledge from several research areas—such as scaling, biomechanics, control systems and neuroscience. In the coming sections of this introduction, I provide a brief background on concepts from these research areas that occur repeatedly in my own research. I review scaling theory (1.1), engineering control systems theory (1.2), the neural control of locomotion (1.3), and the components of response time (1.4). Finally, I describe the aims and approaches used in this thesis (1.5).

1.1. Scaling approach

Scaling is the study of how a change in size of a system affects its features and behavior. It was originally used in engineering applications, such as the design of buildings, bridges and ships. For example, engineers use the scaling approach to understand how the forces and stresses experienced by a bridge will change depending on its size, and select the appropriate architecture and construction materials. Engineers also produce scaled down replicas of large machines such as ships or airplanes and conduct tests on them to predict how the full scale model will perform in the real world (McMahon and Bonner, 1983). In the scaling approach, we first develop a theoretical model of the system that can be scaled to any size. We then use it to make predictions about how the features of the system will change based on fundamental design rules. We can then compare these predictions against actual measurements to understand the system better. As terrestrial mammals span eight orders of magnitude in body mass, we can apply the scaling approach to understand their biology too.

Size is an important factor in determining the characteristics of an animal. Due to the rules of physics, size forces conditions on the morphology and behavior of an animal. Bonner described five rules about how size affects biology (Bonner, 2011):

1. Strength and force varies with size ($\text{Strength} \propto M^{2/3}$),

2. Surfaces that permit diffusion of oxygen, food and heat vary with size ($\text{Surfaces} \propto M^{2/3}$),

3. Division of labor and complexity of organism changes with size,

4. The rate of various living processes varies with size: metabolism, generation time, longevity, speed of locomotion,

5. The abundance of species in nature varies with size,

where M is the body mass of the animal.

We know of several differences between small and large animals in their movements—for example, small animals are non-cursorial while large animals are cursorial, small animals have a crouch posture while larger animals are columnar, small animals have overdamped limbs and joints while large animals have underdamped limbs. The neural control of locomotion thus must also change with animal size. By probing how neural control is different, we can gain insights into the nervous system which might not be evident if we look only at one animal species.

Dimensional analysis is a related technique that is helpful in the analysis of systems that scale with size. By dimensional analysis, we can determine the constitution of the parameters and variables in a system in terms of the fundamental quantities of Newtonian mechanics (mass, length and time). We can then non-dimensionalize the equations that represent the theoretical model used in the scaling approach. This has several advantages. The parameters and variables in the non-dimensional form of the equation do not have measured units, simplifying the equation and preventing unit conversion errors. Non-dimensionalization can reveal intrinsic parameters that provide better insights into the

behavior of the system. Finally, we can obtain a general set of results for the non-dimensionalized system, and can redimensionalize the results to describe the behavior of systems with any set of parameters.

1.1.1. Power laws

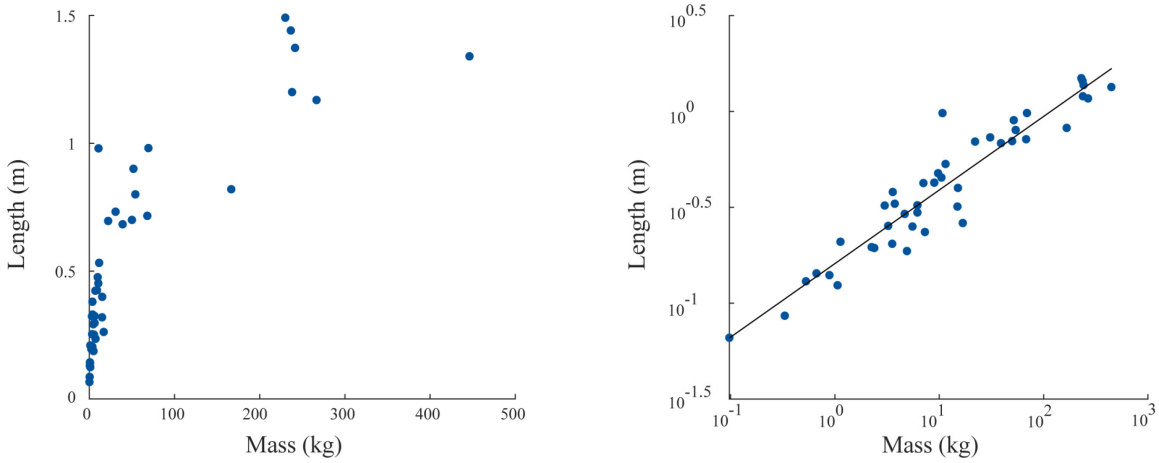

Fig 1.1 Power law fits and its log transform.
On the left is a plot of the forelimb length of 44 species of terrestrial mammals against their mass from Kilbourne and Hoffman (Kilbourne and Hoffman, 2013). On the right is a log-log transform of the same plot. The black line represents a linear fit to the data. The log transform of the power law makes the data more evenly spread out, and easier to visualize and understand.

Physiological and morphological features that are influenced by animal size can often be expressed as a power law known as the allometric equation, expressed in the form:

$$Y = aM^b \tag{1.1}$$

$$Log(Y) = Log(a) + b\,Log(M) \tag{1.2}$$

where Y is the feature being quantified, a and b are constants of the allometric equation, and M is the body mass of the animal. The allometric equation (Eqn 1.1) is exponential in shape while its log transformed equation (Eqn 1.2) is linear (Fig 1.1). In practice, we collect the values of the mass and feature Y of many different animals. We then log transform the data and plot the values of the feature against mass, and perform a linear fit to extract the values of a and b. b is the slope of the linear fit and describes how the feature of interest changes with size (Alexander, 2003). $Log(a)$ is the intercept of the linear fit. a is the

coefficient or the value of the feature Y for a 1 kg animal, if the mass units were in kilograms. We can compare the exponent obtained from the allometric equation to predictions from design principles such as geometric similarity, dynamic similarity, elastic similarity and stress similarity.

Note that the power law fit greatly simplifies our description of the feature, and we lose the complexity and great variation seen from species to species. Therefore, we may not use these scaling laws to accurately predict a feature in any individual species. For example, a hippo and giraffe may both measure 1000 kg but have vastly different anatomies. By removing the complexity and detail, and reducing the description of the feature to a power law, we might gain insight into underlying mechanisms that are based on fundamental physical principles.

1.1.2. Geometric similarity

Two objects are said to be *geometrically similar* if they have exactly the same shape, but are of different sizes. When two objects conform to this principle of geometric similarity, the ratio of the linear dimension of the first object to the corresponding linear dimensions of the second object will remain constant. Furthermore, the surface area of an object would be proportional to the square of the linear dimension, and its volume to the cube of the linear dimension. If we extrapolate these assumptions to hypothetical animal bodies and consider the density of animals to be similar, we can deduce the following predictions:

1. Linear features of the geometrically similar bodies (limb length, nerve length) scale $\propto M^{1/3}$.
2. Surface area features (skin area, lung surface area, muscle cross-sectional area) scale $\propto M^{2/3}$.
3. Volume of any part of the body, and assuming constant density, mass of body segments scales $\propto M^{1}$.

In nature, animal features evolve under various selective pressures including size, physical stress, energy minimization and injury prevention, which may cause allometric equation exponents to deviate away from geometric similarity. When the empirically

measured exponent exceeds or is less than the value expected from geometric similarity, it is called positive and negative allometry, respectively. For example, Kilbourne and Hoffman found that limb masses scale with geometric similarity while limb lengths scale with positive allometry (Kilbourne and Hoffman, 2013).

1.1.3. Dynamic similarity

Scaling has also been used to understand the dynamics of animal movement. While the principle of geometric similarity provides theoretical predictions for animal anatomical changes with size, the principle of dynamic similarity provides predictions for animal locomotor changes with size. For two animals to move in a dynamically similar fashion, not only do they have to be geometrically similar (i.e. lengths in constant ratio of each other), they must also have their movement times be in another constant ratio, and the forces exerted in yet another constant ratio. All cursorial land mammals walk at slow speeds, trot at intermediate speeds and gallop at fast speeds. Alexander et. al. (1983) showed that these land mammals of different sizes adopt similar gaits and move with dynamic similarity, when travelling at similar values of a dimensionless number called the Froude number (Alexander and Jayes, 1983). This allows us to predict the speeds at which different sized animals will change their gait from walking to trotting to galloping, and compare their gait features such as duty factor, stride lengths and footfall patterns. For example, animals will switch between a trot to a gallop at a Froude number of two to three. The theory of dynamic similarity held up when compared to several previous studies. For example, when moving at a slow gallop, Biewener (1983) found that the duty factor of differently sized animals does not vary significantly, it scaled with $0.41M^{-0.006}$ (Biewener, 1983). Heglund et. al. (1974) found that the stride frequency at the trot gallop transition speed scaled with $269M^{-0.14}$ strides per minute, and the exponent matches the prediction of 1/6 made by dynamic similarity (Heglund et al., 1974). We can also compute characteristic movement times for an animal based on its size. The time for an animal to fall to the ground from a height equal to its leg length and the natural time period of oscillation of an animal limb represented as a simple pendulum both scale with $M^{1/6}$, which again matches predictions by dynamic similarity.

1.1.4. Scaling insights

Scaling studies have given us several insights into the features and behavior of animals. For example, geometric similarity predicts that the cross-sectional diameter d of skeletal support elements such as muscles and bones scales with $M^{1/3}$ being a linear feature, and the cross-sectional area $A = \pi(d/2)^2$ scales with $M^{2/3}$. However, the load acting on the skeletal elements (F) scales with the animal's body mass M^1. Therefore, according to geometric similarity, the axial, transverse and torsional stresses $\sigma = F/A$ scales with $M^{1/3}$, indicating that larger animals should suffer from excessive stresses on their skeletal elements making them susceptible to fractures and injury. Actual studies revealed that the transverse stresses were more concerning than axial stresses, and that cross-sectional diameter of the skeletal support elements did scale with geometric similarity. Instead of evolving thicker bones to support their body weight, larger animals use a more upright (columnar) posture to reduce the stress being applied to their muscles and bones (Alexander, 2003; Biewener, 2005). On the other hand, smaller animals use a crouched posture which give them more maneuverability. Kleiber showed that the metabolic rate of animals scale with $M^{0.75}$, indicating that larger animals have relatively less calorific needs compared to smaller animals (McMahon and Bonner, 1983). Scaling studies have also been used to predict the behavior of extinct animals. Economos estimated that the metabolic cost of gravity limits the size of land mammals to 20,000 kg, matching the size of the extinct species Baluchitherium (Economos, 1981), and Hutchinson et al. studied the locomotion of the Tyrannosaurus Rex to conclude that it was not a fast runner (Hutchinson and Garcia, 2002). While the scaling approach has been applied to quantify several features of animal locomotion, it has rarely been applied to the neural control of locomotion (More and Donelan, 2018), which is my aim in this thesis.

1.2. Control theory

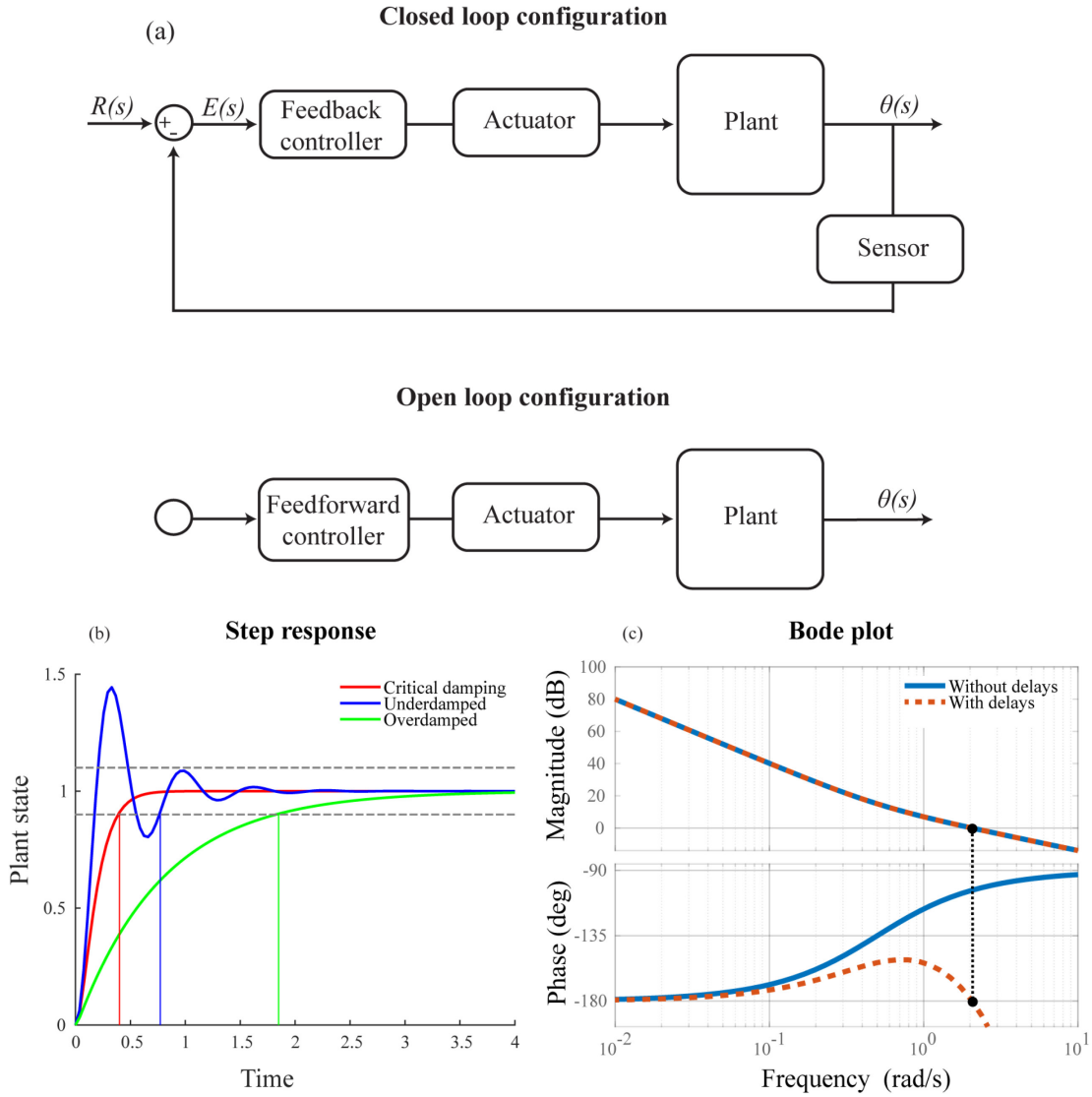

Fig 1.2 Control systems theory.
(a) Block diagrams of open loop and closed loop control systems. In the open loop configuration, the controller generates commands without considering the state of the plant $\theta(s)$. In the closed loop configuration, the controller compares the state of the plant $\theta(s)$ to a desired reference state $R(s)$, and uses the error between them $E(s)$ to generate the actuator commands. (b) Underdamped (blue), critically damped (red) and overdamped (green) responses of a feedback control system. The black horizontal dotted lines at 0.9 and 1.1 denote 10% settling time threshold bands, and the vertical lines at 0.4 (critically damped), 0.8 (underdamped) and 1.85 (overdamped) represent the settling times of the three curves. (c) Bode plot of a control system with the magnitude plot on top and the phase plot at the bottom. In the phase plot, the blue line represents the control system without delays, and the dashed red line represents the control system with delays. The time delays cause a -180° phase shift which results in instability at the gain crossover frequency of 2.06 rad/s.

Control systems is a field of engineering which develops techniques to evaluate and regulate the behavior of dynamical systems. The behavior of dynamical systems can be mathematically described by differential equations with time derivatives, and control theorists have developed techniques to manipulate these equations and control dynamical systems. There are two classes of control systems: linear and nonlinear. Linear control systems have special properties of homogeneity and additivity which make them simpler to analyze and more mathematically tractable than non-linear systems. If you scale the input to a linear control system, the output of the control system also gets scaled by the same amount. Similarly, if you change the properties of the plant of a linear control system to increase its natural frequency, all time characteristics of its response behavior also change by the same amount. The output of a linear control system to the sum of various inputs will be equal to the sum of outputs to each individual input. These properties allow us to use mathematical techniques to fully describe the behavior of a linear control system. Some examples of these techniques for linear control systems are transfer functions, state space representations, Routh-Hurwitz stability analysis, root-locus analysis, Bode plots and Nyquist plots (Åström and Murray, 2008; Nise, 2011). Using Laplace transforms and Fourier transforms, we can convert the time domain representation of the differential equation to a frequency domain representation. The frequency domain representation of the system reveals several insights into its performance which would be difficult to deduce in the time domain. For example, we can look at the root-locus representations of transfer functions to separate out the exponential and sinusoidal components of the system's response, or use Bode plots to predict the frequencies that can cause instability. Nonlinear control systems might not have additive and homogenous properties, making them much less predictable and difficult to analyze. For example, time delays in the control pathways, or limits on the force capacity of the actuator, or effects of gravity on the plant can all make a linear control system nonlinear.

Control systems have two main configurations, feedforward and feedback (Fig 1.2a). In a feedforward (open loop) configuration, the controller produces predefined control signals to regulate the "plant" (the dynamical system being controlled). But the controller does not sense if the plant is behaving as intended; thus the loop is left open. In a feedback (closed loop) configuration, the controller is able to sense the behavior of the

plant and uses these feedback signals to calculate the controller output. There are several types of controllers under both feedforward and feedback configurations which are designed for specific tasks —some examples are on-off, bang-bang, Proportional Integral Derivative (PID), Linear Quadratic Regulator (LQR), robust, adaptive and Model Predictive Control (MPC) (Bechhoefer, 2021). Under the feedforward control configuration, bang-bang controllers are the fastest and most aggressive type (Rao and Bernstein, 2001). The controller first commands the plant to use all available force to accelerate rapidly towards the target state. Then at a predefined time, the controller switches the force direction to rapidly decelerate the plant and bring it to rest at the target state. Under bang-bang control, we must optimize the switching time of the force direction to get the fastest response. Proportional-Integral-Derivative (PID) control is a simple and intuitive feedback controller type, which is popular in engineering applications and often tested as a starting option. In PID control, we first compute an error signal (e) between the present state of the plant and the target state. We determine the proportional component of the controller commands by multiplying this error by a proportional gain (K_p). Thus, the command will act to rapidly reduce the error based on the magnitude of $K_p e$. However, this command equation resembles the formula of a spring, and can result in oscillations around the target state. Therefore, we add a derivative component by differentiating the error signal and multiplying it by a derivative gain (K_d)—this component will act as a damper and prevent oscillations. In some cases, the forces generated by the controller might be opposed by external forces (such as forces due to gravity or friction), resulting in steady state error. Therefore, the error signal is also integrated and multiplied by an integral gain (K_i), to add up the small steady state errors and generate a corrective command that moves the plant to the exact target state. When the three gains are optimally tuned, PID controllers can produce fast, stable and effective control.

Feedback control systems have a peculiar flaw—trying to control an otherwise stable dynamical system can sometimes make it unstable. We can understand why this happens by analyzing the Bode plot of a control system (Fig 1.2c). A stable control system acts to move the dynamical system towards the desired state and dampen out any oscillations. However, instability occurs when a control system outputs signals with

frequencies that are phase shifted by -180 degrees; these feedback signals further amplify the inputs, causing growing oscillations that make the system go out of control. Bode plots allows us to determine stability margins to prevent this situation from occurring. Time delays from signal transmission and processing can also cause phase shifts, which reduces the stability margins of the control system.

We can evaluate the responsiveness of a feedback control system using its step response characteristics, which quantifies how the system behaves when it is required to suddenly reposition the plant (a step change in its target state). Ideally, when a feedback control system is switched on and given a target state to reach, it should rapidly move from its initial state to the target state and come to rest there. However, due to the dynamics of feedback control systems, this is rarely the case. In Fig 1.2b, I have shown the behavior of three types of step responses (an underdamped, overdamped and critically damped response). In an underdamped response, the state of the plant overshoots the target before it returns back towards it, and then continues to oscillate about the target state forever (Fig 1.2b blue line). In an overdamped response, the state of the plant approaches the target state asymptotically but never fully reaches the target state (Fig 1.2b green line). In between these two cases is the critically damped response—the state does not overshoot and approaches the target faster than an overdamped response, but slower than an underdamped response (Fig 1.2b red line). Settling time is a step response measure that quantifies how long the plant takes to move from its initial state to within certain thresholds of the target state, and stay within those settling time thresholds. In Fig 1.2b, I indicate when the responses reach within 10% settling time thresholds for illustration purposes. Note that the underdamped response is faster to reach the thresholds than the critically damped response, but takes longer to remain within the thresholds than the critically damped response. To quantify the responsiveness of a feedback control system, we need to first define the settling time thresholds and allowable overshoot. The choice of settling time thresholds and allowable overshoot and can significantly change the values we obtain for response time, even if the response remains the same.

In this thesis, I use techniques from control systems theory to understand the neural control of movement in animals. Although control theory was developed for synthetic

systems, they have proven to be very useful to probe biological systems (Cowan et al., 2014; Madhav and Cowan, 2020). Both synthetic and biological control systems have to contend with limitations such as time delays and saturation limits which also make the behavior of the control system nonlinear, and control theorists have developed techniques to study their effects and compensate for them. Here, I have developed simple feedforward and feedback control systems with time delays and saturation limits, to model the control of fast perturbation responses in animals.

1.3. Neural control of locomotion

The nervous system controls locomotion using a hierarchical structure where the different levels interact with one another, and each of these levels act with characteristic amounts of latency. From a neuroanatomy perspective, the control of locomotion involves the central and peripheral nervous systems, the visual, vestibular, cutaneous and proprioceptive sensors, and even the muscles. These levels include preflexes, reflexes and supraspinal motor centers (Daley, 2018; Rossignol et al., 2006). Preflexes arise from the intrinsic mechanical properties of the musculoskeletal system and act instantaneously to stabilize the body against perturbations (Brown and Loeb, 2000; Gordon et al., 2020). For example, consider a joint being held at a specified angle due to the coactivation of two antagonistic muscles. If the joint angle is perturbed, the force-velocity properties of the muscles will dampen out the perturbation, and the force-length properties will act as a spring to return the joint to the specified angle. The level of coactivation of the muscles modulate the strength of the preflex. While the above example is neuraly modulated, the passive dynamics of a mechanical system can also contribute to rejecting perturbations. For example, passive dynamic walking models are inherently stable in the sagittal plane, and can respond to small perturbations instantaneously, without the need of neural control (Kuo, 1999).

Reflex circuits and Central Pattern Generators (CPGs) at the spinal cord form the next level of control in the hierarchy. They act with more latency than preflexes, due to signal transmission and processing delays (Pearson and Gordon, 2000). Activation of peripheral receptors in muscles, joints and skin result in coordinated muscle activation

through neural circuits, known as reflexes. One example is the stretch reflex, where the muscle spindle discharges in response to an unanticipated lengthening of the muscle. The discharge results in the stimulation of pathways in the spinal cord that cause activation of the muscle, and inhibition of its antagonistic muscle. Depending on the forces acting across the muscle, the muscle could contract concentrically back to its commanded length, or contract eccentrically to counteract the forces stretching the muscle—acting as a feedback system. Central pattern generators are neural circuits in the spinal cord that can independently produce oscillatory signals without any external input or stimulation (Taga, 1995a, 1995b). These oscillatory signals generate the motor commands that produce rhythmic movements, although they usually work in conjunction with reflex feedback during locomotion.

Supraspinal motor centers within the motor cortex, cerebellum and basal ganglia form the highest level of control, and act with the longest latency. These centers receive sensory feedback from afferents and perform motor planning tasks (Rossignol et al., 2006). For example, proprioceptive signals from the limbs travel through the dorsal spinocerebellar tract (hindlimbs) and cuneocerebellar tract (forelimbs) in the spinal cord, and onto the mossy fibers in the cerebellum. Then, cerebellar granule cells process this information along with efference copies of motor commands from the cerebral cortex, and finally send out signals to the muscles from cerebellar nuclei. Similarly, proprioceptive signals are presumed to travel through the dorsal column medial lemniscus pathway to the brainstem nuclei, and then to the thalamus and motor cortex (Dallmann et al., 2021). Supraspinal centers can increase the strength of preflexes by modulating central pattern generator activity and increasing coactivation, and modulate reflexes by changing reflex loop gains through presynaptic inhibition/excitation (Pearson and Gordon, 2000). Studies hypothesize that supraspinal motor centers also hold the internal models involved in predictive control, state estimation, motor learning, and compensation for sensorimotor delays and noise (Herzfeld and Shadmehr, 2014; Miall et al., 1993; Wolpert et al., 1998), while Kuo et al. have suggested that CPGs can also function as state estimators (Kuo, 2002; Ryu and Kuo, 2021).

Using this hierarchical structure for neural control, animals are able to generate a vast repertoire of movements. Animals locomote using rhythmic movements such as walking, running, hopping, flying and swimming. Central pattern generators can produce the feedforward oscillatory motor commands required for locomotion, while feedback signals from reflex pathways help regulate the timing and magnitude of the rhythmic movements (Dallmann et al., 2021; Ryu and Kuo, 2021; Taga, 1995b). On the other hand, goal directed movements such as reaching and foot placement rely predominantly on feedback control from the supraspinal motor centers, and computational models indicate that the "optimal feedback control method" works well in predicting the generated motor commands (Todorov, 2004; Todorov and Jordan, 2002). Additionally, animals must be able to reject perturbations and maintain posture and stability. These perturbations responses require a combination of feedforward and feedback control and can involve all three levels of the neural control hierarchy (Daley, 2018; Daley et al., 2009; Daley and Biewener, 2011; Gordon et al., 2020). We do not fully understand how these different levels interact with one another to control movement, and which algorithms they use process information and generate motor commands (Zuur et al., 2010).

In this thesis, I choose to focus only on fast perturbation response movements, which are controlled through spinal pathways. I study how these responses are affected by time delays and muscle force capacity limits, and how they change with animal size. My results can help better understand the performance and limitations at the spinal level of control, and give insight into the control choices that the nervous system makes in this context.

1.4. Response time and its component delays

The ability to sense a perturbation, and respond quickly and accurately is important for survival. Animals of all sizes would face evolutionary pressures to have fast response times—although there are exceptions in nature such as sloths and tortoises who overcome the need to be fast by camouflage or armor. The tiny shrew needs a fast response time to escape from its predators. While an adult elephant does not have any natural predators, it also needs a fast response time to recover from a trip or loss of balance, as a simple fall for

such a large animal could result in injury or death. I am interested in how response times change with animal size, and how the limitations of the mammalian neuro-musculoskeletal system affect response time.

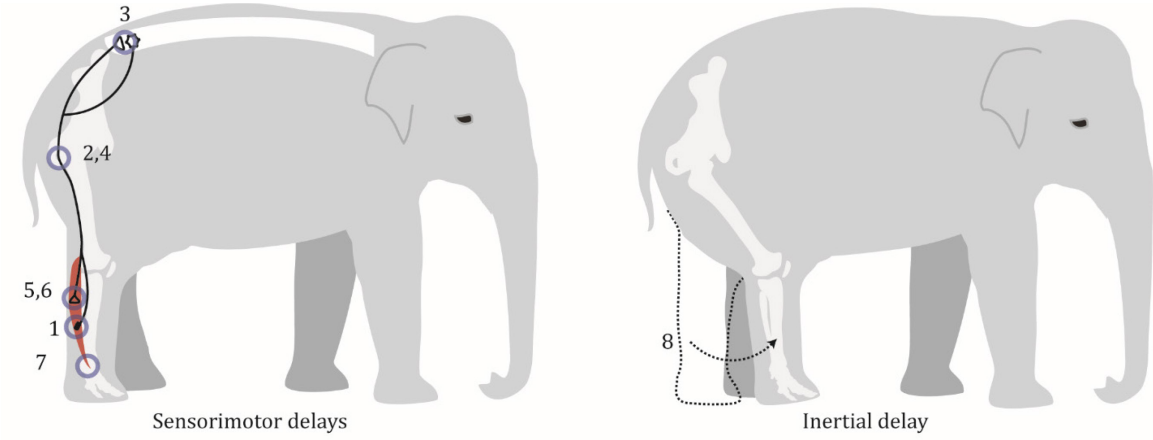

Fig 1.3 Components of perturbation response time.
We can break down the time required to complete a fast perturbation response into several components. Consider an animal that has encountered a trip. There will be a delay in sensing the trip (1. sensing delay), a delay to transmit the signal to the spinal cord (2. nerve conduction delay), a delay for the sensory information to be processed at the synapse in the spinal cord, and for the appropriate motor commands to be generated (3. synaptic delay), another nerve conduction delay to transmit the motor commands to the appropriate muscles, a delay to transmit the signal across the neuromuscular junction (5. neuromuscular junction delay), a delay to transmit the signal across the muscle and start cross bridge cycling (6. electromechanical delay), and a delay to generate forces in the muscle (7. force generation delay). We group these seven delays under the term *sensorimotor delays.* Finally, there is a delay in repositioning the limb such that the animal regains its posture and balance, which requires producing forces to overcome inertia (8. inertial delay).

In order to understand and quantify response time, we can break it down into several component delays. For example, consider the elephant in Fig 1.3, that has encountered a trip to its hindlimb. In order to respond as quickly as possible to this perturbation, the elephant's nervous system would have to sense the trip, transmit the action potentials to the spinal cord, process the sensory information, and send the appropriate motor commands the muscles. I termed these neural transmission and processing delays as *sensorimotor delays.* The muscles then have to lift the limb away from the source of the trip and place it at a new location to regain stable balance and posture. I termed this delay in overcoming inertia and repositioning body segments as *inertial delay*. In this thesis, I quantify response time as the sum of sensorimotor delay and inertial delay. I also explore how using different control policies to generate the motor signals affect response time.

1.4.1. Scaling of sensorimotor delays and resolution

Previous research in the Locomotion Lab, Simon Fraser University studied how aspects of sensorimotor responsiveness and resolution changed with animal size (More et al., 2013, 2011, 2010; More and Donelan, 2018). *Responsiveness* refers to how quickly an animal can sense and respond to a perturbation. *Resolution* refers to how precisely the animal can sense the perturbation, and how finely graded its motor responses can be. More et al. showed that for a given nerve thickness, there is a trade-off between responsiveness and resolution (More et al., 2010). Peripheral nerves contain thousands of both sensory nerve fiber axons and motor nerve fiber axons. Faster nerve conduction velocities would improve responsiveness, and depend on the diameter of the axons. Having more sensors within a given volume of tissue, or having more motor units in a muscle would improve resolution; this depends on the number of axons that can be packed into a nerve. An animal can increase its nerve conduction velocity by having larger diameter axons in its nerves, but will have to contend with fewer axons in the nerve, compromising resolution. Alternatively, it could have a larger number of small diameter axons, and face slower conduction velocities.

More et al. quantified the scaling of nerve conduction velocities and number of axons in the peripheral nerves of terrestrial mammals. They found that nerve conduction velocities in the sciatic nerve of mammals scale as $63.5M^{0.04}$ m/s; while mammalian leg lengths scale as $0.162M^{0.37}$ m (Kilbourne and Hoffman, 2013; Thangal and Donelan, 2020). More et al. also quantified that the number of axons in the sciatic nerve in mammals scale as $13587M^{0.36}$ (More, 2013). Assuming geometric similarity, we would expect volume and cross-sectional area of the regions innervated by the sciatic nerve to scale with M^{1} and $M^{2/3}$ respectively. These results show that as animal size increases, they face relatively longer nerve conduction delays and reduced resolution, which can detrimentally affect their control of locomotion.

Next, More et al. quantified the scaling of each of the components of sensorimotor delay using both electrophysiological experiments and systematic literature reviews (More and Donelan, 2018). They focused on data from the sciatic nerve and medial

gastrocnemius, but sometimes included data from other lower limb muscles if there was scarcity of data.

1. They defined *sensing delay* as the time between the change in length of the muscle and the generation of action potentials in the afferent Ia sensory nerve fibers. As there was limited information in the literature which was insufficient to indicate any change with size for sensing delay, they averaged the three measurements available from cats and assumed sensing delay is constant with animal size at 0.6 ms.

2. They defined *nerve conduction delay* as the time to transmit action potentials from the muscle spindles to the spinal cord along the sensory nerve fibers, and from the spinal cord to the muscles along the motor nerve fibers. They quantified nerve conduction delay as twice the leg length divided by nerve conduction velocity (determined from the sciatic nerve). Nerve conduction delay scaled as $5.3M^{0.30}$ ms.

3. They defined *synaptic delay* as the time to transmit action potentials across the monosynaptic connection from the sensory nerve fiber to the motor nerve fiber in the sacro-lumbar spinal cord. Data from four species did not indicate significant changes with animal size; they averaged the available measurements and assumed synaptic delay is 0.7 ms for all animal sizes.

5. They defined *neuromuscular junction delay* as the time for the motor signals to cross the neuromuscular junction between the motor nerve and the muscle surface, and quantified it as the time between electrical activity at the end of the motor nerve fiber and the detection of electrical activity on the muscle. Based on measurements from four species, they assumed that neuromuscular junction delay does not change with animal size and is constant at 0.9 ms.

6. They defined *electromechanical delay* as the time for the action potentials that have crossed the neuromuscular junction to transmit through the muscle, release Ca^{2+} ions from the sarcoplasmic reticulum, and initiate cross bridge cycling. They determined this by using measurements of the time between electrical activity in the muscle and the detection of force from the muscle, from single twitch response studies made in the

intact medial gastrocnemius at its resting length. Electromechanical delay scaled as $4.3M^{0.21}$ ms.

7. They defined *force generation delay* as the time to reach peak twitch force after force is detected in the muscle. They searched for measurements made from single-twitch non-potentiated responses in the medial gastrocnemius at its resting length, made by stimulating a single motor nerve fiber or multiple fast motor units together. Force generation delay scaled as $17.6M^{0.20}$ ms.

These component delays added together represented total sensorimotor delay which scaled as $31M^{0.21}$ ms. Sensing delay, synaptic delay and neuromuscular junction delay share biophysical processes which support the assumption that they do not change significantly with animal size. Synaptic delay and neuromuscular junction delay involve the release of neurotransmitters from a presynaptic neuron, the neurotransmitters diffusing across the short distance of the synaptic cleft, the neurotransmitters binding to receptors on a post synaptic membrane and changing its conductance, and finally resulting in action potential in the post synaptic membrane. In sensing delay, a stimulus causes a change in conductance in a membrane, resulting in an action potential in the sensory nerve fiber. The biophysical features that affect these delays, such as the speed of neurotransmitter diffusion, size of the synaptic clefts, functions of ion channels or the structure of mechanoreceptors, do not change significantly with animal size. Thus, they expect these delays do not change significantly with size either. In chapters 2 and 3 of my thesis, I use computational modeling to determine the scaling of inertial delay, allowing me to determine the scaling of total response time.

1.5. Aims and approach

My goal was to quantify how the fastest perturbation response times scale with animal size. As animal size increases, the neural control of locomotion faces two prominent challenges—their muscles get proportionally weaker, and the time delays within their control pathways get longer. I studied how these two limiting factors affect response times in animals of different sizes. I designed simple computational models that can be scaled

with animal size, and parameterized them using data from the literature. My models represented two perturbation response scenarios commonly encountered during locomotion: the swing task represented an animal repositioning its limb after a trip during the early swing phase (stumble corrective response) (Rossignol et al., 2006), and the posture task represented an animal recovering its posture after a push forward in the sagittal plane (Horak and Nashner, 1986; Rushmer et al., 1983). In chapters 2 and 3, I quantified the scaling of inertial delays. In chapters 4 and 5, I studied how two different control configurations—feedforward control and feedback control—affected response time. Before studying more biologically realistic models, I first used simple approximations in chapter 2 and 4 to provide intuitive understanding of how various factors affected perturbation response behavior. I kept these models as simple as possible, and used them to make predictions that could be verified in the following chapters. In chapters 3 and 5, I used numerical simulations of more biologically realistic models to estimate the scaling of response times. Below, I have provided short descriptions for each chapter of this thesis.

In chapter 2, I used a simple approximation (a single degree-of-freedom rotational system) to understand how inertial delays scale with animal size. By ignoring gravity, the equations of motion of the system are linear. I analytically derived the equations of motion, and tested how inertial delays would scale under assumptions of geometric and dynamic similarity. These theoretical calculations showed that if animal muscles could produce forces that scaled with dynamic similarity, larger animals would have the same relative inertial delays as smaller animals. On the other hand, if animal muscles only produce forces that scaled with geometric similarity, larger animals would face relatively longer inertial delays than smaller animals, disproportionately burdening them.

In chapter 3, I built on the results from chapter 2, and quantified the scaling of inertial delays using numerical simulations of more biologically realistic models. I parameterized each model with values collected from the scaling literature for terrestrial mammals, and considered gravity. I represented the swing task using a distributed mass pendulum, parameterized it with inertial values corresponding to the forelimb of a terrestrial quadruped, and actuated it with torques derived from the force capacity of the triceps muscle. I represented the posture task as an inverted pendulum with inertial

properties of the whole animal, and actuated the model with torques equalling that from four plantarflexors. I used optimization to determine the optimal parameters that minimized inertial delay time, and used Monte Carlo simulations to determine the confidence intervals. I compared inertial delays to sensorimotor delays, and to available movement time, and discussed how it could affect small and large animals differently. I showed that the scaling of inertial delays depended both on movement task and movement size, and that inertial delays scaled faster than sensorimotor delays and available movement time.

In chapter 4, I used simple models to study how time delays and saturation limits affected response times under feedback control. I first used a linear feedback control system under PD control to show how time delays cap the controller gains that can produce stable behavior. I then non-dimensionalized a time-delayed and force-limited feedback control system, and studied how these limitations affected response times. I showed that perturbation response times in animals can either be limited by the force generation capacity of muscles (force-limited) or by sensorimotor time delays which constrain the maximum feedback gains that can be used to produce stable responses (delay-limited). I also provided predictive equations generated using curve fitting for the relationship between saturation limits and response time, for the swing task and posture task.

In chapter 5, I built on the results from chapter 4, and quantified the scaling of response times under feedback and feedforward control on more biologically realistic models. I considered gravity and parameterized the model with values from the scaling literature. I used optimization to determine the optimal parameters that produced the fastest response times. I compared response times under feedback and feedforward control to each other and to available movement times. I discussed how feasible each form of control is for fast perturbation responses, and how it affects small and large animals differently. I showed that while feedforward control can fully activate muscles and produce fast responses, long sensorimotor delays force feedback control to use low gains to ensure stability, allowing only a fraction of the muscles' force capabilities to be utilized. That is, the effectiveness of feedback control within the size range of terrestrial mammals is delay-limited rather than force-limited.

Chapter 2. Scaling of inertial delays in a simple biomechanical system

2.1. Introduction

Independent of animal size, a fast response time is important to an animal's survival. A tiny shrew needs to react quickly to escape from a predator, and a massive elephant needs to recover quickly from a loss of balance to prevent a fall. Response time—measured as the total delay between the onset of a perturbation and the completion of the corrective movement that is in response to the perturbation—is not just important for relatively rare escapes and falls, but also for more common motor control tasks. This is because time delays within the neural pathways can destabilize feedback control, requiring animals to have compensatory neuromechanical strategies (Miall et al., 1993; Milton, 2011; More and Donelan, 2018; Wolpert et al., 1998). Response time is relevant to the control of movement both in terms of its absolute duration and its duration relative to the available movement time. For example, the absolute duration of the corrective response matters to avoid a snakebite, which can be equally deadly for small and large animals alike. And the relative response time matters to avoid a trip when galloping, where the corrective response may need to occur within a limb's swing duration, which takes longer in larger animals (Alexander, 2002; Heglund et al., 1974; Heglund and Taylor, 1988).

Response time is determined, in part, by neuromuscular physiology (Burke et al., 1973; Grillner, 1972; More et al., 2010; More and Donelan, 2018). Consider an animal whose foot catches on a vine—the lengthening of the limb muscles activates the stretch reflex, which resists muscle stretch and helps the animal recover its posture (Lloyd, 1943; Zehr and Stein, 1999). This stretch reflex consists of several component delays. There are delays which represent the time it takes to sense the trip, transmit the action potentials through both the sensory and motor nerves, process the response at the synapses in the spinal cord, and begin to generate muscle force. I group these component delays together and refer to their sum as *sensorimotor delay* (Section 1.4) (More and Donelan, 2018). After the sensorimotor delays, the corrective response to a perturbation often requires that the animal reposition its body. If muscles could instantaneously generate infinite force, or if

the body and its segments were massless, this could be accomplished instantly. But of course, muscles have finite strength and bodies have inertia. Consequently, the animal's inertia impedes the acceleration generated by muscles, further delaying response time. I refer to this last contributor to response time as *inertial delay* and define it as the absolute time between the onset of the corrective movement that is in response to a perturbation and the completion of this corrective movement. A corrective movement is a dynamic process whose duration depends on the movement task and the magnitude of this movement. The duration depends on the corrective movement task because the time to swing a limb to a new position, for example, may be different from that required to reject a push to the torso to avoid a fall. This is because the two tasks involve different muscles, resulting in different force capacities, and different parts of the body, resulting in different inertial properties. It depends on the magnitude of the required movement because, all else being equal, less time is required to accomplish small adjustments to the body's position and velocity than large adjustments. I model these dynamic effects of inertia as a delay by determining the duration required for a movement, while controlling for movement magnitude and movement task.

In this chapter, my objective is to understand how inertial delays scale with animal size, both in absolute terms and relative to available movement time, under the theoretical scaling design rules of geometric similarity and dynamic similarity. Towards this goal, I first derived scaling relationships for the time available to produce a corrective movement under two scenarios: the natural time period of a swinging limb, and the time required for an animal to fall to the ground (Section 2.3.1). Next, I focussed my study on two different tasks designed to represent perturbation response scenarios commonly encountered during animal locomotion (Section 2.3.2). The swing task represented an animal repositioning its limb to produce a corrective foot placement after a trip, and the posture task represented an animal recovering its posture after a push forward in the sagittal plane. I derived analytical expressions for the scaling of inertial delay using linear models and parameterizing them using two scaling design rules: assuming that muscle forces scale with $M^{2/3}$ under geometric similarity and M^{1} under dynamic similarity. This helps build intuition for the dependence of inertial delay on perturbation task, movement magnitude, muscle force, muscle moment arm, and inertial properties.

2.2. Methods

I performed all the analytical derivations in this chapter by hand. I used two scaling design rules to parametrize my models: geometric similarity and dynamic similarity. I assumed that animal morphological features scale with geometric similarity. Two animals are geometrically similar if they have exactly the same shape, even if they are of different sizes (Alexander, 2003). More specifically, it requires that linear features between animals, such as leg length, scale with $M^{1/3}$, surface area features scale with $M^{2/3}$, and volumes and masses of body segments scale with M^{1} (McMahon, 1975). The theory of dynamic similarity states that two animals will locomote in a dynamically similar fashion when they are travelling at equal values of a dimensionless velocity called the Froude number (Alexander and Jayes, 1983). For two animals to be dynamically similar, their physical dimensions, the time periods of their gait, and the forces that they apply must be in constant ratios to each other. The forces applied during their movements must also scale with M^{1}.

2.3. Results

2.3.1. Scaling of available movement times

I used characteristic movement times to understand how much time an animal has available to respond to a perturbation and complete the corrective movement. I compared response times to these available movement times to gauge whether the time required to respond may hinder neural control of movement (Hooper, 2012). Here, I analytically quantified the scaling of two characteristic movement times: the time it would take an animal to fall to the ground, and the time an animal's leg is in swing phase when running.

As response time becomes longer relative to fall time, it becomes more difficult for an animal to stop a fall and regain balance. To analytically derive the scaling of fall time, I used the equations for a body falling under constant acceleration due to gravity (Halliday et al., 2010). Consider an animal of mass M, falling from the height of its leg L to the floor under the force of gravity. F_g is the force of gravity, where g is the acceleration due to gravity. The equations for acceleration $\ddot{y}(t)$, velocity $\dot{y}(t)$ and position $y(t)$ are:

$$\ddot{y}(t) = \frac{d^2y}{dt^2} = \frac{F_g}{M} = \frac{-gM}{M} = -g \tag{2.1}$$

$$\dot{y}(t) = \int \ddot{y}\, dt = -gt + \dot{y}_0 \tag{2.2}$$

$$y(t) = \int \dot{y}\, dt = \frac{-gt^2}{2} + \dot{y}_0 t + y_0 \tag{2.3}$$

The initial velocity $\dot{y}_0$ is 0 and initial position y_0 is L. Assuming geometric similarity, the time t_f required for an animal to fall to the floor is:

$$t_f = \sqrt{\frac{2L}{g}} \propto \sqrt{L} \propto M^{1/6} \tag{2.4}$$

It would take longer for an animal to fall like an inverted pendulum, rather than crumple to the ground as derived above, but the dependence on mass would not change. Similar to falling, if response time exceeds the natural time period of the swinging limb, or some fraction of this period, the animal may have difficulty recovering if the swing is perturbed. I used the natural time period of a pendulum with the properties of an animal limb as a proxy for swing duration (Halliday et al., 2010; Mochon and McMahon, 1980). Assuming geometric similarity, the natural time period t_s of a pendulum scales as:

$$t_s = 2\pi \sqrt{\frac{L}{g}} \propto \sqrt{L} \propto M^{1/6} \tag{2.5}$$

Thus, like time to fall, swing period depends on $M^{1/6}$. Swing duration calculations based on values reported in the literature estimate that it scales with $M^{0.14}$ at trot-gallop transition speeds and with $M^{0.13}$ at maximum sprint speeds (More and Donelan, 2018). Thus, characteristic movement times scale approximately with $M^{1/6}$ based on both theoretical considerations and empirical measurements. I use these characteristic movement times to normalize the absolute response time.

These relative response times are a measure of how long response time is when compared to the time available to complete the response. It is unlikely that animals have to complete a corrective movement in exactly the duration of the swing phase at sprint speeds. It is possible that they can recover from a perturbation if the corrective movements take longer, and it is also possible that the corrective movements have to be completed in an even shorter period of time. Nevertheless, swing duration seems like a reasonable benchmark for the stumble corrective response in the swing task, rather than distributing the corrective movement across multiple limbs and multiple phases of the gait cycle. Furthermore, swing duration, fall duration, and pendulum period share a common scaling exponent providing me with some assurance that relative response time will not depend strongly on size as a consequence of my choice of available movement time.

2.3.2. A simple model of inertial delay

Model

To obtain theoretical estimates for the scaling of inertial delays, I first considered a simple single degree of freedom rotational system operating without the effect of gravity (Fig 2.1). These equations of motion are linear, allowing me to analytically derive the scaling of inertial delays. These estimates will support subsequent numerical simulations and provide intuition about how various factors contribute to inertial delays. This system is an angular version of a sliding block model and can be analytically described as a double integrator—a simple and well-studied dynamical system (Rao and Bernstein, 2001; Srinivasan, 2010).

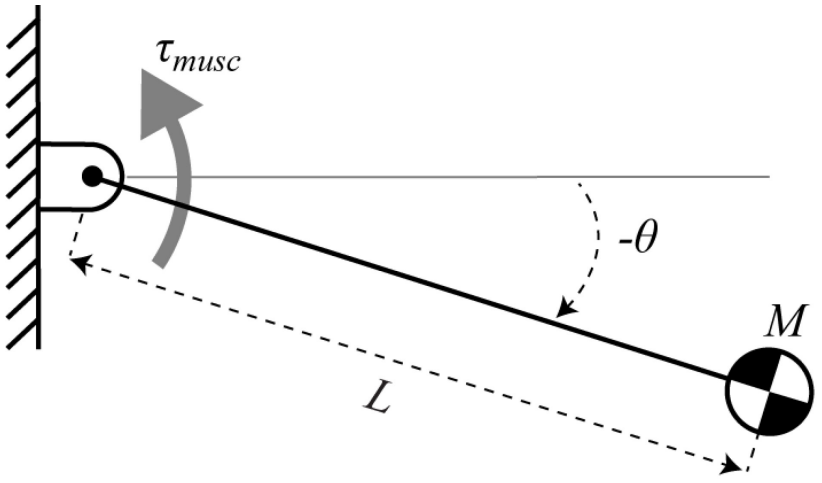

Fig 2.1 Simple model for inertial delay.
A single degree of freedom rotational system with a rod of length L and point-mass M rotates about a pin joint actuated by torque τ_{musc}. θ is the angle from the horizontal with positive angles in the counter-clockwise direction. This model ignores gravity and assumes the rod is massless.

Scaling of model parameters

Assuming the system's morphological features scale with geometric similarity, its length would scale with $M^{1/3}$, mass with M^1 and moment of inertia (ML^2) with $M^{5/3}$. I considered two scenarios for the scaling of maximum muscle force. In the first scenario, I assumed that muscle force maintains dynamic similarity between animals of different sizes by scaling force in direct proportion to animal mass: $F_{musc} \propto M^1$ (Alexander and Jayes, 1983). In the second scenario, I instead assumed muscle force scales with cross-sectional area exponent of geometric similarity: $F_{musc} \propto M^{2/3}$ (Biewener, 1989a). In this model, the applied muscle torque τ_{musc} is the product of a constant muscle moment arm R_{musc} and the muscle force.

$$\tau_{musc} = F_{musc} R_{musc} \qquad 2.6$$

I also assumed that the muscle moment arm scales with geometric similarity too ($M^{1/3}$).

Analytical derivation for the swing task

The swing task represents an animal repositioning its swing leg to control foot placement and maintain stability during walking and running (Daley and Biewener, 2006; Kuo, 1999; Mcgeer, 1990; Seyfarth et al., 2003; Wong and Donelan, 2017). For the swing task, the pendulum is required to move from rest at an initial angle θ_0 which I set as 0°, to

a final angle θ_f under the control of muscle torque τ_{musc}. The fastest way to complete this movement is to apply a constant torque to accelerate from 0 to $\theta_f/2$, then reverse the direction of torque to decelerate and stop at θ_f. Since the movement is symmetrical, I considered only the first half from 0 to $\theta_f/2$. The equations for the angular acceleration $\ddot{\theta}(t)$, angular velocity $\dot{\theta}(t)$ and angle $\theta(t)$ are:

$$\ddot{\theta}(t) = \frac{d^2\theta}{dt^2} = \frac{\tau_{musc}}{ML^2} \tag{2.7}$$

$$\dot{\theta}(t) = \int \ddot{\theta}\, dt = \frac{\tau_{musc}}{ML^2} t + \dot{\theta}_0 \tag{2.8}$$

$$\theta(t) = \int \dot{\theta}\, dt = \frac{\tau_{musc}}{2ML^2} t^2 + \dot{\theta}_0 t + 0 = \frac{\theta_f}{2} \tag{2.9}$$

Because the initial velocity $\dot{\theta}_0$ is 0, and my desired final angle is $\theta_f/2$, I can rearrange Eqn 2.9 to solve for t. The total inertial delay is twice this time to account for the time spent in each half of the total movement:

$$t_{ID} = 2\sqrt{\frac{ML^2\,\theta_f}{\tau_{musc}}} \tag{2.10}$$

Eqn 2.10 shows that inertial delay is proportional to the square root of both the movement magnitude (θ_f) and the moment of inertia of the pendulum (ML^2), and inversely proportional to the square root of the applied torque. Therefore, doubling muscle torque would only cause an approximately 30% reduction in inertial delay and quadrupling muscle torque would only result in a 50% reduction. These calculations indicate that while inertial delay in the swing task does depend on actuator limits, increasing muscle torque may not be an effective option to reduce inertial delay. Instead, an animal could reduce its leg length (L), which would directly reduce inertial delay.

Next, I considered two different scenarios for the scaling of muscle force. Assuming muscle force scales with dynamic similarity ($F_{musc} \propto M^1$), I determined the scaling of inertial delay by substituting Eqn 2.6 into Eqn 2.10:

$$t_{ID} = 2\sqrt{\frac{ML^2\theta_f}{F_{musc}R_{musc}}} = 2\sqrt{\frac{c_1 M^{5/3}\theta_f}{c_2\, M^{4/3}}} \propto M^{1/6}.\sqrt{\Delta\theta} \qquad 2.11$$

where c_1 and c_2 are constants of proportionality. Since θ_0 is 0, I substituted θ_f with $\Delta\theta = (\theta_f - \theta_0)$, representing the movement magnitude.

$$t_{rel} = \frac{t_{ID}}{t_{char}} \propto \frac{M^{1/6}}{M^{1/6}} \propto M^0 \qquad 2.12$$

where t_{ID} is the inertial delay, t_{char} is the characteristic movement time, and t_{rel} is the relative delay. Therefore, if muscles produce forces proportional to their mass, inertial delay will scale with the same exponent as characteristic movement times (Eqns 2.4, 2.5), and relative delay would be independent of animal size. As much as animals are like this simple model with its assumptions, large and small animals would be dynamically similar in their response to disturbances and relative delay would not change with animal size. In this situation, inertial delay would not disproportionately burden larger animals.

Instead, if muscle forces scale with cross-sectional area ($F_{musc} \propto M^{2/3}$), getting relatively weaker with increases in size, inertial delay scales as:

$$t_{ID} = 2\sqrt{\frac{ML^2\theta_f}{F_{musc}R_{musc}}} = 2\sqrt{\frac{c_1 M^{5/3}\theta_f}{c_2 M^1}} \propto M^{1/3}.\sqrt{\Delta\theta} \qquad 2.13$$

$$t_{rel} = \frac{t_{ID}}{t_{char}} \propto \frac{M^{1/3}}{M^{1/6}} \propto M^{1/6} \qquad 2.14$$

In contrast to dynamic similarity, relative delay will grow with animal size proportional to $M^{1/6}$, when muscle force grows only in proportion to cross-sectional area, penalizing larger animals.

Analytical derivation for the posture task

The posture task models a standing animal recovering its balance after being perturbed (Horak and Nashner, 1986; Rushmer et al., 1983; Ting and Macpherson, 2004; Winter, 1995). I represented the standing quadruped with an upright single degree of

freedom rotational system, which starts from an initial position and has an initial clockwise velocity in the sagittal plane due to a perturbation pushing it forward. I defined inertial delay as the time required for muscle torque to return the pendulum to rest back at the initial upright position after recovering from the perturbation. I again used the simple model (Fig 2.1) and ignored the effects of gravity to keep the system linear. For this task, the movement is not symmetrical. To analytically derive the equations for inertial delay in the posture task, it is convenient to break down the movement into three phases: A, B and C. In phase A, the system starts at the initial position with a clockwise velocity due to the perturbation. I then apply a counterclockwise torque to decelerate the pendulum and reject the velocity perturbation, stopping at a clockwise angle. In phase B, I continue to apply the counter-clockwise torque, accelerating the pendulum from rest with a counter-clockwise velocity as it moves back towards its initial position. In phase C, I switch the torque direction again so that a clockwise torque now decelerates the pendulum and brings it to rest at the initial position, thereby completing the response to the velocity perturbation.

In phase A, the pendulum starts from an initial angle ${}_A\theta_0$ with an initial clockwise angular velocity $-{}_A\dot{\theta}_0$. I defined ${}_A\theta_0$ to be the origin with value 0, and counterclockwise movements to be positive. I then applied a counterclockwise torque τ_{musc} that brought the pendulum to rest at a final position $-{}_A\theta_f$. The equations for angular acceleration ${}_A\ddot{\theta}(t)$, angular velocity ${}_A\dot{\theta}(t)$ and angle ${}_A\theta(t)$ are:

$$ {}_A\ddot{\theta}(t) = \frac{d^2\theta}{dt^2} = \frac{\tau_{musc}}{ML^2} \tag{2.15} $$

$$ {}_A\dot{\theta}(t) = \int {}_A\ddot{\theta}dt = \frac{\tau_{musc}}{ML^2}\,{}_At - {}_A\dot{\theta}_0 = 0 \tag{2.16} $$

$$ {}_A\theta(t) = \int {}_A\dot{\theta}\,dt = \frac{\tau_{musc}}{2ML^2}\,{}_At^2 - {}_A\dot{\theta}_0\,{}_At + 0 = -{}_A\theta_f \tag{2.17} $$

Rearranging Eqn 2.16, I expressed the duration of phase A $({}_At)$ in terms of the initial velocity of the perturbation:

$$ {}_{A}t = \frac{ML^2\,{}_{A}\dot{\theta}_0}{\tau_{musc}} \tag{2.18} $$

Substituting Eqn 2.18 into Eqn 2.17 and simplifying provided the final angle of phase A ($_{A}\theta_f$) in terms of the initial velocity $_{A}\dot{\theta}_0$:

$$ {}_{A}\theta_f = \frac{ML^2\,{}_{A}\dot{\theta}_0^{\,2}}{2\tau_{musc}} \tag{2.19} $$

In phases B & C, the system is brought back to rest at the origin from the end position of phase A ($-{}_{A}\theta_f$). The movements in phases B and C are equal and opposite, with a counterclockwise torque initially accelerating the system from rest to a position of $-{}_{A}\theta_f/2$ in phase B, followed by a clockwise torque decelerating the system over the same angular distance to rest at the origin in phase C. Therefore, I only need to evaluate the time required for phase B, since the time required for phase C will be the same. The subtask to be accomplished in phases B and C is the same as that of the entire swing task—begin at rest, move through some angular displacement, and end at rest. The additional feature of the posture task is that the initial velocity perturbation determines the subsequent angular displacement. The equations for the angular acceleration $_{B}\ddot{\theta}(t)$, angular velocity $_{B}\dot{\theta}(t)$ and angle $_{B}\theta(t)$ are:

$$ {}_{B}\ddot{\theta}(t) = \frac{d^2\theta}{dt^2} = \frac{\tau_{musc}}{ML^2} \tag{2.20} $$

$$ {}_{B}\dot{\theta}(t) = \int {}_{B}\ddot{\theta}\,dt = \frac{\tau_{musc}}{ML^2}\,{}_{B}t + 0 \tag{2.21} $$

$$ {}_{B}\theta(t) = \int {}_{B}\dot{\theta}\,dt = \frac{\tau_{musc}}{2ML^2}\,{}_{B}t^2 + 0 - {}_{A}\theta_f \;= \frac{-\,{}_{A}\theta_f}{2} \tag{2.22} $$

Simplifying Eqn 2.22 gives:

$$ \frac{{}_{A}\theta_f}{2} = \frac{\tau_{musc}\;{}_{B}t^2}{2ML^2} \tag{2.23} $$

Substituting the final angle of phase A ($_A\theta_f$) from Eqn 2.19 into Eqn 2.23 and solving for the duration of phase B ($_Bt$) gives:

$$_Bt = \frac{ML^2\ {}_A\dot{\theta}_0}{\sqrt{2}\,\tau_{musc}} \tag{2.24}$$

Solving for the total time for the whole motion (phases A, B and C) gives:

$$t_{ID} = {}_At + 2_Bt = \left(1+\sqrt{2}\right)\frac{ML^2\ {}_A\dot{\theta}_0}{\tau_{musc}} \tag{2.25}$$

Similarly to Eqn 2.10 for the swing task, the analytical derivation in Eqn 2.25 helps understand how the various factors contribute to inertial delay (t_{ID}) for the posture task. It predicts that the inertial delay during posture recovery after a perturbation is directly proportional to the perturbation size $_A\dot{\theta}_0$ and inversely proportional to the muscle torque τ_{musc}.

Since larger animals have heavier bodies, longer limbs and larger muscles, I scaled the size of the perturbation with animal mass to evoke responses with similar relative magnitude. To do this, I expressed the initial angular velocity of the pendulum, representing the applied perturbation, in terms of linear velocity:

$$_A\dot{\theta}_0 = \frac{v}{L} \tag{2.26}$$

where v is the linear velocity caused by the initial perturbation and L is the length of the system. I perturbed each model using an initial linear velocity scaled based on a constant dimensionless velocity v_{ND} (Hof, 1996):

$$v_{ND} = \frac{v}{\sqrt{gL}}, \qquad v = v_{ND}\sqrt{gL} \propto M^{1/6} \tag{2.27}$$

Substituting the values for $_A\dot{\theta}_0$ from Eqn 2.26 and τ_{musc} from Eqn 2.6 into Eqn 2.25 and assuming muscle force scales with dynamic similarity ($F_{musc} \propto M^1$) predicted that the total time for the posture task scales as:

$$t_{ID} = {}_{A}t + 2_{B}t = \left(1 + \sqrt{2}\right)\frac{ML^2v}{F_{musc}R_{musc}L} = \frac{c_1M^1M^{2/3}M^{1/6}}{c_2M^1M^{1/3}M^{1/3}} \propto M^{1/6}.v_{ND} \qquad 2.28$$

$$t_{rel} = \frac{t_{ID}}{t_{char}} \propto \frac{M^{1/6}}{M^{1/6}} \propto M^0 \qquad 2.29$$

If instead muscle force scales with cross-sectional area ($F_{musc} \propto M^{2/3}$), the total time for the posture task would scale as:

$$t_{ID} = {}_{A}t + 2_{B}t = \frac{c_1M^1M^{2/3}M^{1/6}}{c_2M^{2/3}M^{1/3}M^{1/3}} \propto M^{1/2}.v_{ND} \qquad 2.30$$

$$t_{rel} = \frac{t_{ID}}{t_{char}} \propto \frac{M^{1/2}}{M^{1/6}} \propto M^{1/3} \qquad 2.31$$

Similarly to the conclusions from Eqn 2.11 in the swing task, I find that if muscles produced forces proportional to their mass (dynamic similarity), both inertial delays and characteristic movement times would scale with $M^{1/6}$. This would result in constant relative delays regardless of animal size. However, if muscles produced forces proportional to their cross-sectional area, inertial delay would scale with $M^{1/2}$ in absolute time and $M^{1/3}$ when expressed relative to movement time.

The effect of size on inertial delay depended on the task. The effect of size under geometric similarity is steeper in the posture task (Eqn 2.30) than what I found in the swing task (Eqn 2.13). An additional difference is the effect of movement magnitude—inertial delay increases in direct proportion to the size of the velocity perturbation in the posture task, and only with the square root of the angular displacement in the swing task. In chapter 3, I have used computer simulations of nonlinear biomechanical models, parameterized by actual measurements from literature, to refine my estimates for the scaling of inertial delays.

2.4. Discussion

Here I analytically determined how inertial delays, the component of perturbation response time required to physically reposition body segments, scaled under different theoretical scaling design rules. I showed that the time available to complete perturbation responses (available movement time), scaled with $M^{1/6}$ both for the natural time period of a swinging limb and the time required for an animal to fall to the ground. My results showed that the scaling of inertial delays would depend both on movement task and movement size. If muscles of different sized animals could produce forces proportional to their mass ($F_{musc} \propto M^1$), inertial delays in both the swing task and posture task would scale with $M^{1/6}$ in absolute terms and M^0 in relative terms. Therefore, small and large animals would be dynamically similar in their corrective movements, and larger animals would not be disproportionately burdened by longer inertial delays. However, if muscles of different sized animals only produce forces proportional to their cross-sectional area ($F_{musc} \propto M^{2/3}$), inertial delays would scale with $M^{1/3}$ in the swing task and $M^{1/2}$ posture task, in absolute terms. In relative terms, inertial delays would scale with $M^{1/6}$ in the swing task and $M^{1/3}$ posture task. As animals get larger, their inertial delays would also get longer, disproportionately burdening larger animals. My results also show that inertial delays would increase with the square root of the angular displacement in the swing task, and directly with the initial perturbation velocity in the posture task.

These theoretical results provide a better understanding for the contribution of various factors that affect inertial delay, and give me a range of exponents for the actual scaling of inertial delay. These results need to be verified against more realistic simulations which consider the actual scaling of animal features. The scaling of animal features often deviates from theoretical design rules due to physiological limitations or evolutionary pressures. Ignoring competing evolutionary pressures, if inertial delays are potentially a significant source of delay that slows down response times to the extent that it detrimentally affects the neural control of movement and the survivability of the animal, I would expect inertial delays in real life to scale closer to predictions based on dynamic similarity. This would at least eliminate the disproportionate burden on larger animals. Otherwise, if inertial delays are not a significant factor in response time, and need not be compensated

for, I would expect inertial delays to scale based on geometric similarity. These predictions ignore any other evolutionary pressures or physiological constraints which also depend on the same factors that influence inertial delays. Ultimately, the scaling of inertial delays will depend on many different factors which affect the inertial properties of body segments (mass, length, moment of inertia of body segments), and the force generation capacity of muscles (muscle mass, fiber length, cross-sectional area, isometric stress, moment arm). In the next chapter, I have used more detailed models that are scaled with animal size and parameterized with actual scaling values from the literature, and also considered gravity, to obtain more realistic values for the scaling of inertial delays.

Chapter 3. Scaling of inertial delays in legged animals

3.1. Introduction

The scaling of inertial delay depends upon how muscle forces, muscle moment arms, and the body's inertial properties change with animal size. When compared to small animals, larger animals have larger muscles and longer moment arms which increase joint torque, but also heavier and longer limbs which increase moment of inertia (Alexander et al., 1981; Kilbourne and Hoffman, 2013). These properties don't scale precisely with simplified scaling rules such as geometric or dynamic similarity (Alexander and Jayes, 1983; McMahon, 1975). Consequently, it is not clear whether allometric scaling of muscle forces and muscle moment arms offset size-dependent increases in inertial properties, or vice versa. A similar principle is evident in the scaling of skeletal stress, where the disadvantages predicted for larger animals when assuming simplified scaling rules are reduced or eliminated by compensatory size-related changes in other factors, such as posture and moment arms (Alexander, 2003; Biewener, 1990, 1989a).

To understand whether inertial delays are a significant factor in perturbation responses and the neural control of movement, the absolute magnitude of inertial delays should also be compared to that of sensorimotor delay and available movement time, not just their scaling exponents. I can estimate response time as the sum of sensorimotor delays and inertial delays. For a given animal size and perturbation task, inertial delay could exceed sensorimotor delay, becoming the dominant contributor to slowing down perturbation responses, or vice versa. Relative delay (the ratio of response time to available movement time) is also an important indicator of the significance of delays. Longer relative delays would result in poorer stability. At its extreme, relative delays that exceed unity indicate that the animal would not be able to react at all to perturbations within the available time.

My objective is to quantify the scaling of inertial delays in legged animals using numerical simulations of more realistic models, which are parameterized with animal features obtained from literature. My intent is to determine how quickly different sized

animals can produce corrective movements when their muscles act at their force capacity, relative to the time within which those movements need to be performed. I again modeled two perturbation response scenarios: a swing leg repositioning task (swing task), and a posture correction task (posture task). The nonlinear models considered gravity, and I simulated a range of angular repositioning movements in the swing task, and a range of perturbation sizes for the posture task. I actuated my models using bang-bang control and optimized the time to switch the direction of controller torques to obtain the fastest estimates for inertial delay. I compared the more realistic estimates for inertial delay in this chapter to theoretical results based on geometric similarity and dynamics similarity obtained in chapter 2. I estimated response time as the sum of sensorimotor delay and inertial delay. Finally, I compared inertial delay to sensorimotor delay, and response time to available movement time, to understand whether these delays significantly affect neural control of movement. I also studied the sensitivity of my results to my estimates for the isometric torque capacity of muscles, and used Monte Carlo simulations to determine the confidence intervals for the inertial delay scaling results.

3.2. Methods

3.2.1. Swing task: model

I modeled the swing task as a distributed mass pendulum actuated by muscle torque (Fig 3.1a). I defined inertial delay for this task as the time required to swing the pendulum from rest at an initial clockwise angle to rest at a final counterclockwise angle, with identical angles in the clockwise and counterclockwise direction. Unlike my simple model, I included the effects of gravity, did not assume a point mass, and did not linearize the equation of motion. The motion of the pendulum is described by:

$$\ddot{\theta}(t) = \frac{\tau_{musc}}{MOI} + \frac{M_{limb} g L_{COM}}{MOI} \sin\theta(t) \qquad 3.1$$

where τ_{musc} is the muscle torque, L_{COM} is the distance from the pendulum pivot to limb center of mass, M_{limb} is the mass of the limb, and MOI is the moment of inertia of the forelimb about the shoulder joint (Fig 3.1a). I applied the control torque in a bang-bang

profile from $+\tau_{musc}$ to $-\tau_{musc}$ to determine a lower bound for inertial delay; I did not consider realistic muscle dynamics. In this scenario, inertial delay represents the minimum movement time possible, and is limited only by maximal torque (Fig 3.1b top panel).

3.2.2. Swing task: scaling of model parameters

Table 3.1 summarizes the scaling relationships that I used for my swing task parameters. I used scaling equations for forelimb mass, length, distance from shoulder joint to limb center of mass, and moment of inertia from Kilbourne and Hoffman (Kilbourne and Hoffman, 2013). I used scaling equations for triceps muscle mass, muscle length, and moment arm from Alexander et al. (Alexander et al., 1981). I assumed that the triceps is the main muscle flexing the shoulder joint in quadrupeds, because it is a prime mover for this action and because it is the only shoulder muscle for which all the values necessary to compute the scaling of muscle torque are available. Using values for the entire triceps is a further simplification, as only one of the three heads of the triceps move the shoulder (Rushmer et al., 1983). I assumed that parameters for the antagonistic muscle at the shoulder scale in the same way as those for the triceps.

To determine muscle torque for each animal size, I first determined muscle volume by dividing the mass of the muscle by a density of 1060 kg/m^3 (Méndez and Keys, 1960). I found the muscle cross-sectional area by dividing its volume by the muscle length, assuming that muscles have a consistent cross-sectional area. Multiplying the cross-sectional area by the isometric force generation capacity of mammalian muscle, estimated at 20 N/cm^2, gave muscle force (Close, 1972; Rospars and Meyer-Vernet, 2016). Finally, I calculated muscle torque by multiplying the muscle force and its moment arm.

Table 3.1 Swing task input scaling parameters and their confidence intervals.

Parameter	Coefficient (*a*)			Exponent (*b*)		
	Value	95% CI		Value	95% CI	
Forelimb inertial properties (Kilbourne and Hoffman, 2013)						
Mass (kg)	5.82×10^{-2}	4.61×10^{-2}	7.34×10^{-2}	1.00	0.93	1.08
COM length (m)	5.64×10^{-2}	4.98×10^{-2}	6.38×10^{-2}	0.36	0.32	0.40
MOI (kg m^2)	2.52×10^{-4}	1.61×10^{-4}	3.95×10^{-4}	1.75	1.60	1.89
Triceps muscle properties (Alexander et al., 1981)						
Mass (kg)	6.20×10^{-3}	5.54×10^{-3}	6.94×10^{-3}	1.11	1.07	1.15
Muscle length (m)	1.87×10^{-2}	1.72×10^{-2}	2.04×10^{-2}	0.33	0.29	0.37
Moment arm (m)	8.70×10^{-3}	8.13×10^{-3}	9.31×10^{-3}	0.41	0.38	0.44

3.2.3. Swing task: simulation

I performed simulations of the swing task for seven animal masses logarithmically spaced from one gram to ten tons, chosen to span the entire size range of terrestrial mammals (Jürgens, 2002; Larramendi, 2015). For each animal mass, I used the scaling relationships from section 3.2.2 to determine the size-specific parameters for simulation. At each animal size, I varied the initial clockwise angle from 0.01 to 30 degrees to quantify how movement size affected inertial delay. I numerically simulated the swing task using an explicit Runge-Kutta algorithm implemented with MATLAB's ode45 solver (MATLAB R2017b, The MathWorks, Inc., Natick, MA, USA). I used the solver's event detection to determine when the pendulum reached zero angle and, taking advantage of the symmetric nature of the problem, switched the direction of the applied torque from counterclockwise to clockwise. The simulation continued until the solver's event detection halted the simulation when the pendulum reached zero angular velocity, which occurred when the pendulum reached the same counterclockwise angle as it had started in the clockwise direction. Fig 3.1b shows an example simulation. Elapsed simulation time was the inertial delay for each animal size and each initial angle. For each initial angle, I then logarithmically transformed the inertial delay values for the various animal sizes and used least squares linear regression to extract the coefficient and exponent for the scaling of

inertial delay (LaBarbera, 1989). I used Monte Carlo simulations to estimate the 95% confidence intervals.

3.2.4. Posture task: model

I modeled the posture task as an inverted pendulum that has been pushed in the forward direction resulting in an initial body velocity (Fig 3.2a). The task goal is to apply the correct muscle forces to reject the perturbation and return the inverted pendulum to rest at an upright posture. I defined inertial delay for this task as the time required to move from a vertical position with an initial velocity perturbation in the clockwise direction to rest at the vertical position, under the control of muscle torque. Unlike my simple model of this task, I included the effects of gravity and did not linearize the equation of motion. The motion of this inverted pendulum model is described by:

$$\ddot{\theta}(t) = \frac{\tau_{musc}}{ML_{limb}{}^2} + \frac{MgL_{limb}}{ML_{limb}{}^2}\sin\theta(t) \qquad 3.2$$

where τ_{musc} is the muscle torque, L_{limb} is the average length of the forelimb and hindlimb, and M is the total mass of the animal. As in the swing task, I applied the control torque in a bang-bang profile. In this scenario, inertial delay represents the minimum movement time possible, and is limited only by maximal torque.

3.2.5. Posture task: scaling of model parameters

Table 3.2 summarizes the scaling relationships I used for the posture task parameters. I set the length of the inverted pendulum as the average length of the hindlimb and forelimb from Kilbourne and Hoffman, because I wanted the pendulum mass to represent the whole-body center of mass of the animal (Kilbourne and Hoffman, 2013). In contrast, I set the swing task pendulum length to the length of the forelimb. If I had used the length of the forelimb for the posture task inverted pendulum, my values would increase by 8% or less. I used scaling equations for ankle extensor muscle mass, muscle length, and moment arm from Alexander et al. and computed muscle torque using the steps described in section 3.2.2 (Alexander et al., 1981). I assumed that the posture of the animal is

controlled by the ankle extensor muscle groups on the four legs by setting τ_{musc} to be four times the torque applied by one set of ankle extensor muscles.

Table 3.2 Posture task input scaling parameters and their confidence intervals.

Parameter	Coefficient (*a*)			Exponent (*b*)		
	Value	95% CI		Value	95% CI	
Limb lengths (Kilbourne and Hoffman, 2013)						
Forelimb length (m)	1.61×10^{-1}	1.42×10^{-1}	1.82×10^{-1}	0.38	0.34	0.42
Hindlimb length (m)	1.63×10^{-1}	1.47×10^{-1}	1.80×10^{-1}	0.36	0.32	0.39
Ankle extensor muscle properties (Alexander et al., 1981)						
Mass (kg)	5.10×10^{-3}	4.40×10^{-3}	5.92×10^{-3}	0.97	0.92	1.02
Muscle length (m)	1.06×10^{-2}	8.98×10^{-3}	1.25×10^{-2}	0.14	0.06	0.22
Moment arm (m)	9.40×10^{-3}	8.79×10^{-3}	1.01×10^{-2}	0.38	0.35	0.41

3.2.6. Posture task: simulations

I performed simulations of the posture task for seven animal masses logarithmically spaced from one gram to ten tons. For each animal mass, I used the scaling relationships from section 3.2.5 to determine the size-specific parameters. At each animal size, I scaled the perturbation size based on dimensionless velocity (Eqn 2.27) to evoke a proportional response from each animal size. The inverted pendulum can reject the perturbation and return to rest at the vertical position only up to a certain limit—if the initial clockwise velocity is too large, the counterclockwise torque cannot prevent the inverted pendulum from falling to the ground. The largest perturbation that a 10,000 kg animal could reject and return to vertical was 0.49 dimensionless velocity, so I varied the initial perturbation from 0.01 to 0.49 dimensionless velocity. As with the swing task, I numerically simulated the motion in MATLAB. I used optimization to determine when to switch between the maximum counterclockwise and clockwise torques such that the pendulum reached the original upright posture at the same instant that the velocity went to zero. For each perturbation magnitude and animal size, I seeded the optimization with an initial guess of the optimal timing and then used the Trust-region dogleg optimization algorithm

(implemented using MATLAB's fsolve function) (Powell, 1968). It used repeated model simulations to search for the optimal time to switch torque direction. Fig 3.2b illustrates a representative optimal solution. Elapsed simulation time was the inertial delay for each animal size and perturbation magnitude. Similar to the swing task, I repeated the simulations and optimizations for a range of animal masses and used least squares linear regression to extract the coefficient and exponent for the scaling of inertial delay. I then used Monte Carlo simulations to estimate the 95% confidence intervals.

3.2.7. Monte Carlo simulations

I used Monte Carlo simulations to determine the confidence intervals of my inertial delay results, based on the confidence intervals of the input parameters (Buckland, 1984; Preacher and Selig, 2012). I have described the parameters and their confidence intervals for the swing task in Eqn 3.1 and Table 3.1, and for the posture task in Eqn 3.2 and Table 3.2.

Creating probability distributions

Kilbourne and Hoffman had reported the 95% confidence intervals for the exponents of the power laws in their paper, but did not do so for the coefficients (Kilbourne and Hoffman, 2013). Therefore, I processed the raw data provided in the supplementary material to extract this information. I obtained probability distributions for the limb inertial properties using MATLAB's "fitlm" function, which uses a QR decomposition algorithm to compute a linear regression model to the log transformed raw data. Since Alexander et al. had 33 specimens in their study to determine muscle properties, I used the reported mean and 95% confidence intervals to create t-distributions (31 d.o.f.) for each muscle property (Alexander et al., 1981).

Implementing simulations

I then sampled one value for each of the input parameters from their respective probability distributions and numerically simulated the models to obtain one value for inertial delay. For the limb inertial properties, I used MATLAB's "random" function to randomly sample from the linear regression model produced by the "fitlm" function, which

assumes a normal distribution of data. For the input muscle properties, I used MATLAB's "trnd" function to randomly sample from the t-distribution. I ran 10,000 simulations in this way, obtaining a distribution of coefficients and exponents. My final 95% confidence intervals are 1.96 times the standard deviations of these distributions.

3.3. Results

3.3.1. Swing task results

My numerical simulations determined that inertial delay scales with an average of $M^{0.28}$ for the swing task, across movement magnitudes (Fig 3.1c). This scaling exponent falls between my two analytical predictions, which assume that muscle force scales either with dynamic similarity $M^{1/6}$ (Eqn 2.11) or with geometric similarity $M^{1/3}$ (Eqn 2.13). The coefficient of inertial delay in my numerical simulations increased with the square root of movement size (Fig 3.1c top), as predicted by my analytical analysis (Eqn 2.11). As movement size increased from 1 degree to 60 degrees, the coefficient increased from 5.8 ms (4.0–7.5 ms) to 43 ms (30–57 ms), while the exponent remained fairly steady about 0.28 (0.22–0.34) (Fig 3.5). Here and elsewhere, I report my results as "mean (lower – upper 95% confidence intervals)".

I tested the sensitivity of my numerical results to the applied muscle torque. Varying the torque from half to four times its original value only increased the scaling exponent of inertial delay from $M^{0.276}$ to $M^{0.279}$. This indicates that my results for the scaling of inertial delay are robust to possible inaccuracies in my estimates for the torque produced by muscles that flex and extend the shoulder joint. I have provided a short description of these tests in section 3.3.5.

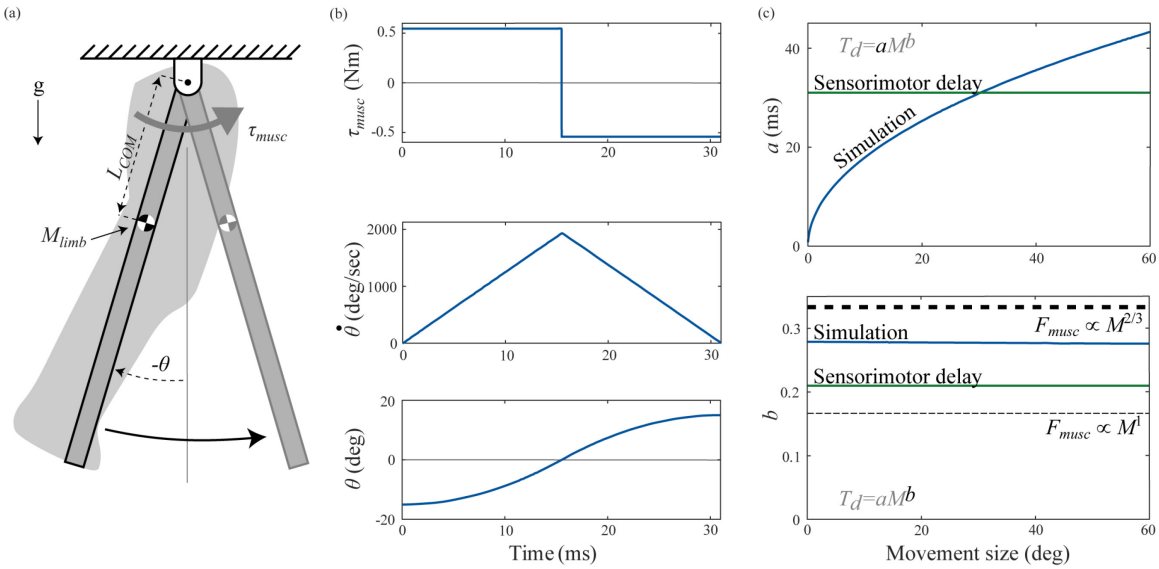

Fig 3.1 Swing task.
The model represents repositioning of the swing leg as part of the response to a trip. (a) I modeled the swing task as a distributed mass pendulum actuated by muscle torque τ_{musc}. My model incorporates the distance from the pendulum pivot to limb center of mass (L_{COM}), mass of the limb (M_{limb}), and moment of inertia of the forelimb about the shoulder joint (MOI). (b) Angle (θ), angular velocity ($\dot{\theta}$), and torque (τ_{musc}) profiles in the swing task for a one kg animal for a 30 degree movement, the movement magnitude for which inertial delay equals sensorimotor delay in a one kg animal. (c) Variation in coefficient a and exponent b of the power law for inertial delay from numerical simulations with movement magnitude (dark blue), sensorimotor delay (dark green), and theoretical predictions for the inertial delay exponent based on scaling of muscle force with cross-sectional area $\propto M^{2/3}$ (thick dashed line) and dynamic similarity $\propto M^1$ (thin dashed line).

3.3.2. Posture task results

My numerical simulations determined that inertial delay scaled with an average of $M^{0.35}$ for the posture task, across perturbation magnitudes (Fig 3.2c). The exponent again fell between those of the analytical predictions assuming muscle force scaling based on dynamic similarity ($M^{1/6}$; Eqn 2.28) and on geometric similarity ($M^{1/2}$; Eqn 2.30). Varying the perturbation size from 0.01 to 0.49 dimensionless velocity caused the coefficient to increase nearly linearly from 1.5 ms (1.1–1.9 ms) to 81 ms (53–102 ms), while the exponent again remained fairly steady about 0.35 (0.24–0.46) (Fig 3.5). This linear dependence on perturbation size was captured by my simple model of this task (Eqn 2.25).

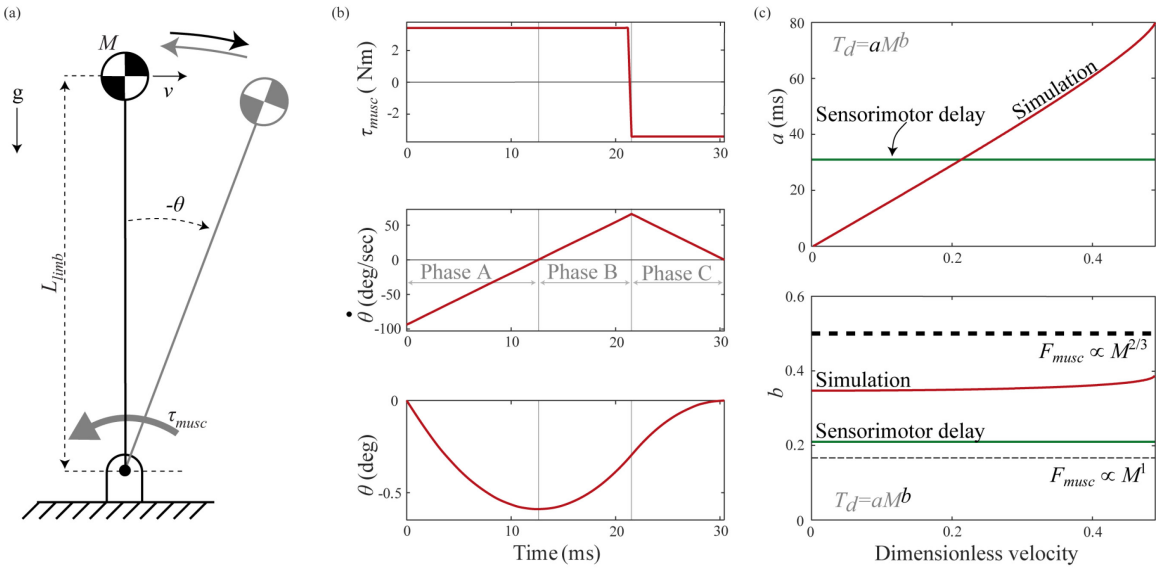

Fig 3.2 Posture task.
The model represents an animal recovering its posture after a balance perturbation. (a) I use an inverted pendulum with a point-mass body and massless rigid legs, pivoting about a ground-mounted pin joint. My model considers limb length (L_{limb}), mass of animal (M), and actuating muscle torque (τ_{musc}). (b) Angle (θ), angular velocity ($\dot{\theta}$), and torque (τ_{musc}) profiles in the posture task for a one kg animal for movement of 0.21 dimensionless velocity, the perturbation size for which inertial delay equals sensorimotor delay in a one kg animal. (c) Variation in coefficient a and exponent b of the power law for inertial delay determined from numerical simulations with perturbation size (red), sensorimotor delay (dark green), and theoretical predictions for the inertial delay exponent based on scaling of muscle force with cross-sectional area $\propto M^{2/3}$ (thick dashed line) and dynamic similarity $\propto M^1$ (thin dashed line).

3.3.3. Inertial delays, sensorimotor delays and response time

In both the swing and posture task, inertial delay increases more steeply with animal size than sensorimotor delay. Previous research in my lab has studied sensorimotor delay in terrestrial mammals of varying sizes and found that it scales with $M^{0.21}$ (More and Donelan, 2018). Here I found that swing and posture task inertial delays scaled with an average of $M^{0.28}$ and $M^{0.35}$ across perturbation magnitudes, respectively. This does not necessitate that inertial delays always exceed sensorimotor delay because inertial delays also depend on the movement magnitude—for very small position changes and velocity perturbations, inertial delays are far shorter than sensorimotor delay at all animal sizes. But as movement magnitudes increase, there reaches a magnitude at which inertial delay first matches, and then exceeds sensorimotor delay. This occurs at smaller movement magnitudes in larger animals (Fig 3.3). For the swing task, inertial delay exceeded sensorimotor delay when the limb swung through angles greater than $30M^{-0.14}$ degrees,

corresponding to 63 degrees in a five gram shrew and only 9 degrees in a five ton elephant. Shrews experience these limb angles only while galloping, but elephants experience them at slower speeds (McMahon, 1975). For the posture task, inertial delay exceeded sensorimotor delay for velocity perturbations greater than $0.21M^{-0.14}$ dimensionless velocity, corresponding to 0.44 in a five gram shrew and only 0.06 in a five ton elephant. For a shrew, this perturbation magnitude is equivalent to its walk-trot transition speed, but for an elephant it is equivalent to a much slower speed (Alexander and Jayes, 1983). Because day-to-day activities generally involve smaller movements and less extreme perturbations, in most situations sensorimotor delay likely dominates response time for smaller animals while inertial delays dominate for larger animals (Fig 3.4).

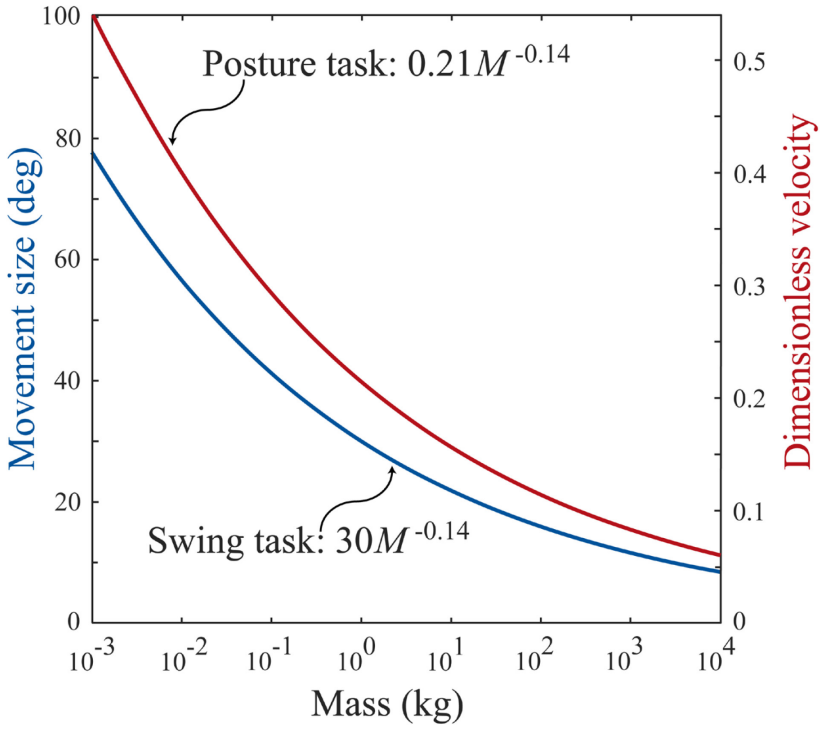

Fig 3.3 Scaling of movements for which inertial delay equaled sensorimotor delay.
The blue line represents the swing task values, with Y axis shown on the left. The red line represents the posture task values, with Y axis shown on the right.

The dependence of both sensorimotor and inertial delays on animal size results in relatively long response times in larger animals. I estimated response time as the sum of sensorimotor delay and inertial delay. If this response time equals or exceeds the available movement duration, an animal cannot complete the task within the available time. Here, I

used swing duration at maximum sprint speed, which scaled as $148M^{0.13}$ ms, as the available movement time for fast locomotion (More and Donelan, 2018). I calculated relative response time as the response time normalized by the available time—it scaled as $0.42M^{0.08}$. Inertial delay depends on movement magnitude, and here I assumed a 30° swing movement because at this magnitude, inertial delay matches sensorimotor delay in a one kg animal. The fraction of swing duration taken up by sensorimotor delay doubled over seven orders of magnitude of animal mass, while that of inertial delay increased almost six-fold (Fig 3.4). At maximum running speed, response time required only about 30% of swing duration for a five gram shrew but about 80% for a five ton elephant. For larger perturbations, response time could exceed available time in the largest animals. These relatively slower response times in larger animals, may hinder their effective control of movement. While I considered sensorimotor delays and inertial delays separately in this chapter, I studied how these delays combine together under feedforward and feedback control in chapter 5, and revisited relative response time (Fig 5.4 and 5.6).

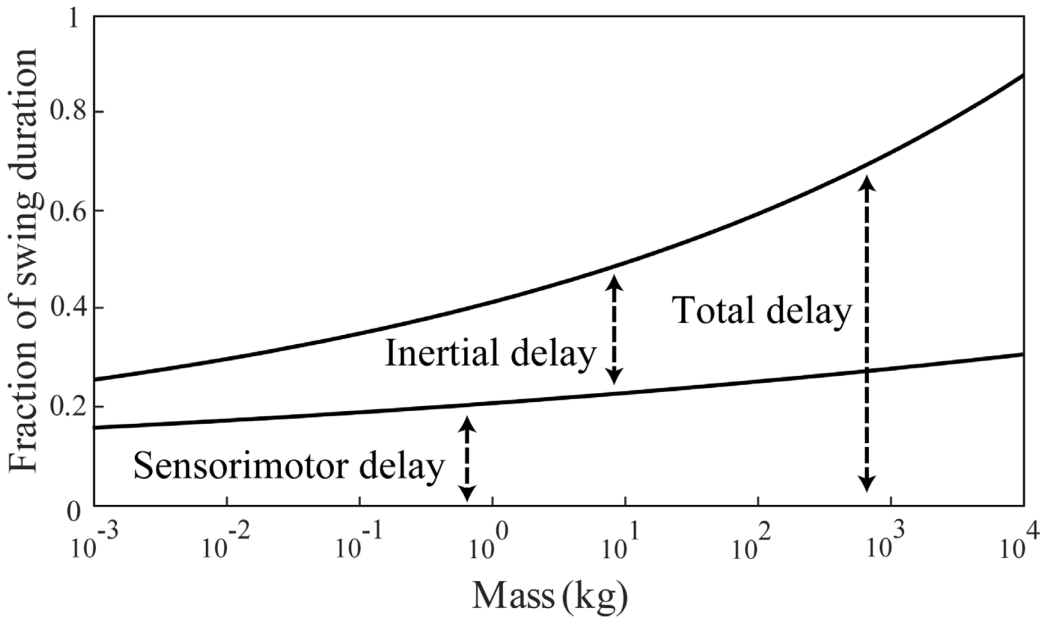

Fig 3.4 Relative response time.
Inertial delay and sensorimotor delay expressed as fractions of swing duration at maximum sprint speed. Inertial delay is shown for a movement of 30 degrees in swing task. At this movement size, inertial delay matches sensorimotor delay in a one kg animal.

3.3.4. Confidence intervals for the scaling of inertial delay

Using Monte Carlo simulations, I propagated the uncertainty in the input scaling values for the limb inertial properties and muscle properties through to my estimates for the scaling of inertial delay. The confidence intervals for the coefficients grew with movement size, while it remained constant for the exponents (Fig 3.5). The swing task exponent had a mean value of 0.28 and the 95% confidence intervals ranged from 0.22 to 0.34. The posture task exponent had a mean value of 0.35 and the confidence intervals ranged from 0.24 to 0.46. As the mean of the swing task exponent fell within the posture task exponent's confidence intervals, the two perturbations tasks are not statistically different.

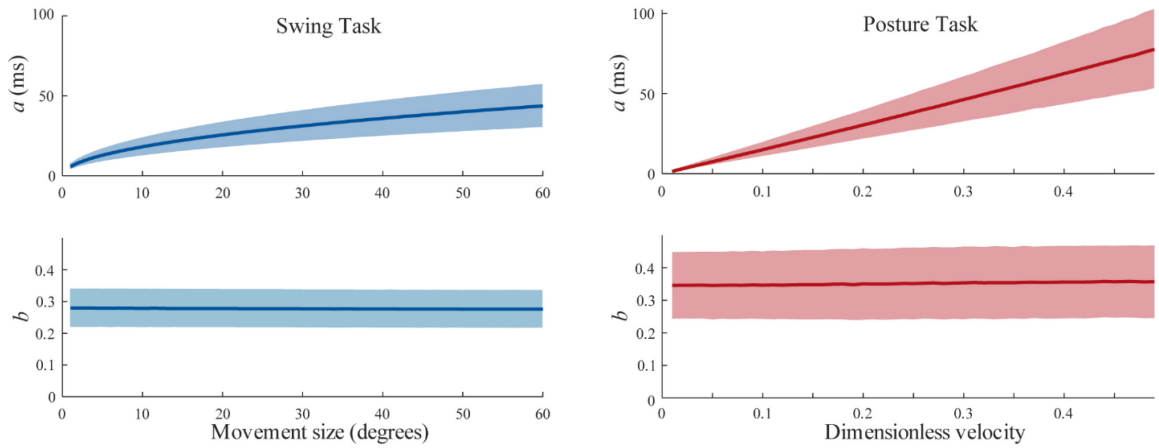

Fig 3.5 95% confidence intervals for the coefficient and exponent of inertial delay.
The shaded region represents the 95% confidence interval for the swing task on the left and the posture task on the right. Values for the coefficient (a) of the power law are shown on top, and for the exponent (b) are shown on the bottom graphs.

3.3.5. Effect of changing muscle torque on inertial delay scaling

Due to sparse information on the scaling of muscles involved in swinging the limb or correcting posture, and widely varying estimates for the isometric force production capacity of mammalian muscle, I am limited in the accuracy of my estimates for muscle torque. Therefore, I tested the sensitivity of my numerical results to the applied muscle torque.

Swing Task

I varied the applied torque from zero to four times the original value, for a 30 degree movement in the swing task. The period of an unactuated forelimb scaled as $281M^{0.19}$ ms. Inertial delay when using half the original muscle torque value scaled as $43.3M^{0.276}$ ms, while at four times the original scaled as $15.6M^{0.279}$ ms (Fig 3.6).

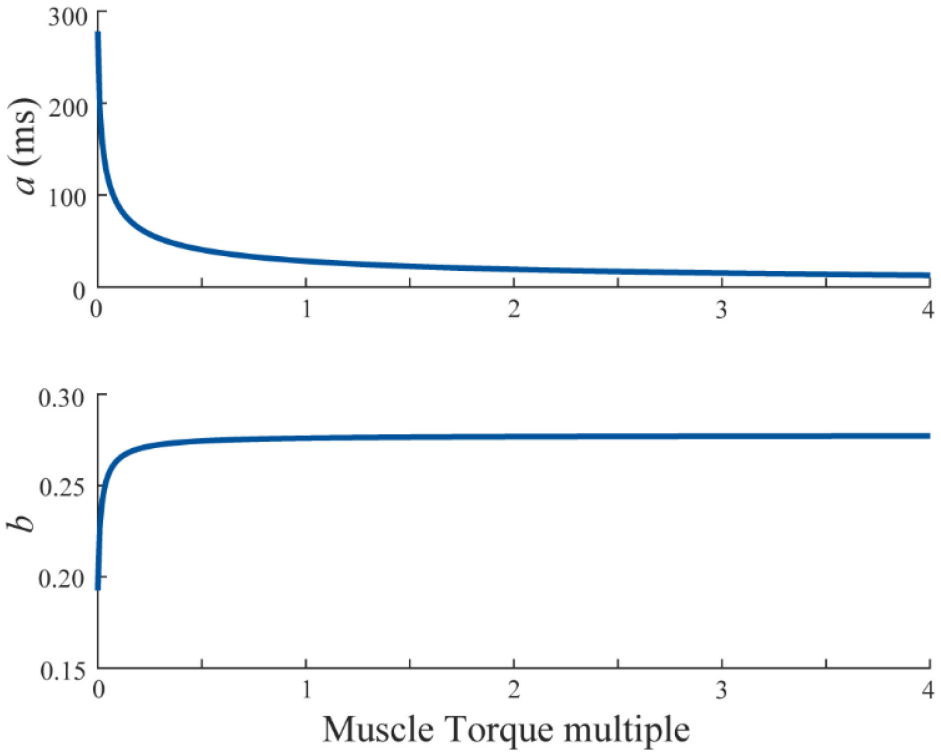

Fig 3.6 Effect of muscle torque on the scaling of inertial delay for the swing task.
I varied muscle torque from 0 to 4 times the initial estimate. I show the coefficient and exponent of the power law for a 30 degree movement in the swing task. A value of 0 for muscle torque represents an unactuated pendulum. The exponent levels off at a value of 0.28, while the coefficient decreases with inverse proportionality to the square root of muscle torque.

Posture Task

I varied the applied torque from 0.5 to four times the original value, for a perturbation of 0.21 dimensionless velocity for the posture task. If no torque is applied, the inverted pendulum would fall to the floor. Therefore, the lower limit of the range of torques tested was set to 0.5 times the original value. Inertial delay when using half the original muscle torque value scaled as $64.6M^{0.363}$ ms, while at four times the original scaled as $7.6M^{0.346}$ ms (Fig 3.7).

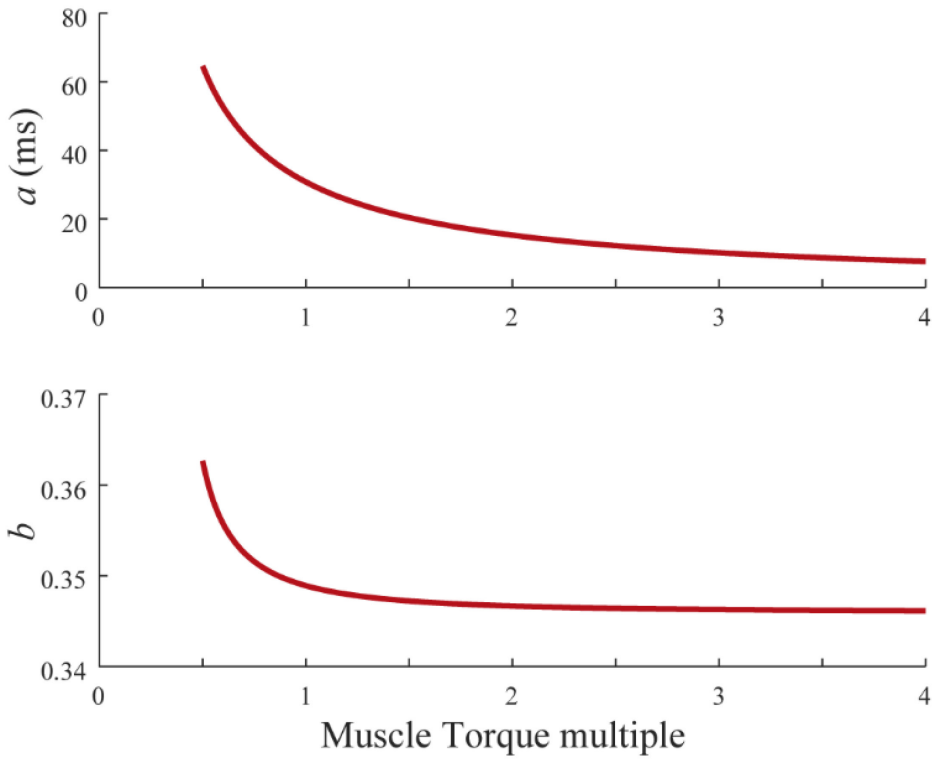

Fig 3.7 Effect of muscle torque on the scaling of inertial delay for the posture task.
I varied the muscle torque from 0.5 to 4 times the initial estimate. I show the coefficient and exponent of the power law for a perturbation of 0.21 dimensionless velocity for the posture task. The exponent levels off at a value of 0.346, while the coefficient decreases with inverse proportionality to muscle torque.

3.4. Discussion

Here I studied how inertial delays scale with animal size in terrestrial quadrupedal mammals. Inertial delay is the component of response time associated with overcoming inertia to move body segments or reject a perturbation. I quantified it by modeling two scenarios commonly encountered during animal locomotion—a swing task and a posture task. The scaling of inertial delays depended on both the movement task and movement magnitude. Over the perturbation magnitudes that I considered, inertial delays scaled with an average of $M^{0.28}$ for the swing task and $M^{0.35}$ for the posture task, which are both steeper than sensorimotor delays at $M^{0.21}$ (More and Donelan, 2018). In chapter 2, I had used analytical derivations to show theoretically that if animal muscles could produce forces proportional to an animal's mass, as required for dynamic similarity, inertial delays would scale at the same rate as characteristic movement times and relative delay would be independent of animal size. However, if muscles only produce forces proportional to their

cross-sectional area, which scales with $M^{2/3}$ under geometric similarity, relative delay will increase with animal size and disproportionately burden larger animals. My numerical predictions for the scaling exponent fell between these theoretical predictions—indicating that muscle forces that scale more steeply than with cross-sectional area, and moment arms that scale more steeply than assumed by geometric similarity, partly, but not completely, overcome the increases in inertia with animal size.

Previous work has suggested that animals may be more acutely challenged by long sensorimotor delays than by inertial delays (Kilbourne and Hoffman, 2013). My comparison of these two contributors to response time indicates that this is certainly true in all animals when the movement magnitude is small. But for larger movement magnitudes, including magnitudes encountered during day-to-day movements, inertial delay is greater than sensorimotor delay in larger animals (Fig 3.3). But sensorimotor delays appear to always be important—response time is never entirely dominated by inertial delay (Fig 3.4). Whether sensorimotor or inertial delays are more challenging to motor control depends on both the movement magnitude and the animal size.

This study had several important limitations. First, the lack of literature on scaling of muscle properties constrained the accuracy of our estimates for scaling of muscle torque. To my knowledge, only one study reports the scaling of muscle features necessary for determining torques acting about the shoulder and ankle joints in quadrupedal mammals (Alexander et al., 1981). Second, due to the lack of data for other muscles, I assumed that the triceps and the ankle extensors are the dominant muscles involved in moving their respective joints and that their antagonistic muscles scale similarly. Thirdly, I assumed that the isometric stress produced by mammalian muscle is constant at 20 N/cm^2 (Rospars and Meyer-Vernet, 2016), although actual isometric stress values for mammalian muscle vary from 7 to 148 N/cm^2 (Buchanan, 1995; Medler, 2002; Rajagopal et al., 2016). I tested the sensitivity of my results to muscle torque and found little effect on the exponent of the power law for both tasks (Section 3.3.5). Finally, my models are greatly simplified versions of the rather complex multi-jointed, multi-muscled animal. For example, they do not consider size specific features such as crouch vs. columnar posture (Biewener, 1989a) and high vs. low joint damping (Garcia et al., 2000). A more complete model of different sized

animals, like might be possible with OpenSim or a similar approach, may provide more realistic estimates of inertial delay (Delp et al., 2007). However, I don't expect that more complete musculoskeletal models would greatly change the identified scaling exponents which were robust to the major simplifications of the analytical models of chapter 2 when compared to the nonlinear simulations in this chapter.

My estimate of response time as the sum of sensorimotor delay and inertial delay makes several simplifications. Firstly, I assumed that muscles can switch between maximal forces instantaneously. However, actual muscles have properties that limit their rate of force production, such as activation-deactivation dynamics and force-velocity properties (Close, 1972; Loeb et al., 1987; Mörl et al., 2012; Rios et al., 1992; Zajac, 1989). Secondly, I assumed that electromechanical delay, force generation delay and inertial delay are distinct. However, these component delays are dynamic processes that overlap (More and Donelan, 2018; Mörl et al., 2012). Thirdly, I have assumed that sensing delay is independent of animal size. I based this assumption on More and Donelan who had previously studied the scaling of sensing delay, but due to scarcity of data, assumed it to be constant at 0.6 ms across animal size (More and Donelan, 2018). Some sensors, such as muscle spindles, are sensitive to length and length changes (Matthews, 1964). For these sensors, greater inertia may result in longer sensing delays. This is because the same perturbing force will result in slower body accelerations, lower velocities, and smaller length changes of the sensors when inertia is greater. While I have not accounted for this contribution of inertia to sensing delay in my current modeling work, I suspect it is not a major factor—doubling or tripling the nominal sensing delay results in a sensing delay that is still short relative to other contributors. Finally, physiological control rarely works in a purely feedforward fashion without sensory feedback. Feedback control is more resilient to unexpected perturbations and to the inherent noise and delays in biological control systems (Kuo, 2002; Todorov and Jordan, 2002). While superior in these regards, it would only slow the response time that I have estimated here—the optimal feedforward control profile operating at the limits to muscle torque yields a response time that is a lower bound on what is possible with feedback control. I suspect that these limitations make my present estimates of response time conservative, and that a refined model or an experimental

approach will find response times that exceed available movement times, particularly in large animals at fast speeds.

Given the importance of a short response time in controlling movement, how do animals cope with their relatively long sensorimotor and inertial delays? I suspect that animals benefit from several factors that mitigate the need for rapid response times. In smaller animals, these include the innate biomechanical properties of the musculoskeletal system to rapidly counteract perturbations. These stabilizing properties arise from the intrinsic properties of muscle (Brown and Loeb, 2000; Gerritsen et al., 1998), the increased role of joint damping at small sizes (Garcia et al., 2000; Hooper, 2012; Hooper et al., 2009), and the geometry of the legs (Biewener, 1989b). While larger animals have underdamped joints, the greater inertia of their body segments also mean that an animal can withstand larger external perturbations before being destabilized (Kilbourne and Hoffman, 2013). Animals may also benefit from neural prediction to help ameliorate the effects of long response time (Kuo, 2002; Milton, 2011; More and Donelan, 2018; Wolpert and Ghahramani, 2000). This may only be a useful strategy for comparatively larger animals, in which the synaptic delays associated with neural computation are short relative to movement durations (More and Donelan, 2018).

Chapter 4. Analysis of a normalized feedback control system with time delays and saturation limits

4.1. Introduction

Researchers have used techniques from control theory to gain insights into the functioning of biological systems (Cowan et al., 2014; Madhav and Cowan, 2020). We can also represent the neural control of movement as a control system (Fig 1.2). The controller represents the neural computational centers (supraspinal motor centers, central pattern generators and spinal synapses) that generate the motor commands (efferent action potentials), the actuator represents the muscles, and the plant represents the body segments being moved. The various sensory modalities (visual, vestibular, cutaneous, proprioceptive) sense the behavior of the plant and transmit that information back to the controller. The signal pathways represent the nerves that transmit information between the sensors, controller and plant. This biological control system also faces some of the drawbacks seen in synthetic control systems, such as noise and delays in signals, and dead zones and saturation limits in the actuator. We can parametrize this control system model to represent animal locomotion, and develop and test hypotheses to probe how animals control movement. In chapters 2 and 3, I had quantified the scaling of inertial delays (the time required to reposition body segments as part of the perturbation response) under bang-bang control, but did not consider time delays within the control pathways. In chapter 4 and 5, I have incorporated time delays into the control pathways, and limit the torques applied to the plant based on muscle force capacity limits, to understand how these limitations together affect the control of perturbation responses.

The neuromusculoskeletal system has physiological limitations which may constrain its performance. These physiological limitations include the magnitude of forces that muscles can generate, and the speed at which nerves can conduct action potentials (Close, 1972; More et al., 2010). In synthetic systems, time delays and actuator saturation are two well studied limitations of both feedforward and feedback control. Actuator saturation can represent the limited force generation capacity of muscles, while time delays can represent the sensorimotor delays in the nervous system. Actuator saturation reduces

responsiveness because the speed at which a physical system can be repositioned depends on how quickly the system can be accelerated; this depends on the force capacity of its actuators. In the absence of time delays, feedforward and feedback controllers limited by actuator saturation can behave similarly. A theoretical feedforward controller "knows" the saturation limits and generates motor commands that utilize the maximum available forces to produce fast responses (bang-bang control) (Rao and Bernstein, 2001), and a theoretical feedback controller could use very high gains that saturate the actuator and produce fast responses (Libby et al., 2016). But time delays do not equally affect feedforward and feedback systems. While time delays result in slower responses in both feedforward and feedback systems, feedback systems have an additional vulnerability. When feedback control signals are outdated, the motor commands generated are inaccurate, resulting in poor control and reduced stability (Madhav and Cowan, 2020; Milton, 2011). If the delays grow too large, the feedback signal will actively destabilize the system instead of controlling it. In order to remain stable, the feedback controller has to use lower gains which result in lower forces and slower responses. Several studies have explored the effects of these limitations on engineering control systems and proposed methods to deal with them (Goldfarb and Sirithanapipat, 1999; Insperger, 2006; Skogestad, 2001).

My objective is to characterize how time delays and actuator saturation affect the behavior of a feedback control system that represents the neural control of movement in animals, and to quantify how fast the control system can respond given the limitations. First, I have revisited a textbook example from linear control systems theory on Bode analysis and stability margins. I have then proposed a normalized feedback control system under proportional-derivative (PD) control with both time delays and saturation limits. I tested the performance of this system in two tasks as I have done in the previous chapters on inertial delays. In the swing task, the controller has to reposition the plant from rest at the origin, to rest at a new position. In the posture task, the plant has an initial velocity perturbation that needs to be rejected, and the controller must return the plant to rest at the origin. I determined the optimal controller gains that produced the fastest response times, and then characterized how response times change when saturation limits are varied.

4.2. Methods

To understand how time delays and actuator saturation affects feedback control, I developed both linear and nonlinear control system models. First, I used Bode plots to show how time delays cap the controller gains that can be used in a stable linear feedback control system (Section 4.3.1). I performed the derivations both by hand and by using MATLAB's symbolic toolbox (MATLAB R2020a, The MathWorks, Inc., Natick, MA, USA).

I then proposed a normalized feedback control system with both time delays and actuator saturation and used numerical simulations to analyze its behavior. I performed the derivations to normalize the equations for this section by hand (Section 4.3.2). I simulated the normalized feedback control system using MATLAB's Simulink toolbox, and used the ode45 (Runge-Kutta algorithm) variable time step solver with a relative tolerance of 10^{-6} and an absolute tolerance of 10^{-9} (Section 4.3.3). I modeled the plant as a double integrator— it represents single degree of freedom rotational systems which have two states—angle $\theta(t)$ and angular velocity $\dot{\theta}(t)$ (Rao and Bernstein, 2001). I modeled the controller as a proportional-derivative (PD) type controller. I optimized the controller gains using MATLAB optimization functions, fminsearch (simplex algorithm) and fmincon (interior-point algorithm).

I evaluated the performance of the system for two perturbation response tasks: a swing leg reposition task (swing task), and a posture correction task (posture task), similarly to the previous chapters on inertial delays. For the swing task, I set the initial conditions for plant states $[\theta_0, \dot{\theta}_0]$ to [0, 0], and the target state to [1, 0]. I calculated both settling time and overshoot on the angle vs. time curve. For the posture task, I set the initial conditions to [1, -1] and the target state to [1, 0]. I calculated settling time on the angular velocity curve and the overshoot on the angle curve. I used 2% settling time thresholds to calculate settling time. I defined response time as the fastest settling time of the system without any overshoot, and optimized controller gains to search for this specific response.

I varied the actuator saturation limits to understand how saturation limits affect response time in the normalized feedback control system, while keeping time delay fixed.

I used curve fitting to obtain an equation to describe the relationship between response time and saturation limits. I tested out various curves available in the MATLAB fit library such as first, second and third order polynomials, power laws, and single and double exponentials—and reported the equations that provided the least root mean square error (RMSE).

In section 4.3.4, I evaluated whether placing time delays in the feedforward pathway or the feedback pathway changes system behavior, and I derived these equations by hand.

4.3. Results

4.3.1. Linear feedback control system and Bode plots

I used Bode plots to understand how time delays affect a linear feedback control system. Bode plots are tools from linear control systems theory that reveal the stability margins of a feedback control system, which determine the viable range of parameters that one can use while ensuring that the system remains stable. Fig 4.1a shows a block diagram of the linear feedback control system. It does not include time delays or actuator saturation nonlinearities. It represents a PD controlled double integrator, and the second-order differential equation of this system is:

$$I\ddot{\theta}(t) = \tau_{act}(t) = K_p[r(t) - \theta(t)] + K_d\left[\dot{r}(t) - \dot{\theta}(t)\right] \quad 4.1$$

where I is the moment of inertia of the plant, K_p and K_d are the controller gains, and $r(t)$ is the reference signal. $\ddot{\theta}, \dot{\theta}\ and\ \theta$ are the acceleration, angular velocity and angle of the plant, respectively. The controller produced torques τ_{act} to reduce the error between the reference signal and the current state, $e(t) = r(t) - \theta(t)$.

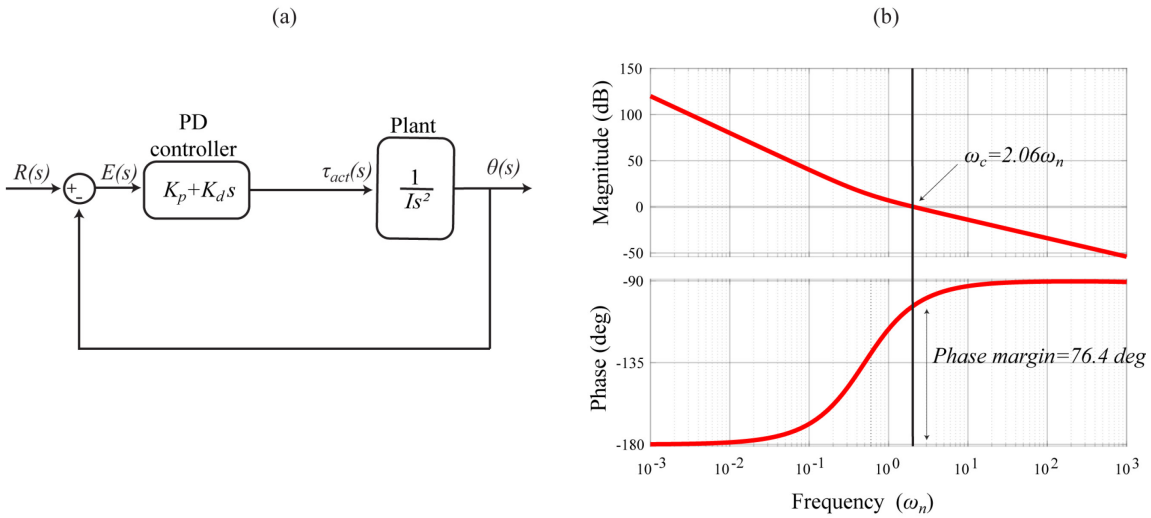

Fig 4.1 Linear feedback control system and Bode plot.
(a) The block diagram of the linear control system, where $R(s)$ is the reference signal, $E(s)$ is the error signal, $\theta(s)$ is the plant output (angle of the plant represented by the double integrator), $\tau_{act}(s)$ the actuating torque, and s indicates that these time-dependent variables are represented in the frequency domain. (b) Bode plot of the open loop transfer function (Eqn 4.2) with the gain crossover frequency (Eqn 4.5) and phase margin (Eqn 4.7) indicated on the plot.

I performed a Laplace transform on Eqn 4.1 to convert it from the time domain to the frequency domain, e.g. $r(t) \rightarrow R(s)$, in order to get a transfer function that maps the commanded angle $R(s)$ onto the plant output $\theta(s)$. The open loop transfer function of the control system is given by:

$$G(s) = \frac{K_p + K_d s}{Is^2} \tag{4.2}$$

The closed loop transfer function of the control system with unity feedback is given by:

$$H(s) = \frac{G(s)}{1 + G(s)} = \frac{K_p + K_d s}{Is^2 + K_d s + K_p} \tag{4.3}$$

The equation for this closed loop control system is equivalent to that for a mechanical mass-spring-damper system. Eqn 4.3 shows that the system has three free parameters $I, K_d \; and \; K_p$. I can derive two more parameters which describe the behavior of the system from these free parameters—the undamped natural frequency $\left(\omega_n = \sqrt{\frac{K_p}{I}}\right)$ and the damping ratio $\left(\zeta = \frac{K_d}{2\sqrt{K_p I}}\right)$ (Åström and Murray, 2008; Ruina and Pratap, 2015). In order

to reduce the free parameters that I have to choose, I assumed that the moment of inertia is constant, and that the system is critically damped by setting ζ to 1, $K_d = 2\sqrt{K_p\, I}$. Therefore, the only parameter that I vary in my control system is the proportional gain, K_p.

A Bode plot of the open loop transfer function provided the stability margins of the control system (Fig 4.1b). If the open loop transfer function $G(s)$ equals -1, the closed loop transfer function in Eqn 4.3 becomes ∞, signifying instability. This occurs when $G(s)$ has a magnitude of 0 dB and a phase of -180° for any input frequency in the Bode plot. In this condition, the feedback signal will actively amplify the error and destabilize the feedback control system, instead of attenuating the error and stabilizing it. The phase margin is the distance of the phase line (Fig 4.1b bottom) from -180°, at the frequency where the gain line (Fig 4.1b top) crosses the 0 dB line. While the feedback control system is presently linear, adding a time delay would make it nonlinear, and the time delay would cause a negative phase shift. The delay that will induce instability—called the delay margin—is the time delay that corresponds to the phase margin.

To determine how the delay margin depended on controller gains and plant inertia, I first found the gain crossover frequency by solving for the frequency at which the gain of the open loop transfer function equaled 1 (0 dB).

$$|G(s)| = \left|\frac{K_p + K_d(j\omega_c)}{I(j\omega_c)^2}\right| = 1 \qquad 4.4$$

Substituting in the value of K_d for critical damping and solving for ω_c gave:

$$\omega_c = \sqrt{\sqrt{5} + 2}\,\sqrt{\frac{K_p}{I}} = 2.06\,\omega_n \qquad 4.5$$

The phase margin is how far the phase of the open loop transfer function at the gain crossover frequency is from 180°:

$$\emptyset(G(s)) = \tan^{-1}\left(\frac{K_d\omega_c}{K_p}\right) - \tan^{-1}\left(\frac{0}{-I\,{\omega_c}^2}\right) = -1.81\,rad \qquad 4.6$$

Eqn 4.6 reduced to a constant value because substituting in Eqn 4.5 for ω_c and the critical damping equation for K_d caused all variable terms to cancel out.

$$Phase\ margin = \pi - 1.81 = 1.33\ rad \quad (76.4\ °) \tag{4.7}$$

I obtained the delay margin—the maximum allowable delay before the system becomes unstable— by dividing the phase margin by the gain crossover frequency:

$$Delay\ margin = \frac{1.33}{2.06\ \omega_n} = 0.647\sqrt{\frac{I}{K_p}} \tag{4.8}$$

Eqn 4.8 reveals that the maximum proportional gain $K_{p_{max}}$ that a control system with a given time delay t_d can use is:

$$K_{p_{max}} = 0.647^2 \frac{I}{{t_d}^2} \tag{4.9}$$

Thus, for a feedback control system with time delay to remain stable, it must limit its controller gains such that:

$$0 \le K_p \le 0.647^2 \frac{I}{{t_d}^2}, \quad K_d = 2 \times 0.647 \frac{I}{t_d}, \quad \omega_n = 0.647 \frac{1}{t_d} \tag{4.10}$$

Therefore, if a control system has time delays, it limits the viable range of controller gains that the system can use while ensuring stability. Eqn 4.10 also reveals proportionalities between the controller gains and system parameters, $K_p \propto \frac{I}{{t_d}^2}$, $K_d \propto \frac{I}{t_d}$, and $\omega_0 \propto \frac{1}{t_d}$. In the next section, I developed a normalized feedback control system and determined the optimal controller gains that produce the fastest response times within this limited range.

4.3.2. Normalized feedback control system with time delays and actuator saturation

I developed a normalized feedback control system (one model which can represent animals of all sizes), and studied how response times are affected by time delays and

actuator saturation limits (Fig 4.2). The equations of motion of the feedback control system before normalization are:

$$I\ddot{\theta}(t) = \tau_{act}(t) \tag{4.11}$$

$$\tau_{act} = sat(\tau_{des}) = \begin{cases} \tau_{iso} & if\ \tau_{des} > \tau_{iso} \\ \tau_{des} & if\ -\tau_{iso} \leq \tau_{des} \leq \tau_{iso} \\ -\tau_{iso} & if\ \tau_{des} < -\tau_{iso} \end{cases} \tag{4.12}$$

$$\tau_{des} = \begin{cases} 0 & if\ 0 < t < t_d \\ K_p[\theta_r - \theta(t - t_d)] + K_d\left[-\dot{\theta}(t - t_d)\right] & if\ t \geq t_d \end{cases} \tag{4.13}$$

where τ_{des} is the controller output subject to saturation limits τ_{iso}, and τ_{act} is the torque applied to plant. I did not consider actuator (muscle) dynamics in my models, and directly applied the controller output as torques to the plant. I also assumed that the controller gets full state information; I did not consider sensory dynamics. Due to time delays t_d, there is an initial deadtime at the start of the simulation where no torques were applied to the plant (Eqn 4.13). I only considered a constant reference target θ_r in my simulations.

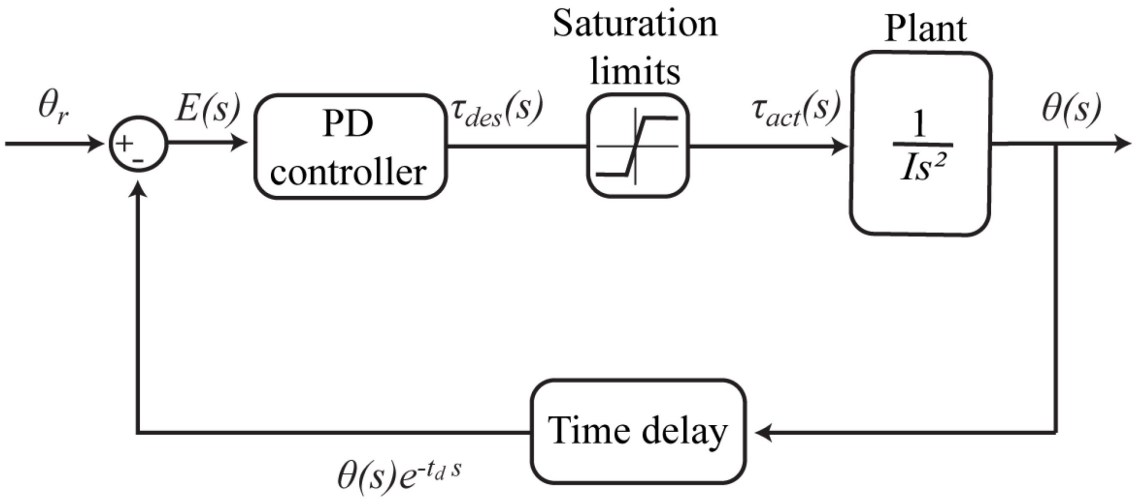

Fig 4.2 Block diagram of feedback control system with time delays and actuator saturation.
θ_r is the reference signal, $E(s)$ is the error signal, $\theta(s)$ is the plant output (angle of the pendulum represented by the double integrator), τ_{des} is the controller output torque, and τ_{act} the actuating torque which has been subjected to saturation limits. $\theta(s)e^{-t_d s}$ is the time delayed feedback signal.

I normalized Eqn 4.13 using three constants which also represent characteristic features of neural control of movement in animals:

- I is the moment of inertia of the double integrator plant, and also represents the moment of inertia of the body segment being moved under neural control by the animal.
- θ_r is the reference target for feedback control, and also represents the size of the movement being commanded under neural control in the swing task. For the posture task, the movement size is represented by the initial perturbation velocity $\dot{\theta}_0$.
- t_d is the time delay in feedback control system, and also represents the sensorimotor delays in the reflex pathways during neural control of movement.

The terms in Eqn 4.11 have dimensions of torque ($M^1L^2T^{-2}$), where M represents mass, L represents length and T represents time dimensions. Therefore, to derive the normalized model, I divided each term in Eqn 4.11 by $\frac{I\theta_r}{{t_d}^2}$.

$$\frac{I\ddot{\theta}}{\left(\frac{I\theta_r}{{t_d}^2}\right)} = \frac{\tau_{act}}{\left(\frac{I\theta_r}{{t_d}^2}\right)} = \frac{K_p[\theta_r - \theta(t-t_d)] + K_d\left[-\dot{\theta}(t-t_d)\right]}{\left(\frac{I\theta_r}{{t_d}^2}\right)} \qquad 4.14$$

$$\bar{\ddot{\theta}} = \bar{\tau}_{act} = \bar{K}_p\left[1 - \bar{\theta}(\bar{t}-1)\right] + \bar{K}_d\left[-\dot{\bar{\theta}}(\bar{t}-1)\right] \qquad 4.15$$

The normalized model is described by Eqn 4.15. Below, I describe how to normalize each of the parameters of the model.

$$\bar{t} = \frac{t}{t_d} \qquad \bar{t}_{resp} = \frac{t_{resp}}{t_d} \qquad 4.16$$

$$\bar{\theta} = \frac{\theta}{\theta_r} \qquad \dot{\bar{\theta}} = \frac{\dot{\theta}}{\left(\frac{\theta_r}{t_d}\right)} \qquad \bar{\ddot{\theta}} = \frac{\ddot{\theta}}{\left(\frac{\theta_r}{{t_d}^2}\right)} \qquad 4.17$$

$$\bar{\theta}_0 = \frac{\theta_0}{\theta_r} \qquad \dot{\bar{\theta}}_0 = \frac{\dot{\theta}_0}{\left(\frac{\theta_r}{t_d}\right)} \qquad 4.18$$

$$\overline{\tau} = \frac{\tau}{\left(\frac{I\theta_r}{{t_d}^2}\right)} \qquad \overline{\tau}_{iso} = \frac{\tau_{iso}}{\left(\frac{I\theta_r}{{t_d}^2}\right)} \tag{4.19}$$

$$\overline{K}_p = \frac{K_p}{\left(\frac{I}{{t_d}^2}\right)} \qquad \overline{K}_d = \frac{K_d}{\left(\frac{I}{t_d}\right)} \tag{4.20}$$

$\overline{t}_{resp}$ is the normalized response time of the model, which I determined using numerical simulations for the swing task and posture task in the next section.

4.3.3. Normalized feedback control system—numerical simulations

Using numerical simulations, I evaluated how changing the perturbation task, controller gains, time delays and actuator saturation limits affected the behavior of the normalized feedback control system. First, I did not set saturation limits and used a fixed time delay ($\overline{t}$=1), and performed a brute force search to determine how controller gains affect settling time and overshoot. Next, I kept time delays constant ($\overline{t}$=1), and varied the saturation limits to understand how this affects response times ($\overline{t}_{resp}$ vs $\overline{\tau}_{iso}$). For each saturation limit, I optimized the controller gains to find the fastest response time (fastest settling time with 2% thresholds and without any overshoot).

Swing task results

A brute force search through a range of controller gains revealed the settling time and overshoot landscapes for the swing task. I calculated both settling time and overshoot on the angle curve for the swing task (Fig 4.3a bottom panel). The settling time landscape is very rough and jagged with several local minima (Fig 4.3b). The overshoot landscape has a flat area with zero overshoot, followed by a region of rapid increase. (Fig 4.3c) The black dot depicts the fastest settling time achieved without constraining overshoot. The red dot corresponds with the fastest settling time without any overshoot; I considered these gains to determine response time. Without setting any saturation limits, controller gains of 0.1617 for $\overline{K}_p$ and 0.6343 for $\overline{K}_d$ produced the fastest normalized response time ($\overline{t}_{resp}$) of 7.09 in normalized time units (Fig 4.3a).

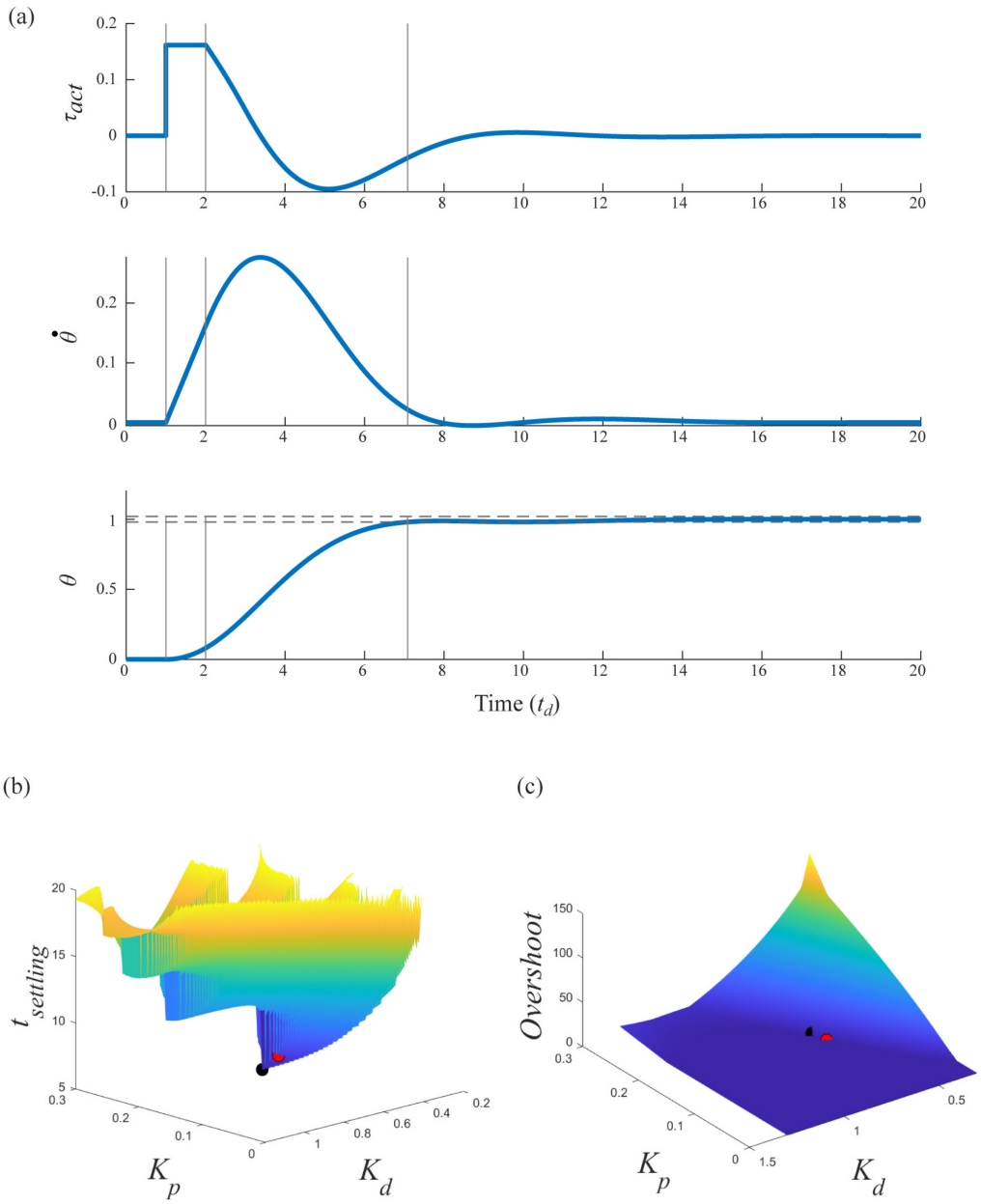

Fig 4.3 Normalized swing task—brute force search.

(a) Normalized torque ($\overline{\tau}_{act}$), angular velocity ($\dot{\overline{\theta}}$) and angle ($\overline{\theta}$) profiles in the swing task for the fastest response. The three black vertical lines depict one time delay period, two time delay periods and the settling time. The two black horizontal dashed lines on the angle graph depict the 2% settling time thresholds. (b & c) The settling time and overshoot landscapes for the normalized swing task model determined through a brute force search for a range of controller gains. The red dot depicts the fastest settling time when overshoot is not allowed. The black dot depicts the fastest settling time when overshoot is not constrained (This response had 1.76% overshoot).

Analysis of the relationship between saturation limits and response time revealed three distinct regions (Fig 4.4). The fastest response without considering saturation limits produced a peak torque of 0.1617, which equals $\overline{K}_p$. Fig 4.4 shows how settling time, overshoot and controller gains changed when I varied saturation limits from 0.3 to 0.001.

- High saturation limits region: For $\overline{\tau}_{iso}$> 0.1610, the peak torque did not reach the saturation limits, and the settling time and controller gains did not change.

- Middle region: For 0.079<$\overline{\tau}_{iso}$<0.1610, the saturation limits clipped the positive region of the torque curve, and settling time increased gradually with lower saturation limits. However, the optimal control gains still remained the same.

- Low region: 0.009<$\overline{\tau}_{iso}$<0.079, the saturation limits clipped both the positive and negative regions of the torque curve, and settling time increased exponentially with lower saturation limits. In this region, the controller gains also increased with lower saturation limits.

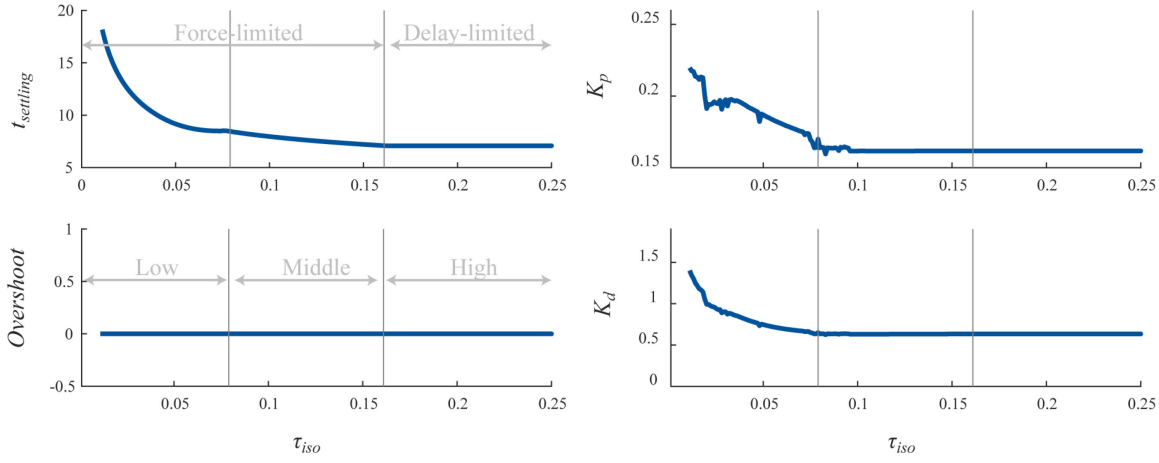

Fig 4.4 Normalized swing task—saturation limits vs. response time.
(a) Changes in settling time and overshoot when saturation limits are lowered from 0.2 to 0. There are three distinct regions in the settling time profile divided by the blue vertical lines. (b) Changes in the optimal controller gains that produce the fastest settling times without overshoot for a range of saturation limits.

I found that the double exponential function gave the best fit (lowest root mean square error) for the middle and low saturation limit regions in the swing task. The swing task $\overline{t}_{resp}$ vs. $\overline{\tau}_{iso}$ relationship can be described by the following function:

$$\overline{t}_{resp} = f(\overline{\tau}_{iso}) = \begin{cases} 7.09 & \overline{\tau}_{iso} \geq 0.162 \\ 5.56e^{-27.1\overline{\tau}_{iso}} + 8.64e^{-1.29\overline{\tau}_{iso}} & 0.079 \leq \overline{\tau}_{iso} < 0.161 \\ 18.33e^{-73.12\overline{\tau}_{iso}} + 10.12e^{-2.88\overline{\tau}_{iso}} & 0.009 \leq \overline{\tau}_{iso} < 0.078 \end{cases} \quad 4.21$$

This analysis showed that for feedback control systems with both time delays and actuator saturation, there are two ranges in the response time vs. saturation limits graph: a force-limited range and a delay-limited range. At the extremes, without saturation limits or delays, infinitely high gains can produce instant response times. If I reduced the saturation limits to 0, or if the time delays were infinitely long, I would have infinite response times. The delay-limited range matched the high saturation limits region ($\overline{\tau}_{iso}$ >0.1617), where the response time was limited purely by time delays. The force-limited range consisted of the middle and low saturation limits regions ($\overline{\tau}_{iso}$ <0.1617), where the saturation limits also begin to limit response time. Extrapolating to animals, this analysis indicates that for an animal to respond quickly, it requires both strong muscles and short sensorimotor delays. Deficiencies in either factor will slow the animal's ability to respond quickly. Whether an animal is delay-limited or force-limited would depend on the relative magnitudes of factors that affect the perturbation response, such as the moment of inertia of the body segment being moved, the sensorimotor delays, the size of the perturbation response movement, and the muscle force capacity.

Posture task results

For the normalized posture task model, I found that the brute force search results were similar to the swing task, while the relationship between response time and saturation limits had several differences. For the posture task, I calculated settling time on the angular velocity curve, and overshoot on the angle curve. I did this to ensure that the settling time thresholds scaled with perturbation size, while not changing with controller gains. The settling time landscape was again very rugged. The red dot in Fig 4.5b depicts the controller gains that produced the fastest settling time; this set of controller gains also caused no

overshoot. Without setting saturation limits, controller gains of 0.1560 for $\overline{K}_p$ and 0.6530 for $\overline{K}_d$ produced the fastest normalized response time ($\overline{t}_{resp}$) of 7.38 in normalized time units (Fig 4.5a).

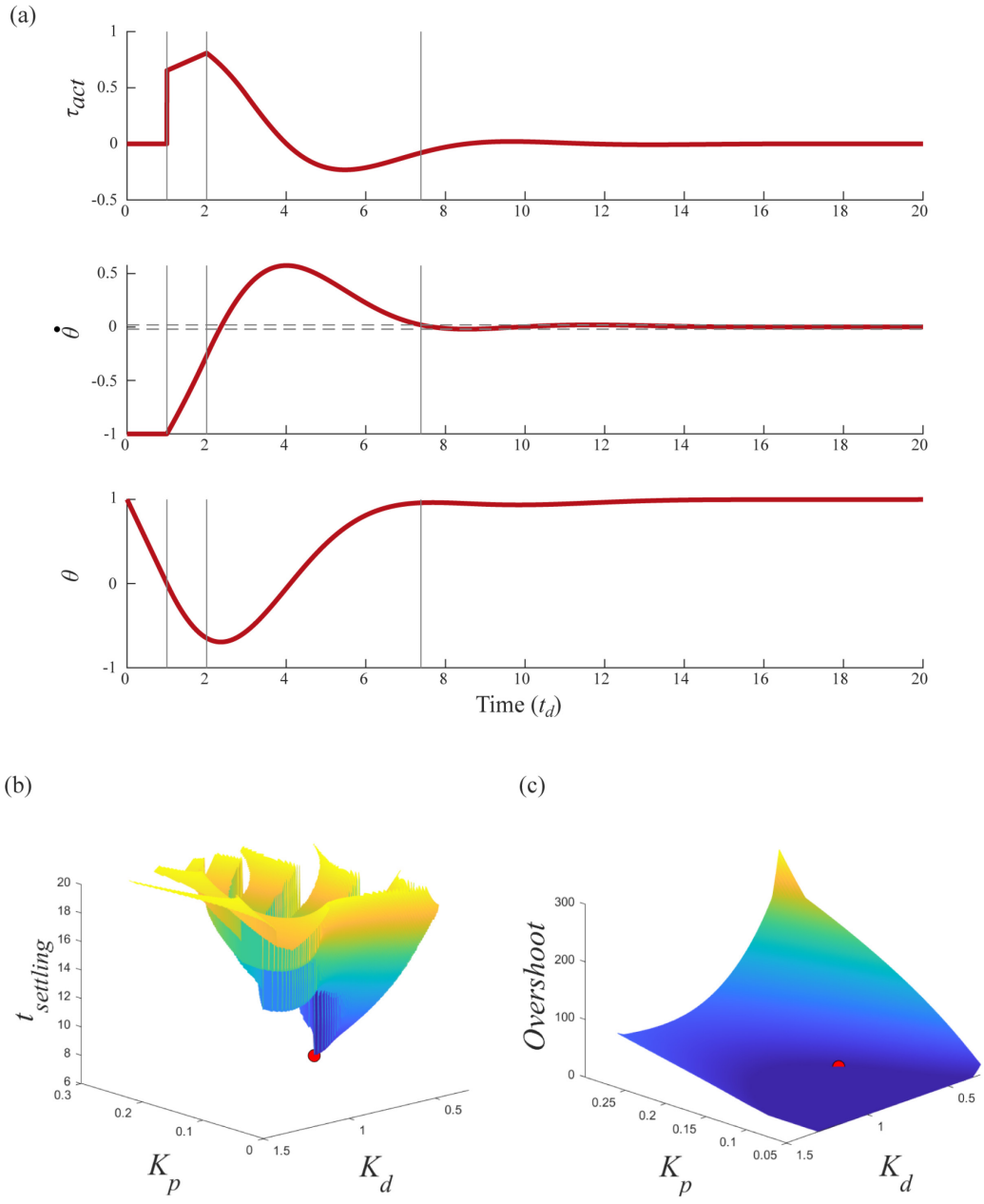

Fig 4.5 Normalized posture task—brute force search.

(a) Normalized torque ($\overline{\tau}_{act}$), angular velocity ($\dot{\overline{\theta}}$) and angle ($\overline{\theta}$) profiles in the posture task for the fastest response. The three black vertical lines depict one time delay period, two time delay periods and the settling time. The two black horizontal dashed lines on the angular velocity graph depict the 2% settling time thresholds. (b & c) The settling time and overshoot landscapes for the normalized posture task model determined through a brute force search for a range of controller gains. The red dot depicts the fastest settling time, and the value does not change if overshoot is allowed or constrained.

Analysis of the relationship between saturation limits and response time again revealed three distinct regions. The fastest response without considering saturation limits produced a peak torque of 0.80. Fig 4.6 shows how settling time, overshoot and controller gains changed when I varied saturation limits from 1.2 to 0.001.

- High saturation limits region: For $\overline{\tau}_{iso}$> 0.80, the peak torque $\overline{\tau}_{max}$ did not reach the saturation limits, and the settling time and controller gains did not change.

- Middle region: For 0.24<$\overline{\tau}_{iso}$<0.79, the saturation limits clipped the positive region of the torque curve, and settling time increased gradually with lower saturation limits. Unlike the swing task where the controller gains did not change in the middle region, the controller gains increased gradually with lower saturation limits.

- Low region: 0.009<$\overline{\tau}_{iso}$<0.24, the saturation limits clipped both the positive and negative regions of the torque curve. Unlike the swing task, the settling time continued to increase at the same rate as in the middle region. The controller gains initially show a shallow dip before increasing rapidly for lower saturation limits.

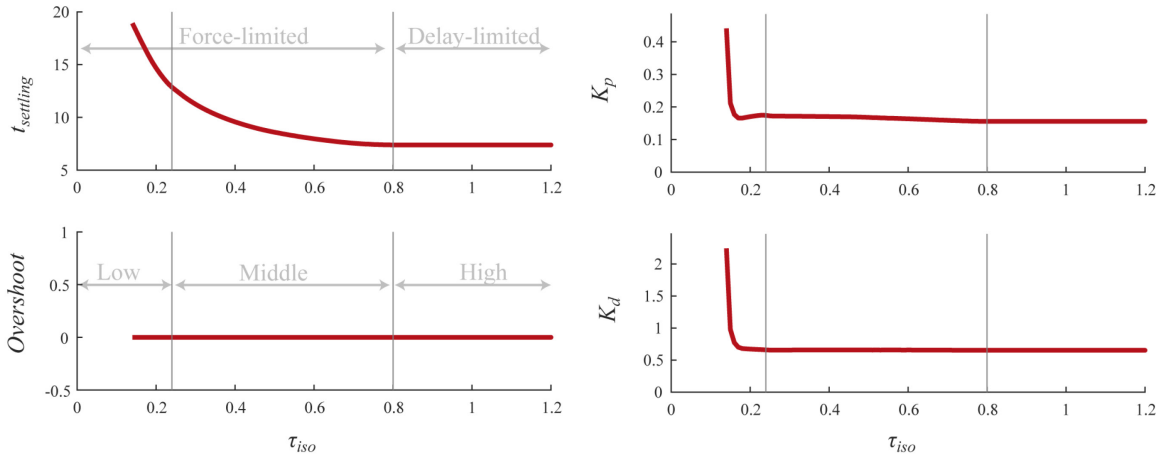

Fig 4.6 Normalized posture task—saturation limits vs. response time.
(a) Changes in settling time and overshoot when saturation limits are lowered from 1 to 0.1. There are three distinct regions in the settling time profile divided by the blue vertical lines. (b) Changes in the optimal controller gains that produce the fastest settling times without overshoot for a range of saturation limits.

I again tried fitting various functions to the settling time curve in the middle and lower regions. I found that a power law with intercept (power2) function produced the

lowest RMSE values. The posture task $\overline{t}_{resp}$ vs. $\overline{\tau}_{iso}$ relationship can be described by the following function:

$$\overline{t}_{resp} = f(\overline{\tau}_{iso}) = \begin{cases} 7.39 & \overline{\tau}_{iso} \geq 0.80 \\ 1.61\,\overline{\tau}_{iso}^{\,-1.10} + 5.17 & 0.14 \leq \overline{\tau}_{iso} < 0.80 \end{cases} \quad 4.22$$

For this analysis, I have studied the effect of saturation limits on response time and kept time delays constant. I could similarly evaluate the effect of varying time delays on response time, while keeping saturation limits constant. As I only consider constant sensorimotor time delays in my more biologically realistic simulations, while using different muscle parameters in the swing and posture task, I have only conducted the first analysis for this thesis.

4.3.4. Delays in the feedforward and feedback pathways

Reflex pathways suffer from several sensorimotor delays (t_{SMD}) which are distributed across them. Between the sensors (e.g. cutaneous receptors, muscle spindles) and the spinal synapse with the motor neuron, there are sensing delays, nerve conduction delays and synaptic delays. I refer to these delays together as sensory delays (t_{SD}). Between the spinal synapse and muscles, there are nerve conduction delays, neuromuscular junction delays, electromechanical delays and force generation delays. I refer to these delays together as motor delays (t_{MD}). In the feedback control model, I placed all the sensorimotor delays in the feedback pathways to simplify the analyses (Fig 4.2). I could instead have placed the motor delays in the feedforward pathway, and the sensory delays in the feedback pathway. Here, I briefly discuss how this assumption does not affect my estimates of response time, as it doesn't affect settling times for a step response.

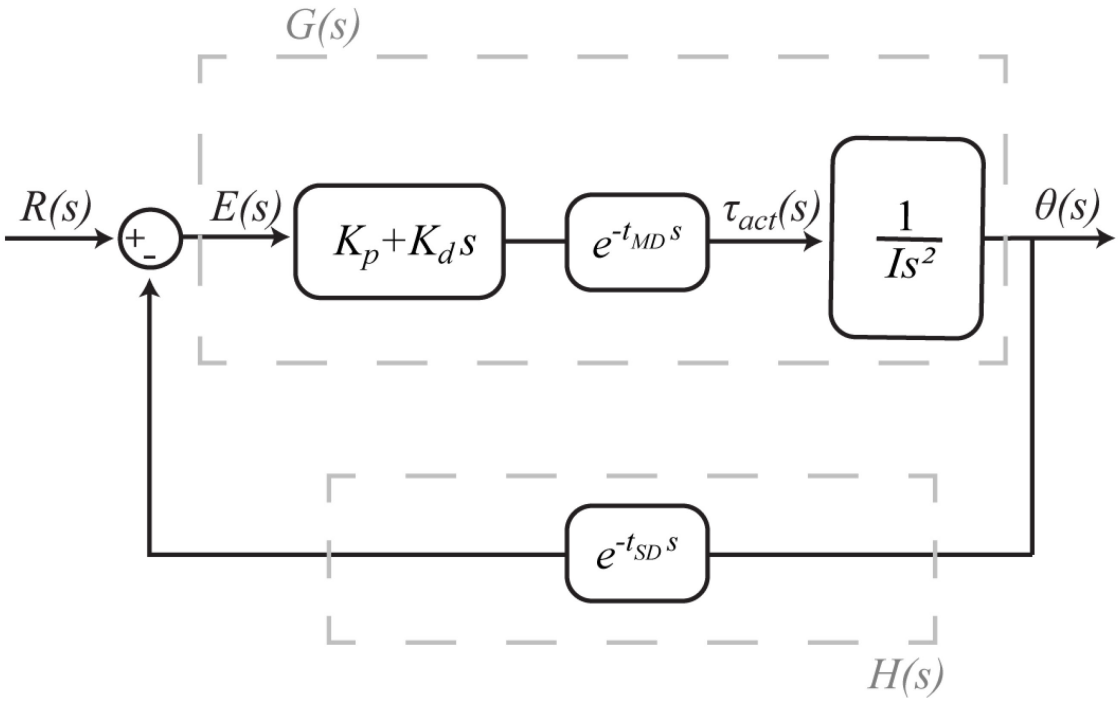

Fig 4.7 Block diagram with delays in feedforward and feedback pathways.
$R(s)$ is the reference signal, $E(s)$ is the error signal, $\theta(s)$ is the plant output (angle of the pendulum represented by the double integrator), and $\tau_{act}(s)$ the actuating torque. K_p and K_d are the controller gains, and $\frac{1}{Is^2}$ is the double integrator plant. $e^{-t_{MD}s}$ is the transfer function that delays the motor commands due to the time delay t_{MD}, and $e^{-t_{SD}s}$ is the equivalent transfer function for the sensory feedback.

The closed loop transfer function of a system $J(s)$, with a transfer function $G(s)$ in the feedforward pathway and $H(s)$ in the feedback pathway is given by $\frac{G(s)}{1+G(s)H(s)}$. Therefore, the block diagram in Fig 4.7 has a transfer function:

$$J(s) = \frac{\theta(s)}{R(s)} = \frac{G(s)}{1 + G(s)H(s)} = \frac{\left(K_p + K_d s\right) e^{-t_{MD}s} \frac{1}{Is^2}}{1 + \left[\left(K_p + K_d s\right) e^{-t_{MD}s} \frac{1}{Is^2} e^{-t_{SD}s}\right]} \quad 4.23$$

$$\theta(s)\left[Is^2 + \left(K_p + K_d s\right) e^{-(t_{MD}+t_{SD})s}\right] = R(s)\left[\left(K_p + K_d s\right) e^{-t_{MD}s}\right] \quad 4.24$$

$$I\theta(s)\, s^2 + K_p\, e^{-(t_{MD}+t_{SD})s}\, \theta(s) + K_d\, e^{-(t_{MD}+t_{SD})s}\, \theta(s)\, s = K_p\, e^{-t_{MD}s}\, R(s) + K_d\, e^{-t_{MD}s}\, R(s)\, s \quad 4.25$$

Converting Eqn 4.25 from the s domain to the time domain:

$$I\ddot{\theta}(t) + K_p\,\theta\big(t-(t_{MD}+t_{SD})\big) + K_d\,\dot{\theta}\big(t-(t_{MD}+t_{SD})\big) = K_p\,r(t-t_{MD}) + K_d\,\dot{r}(t-t_{MD}) \quad 4.26$$

$$I\ddot{\theta}(t) = \tau_{act}(t) = K_p\big[r(t-t_{MD}) - \theta\big(t-(t_{MD}+t_{SD})\big)\big] + K_d\big[\dot{r}(t-t_{MD}) - \dot{\theta}\big(t-(t_{MD}+t_{SD})\big)\big] \quad 4.27$$

The total sensorimotor delay is the sum of the sensory and motor delays:

$$t_{SMD} = t_{MD} + t_{SD} \quad 4.28$$

Eqn 4.27 shows us that if there were separate delays in the feedforward and feedback pathways, the reference signal would be delayed only by the motor delays (t_{MD}), while the sensory feedback would be delayed by the total delays (t_{SMD}).

However, if I combined all the delays and put them in the feedback pathway, I could remove t_{MD} from Eqn 4.27 and replace t_{SD} with t_{SMD} to get:

$$I\ddot{\theta}(t) = \tau_{act}(t) = K_p[r(t) - \theta(t-t_{SMD})] + K_d\big[\dot{r}(t) - \dot{\theta}(t-t_{SMD})\big] \quad 4.29$$

A comparison of Eqns 4.27 and 4.29 clarifies how having delays in both the feedforward and feedback pathways will make the tracking of a time varying reference signal more difficult than if there were delays only in the feedback pathway. However, since I am only considering a step response in my original simulations, the reference signal is constant. Therefore, Eqn 4.27 and 4.29 would be equivalent.

4.4. Discussion

In this chapter, I characterized how time delays and actuator saturation affected the behavior of a feedback control system, and quantified how fast the control system can respond given the limitations. Using the Bode plot of a linear control system, I showed how time delays cap the maximum controller gains that can be used in a stable feedback control system. I then analyzed a normalized feedback control system with both time delays and actuator saturation. This analysis showed that perturbation response times in animals can either be limited by the force generation capacity of muscles (force-limited) or by

sensorimotor time delays which constrain the maximum feedback gains that can be used to produce stable responses (delay-limited). I provided predictive equations generated using curve fitting for the relationship between saturation limits and response time, for the swing task and posture task.

The behavior of this feedback control system is very sensitive to simulation parameters, and I have described three examples here. Firstly, slight changes in the definition of allowable overshoot can significantly change the settling times obtained through optimization. I chose to allow no overshoot in the simulations that I considered to determine response time, by constraining overshoot to zero while optimizing controller gains. I based this partially on control systems theory; I wanted to obtain the equivalent of a critically damped response of a mass-spring-damper system (Fig 1.2). Furthermore, when an animal is trying to accurately place it foots to recover from a trip during a stumble correction response, overshooting the step can cause a fall or further destabilize the response. Secondly, slight changes in the definition of settling time thresholds can cause large discontinuous changes in settling time. This is because the response of a time-delayed feedback control system oscillates continuously. The oscillations are initially large, and they get smaller in amplitude over time, but they never stop even after reaching within the settling time thresholds. A slight change in controller gains could result in an oscillation reaching below the lower settling time threshold (Fig 1.2 underdamped-blue line), causing settling time to jump to the next time point where the oscillations move back within the settling time thresholds. The same thing can happen for a slight change in the definition of settling time thresholds. This feature makes the error landscape of the optimization very jagged, with many discontinuities and local minima (Fig 4.3, 4.5). To ensure that I have obtained the global minimum, I had to try multiple starting points and different optimization algorithms (MATLAB's fminsearch and fmincon optimization functions). Thirdly, in the posture task, we can choose to calculate settling time on the angle profile or the angular velocity profile; this choice can result in different settling times for the same response with the same controller gains. In a linear feedback control system, the settling time does not depend on the size of the perturbation. If you scale the target state of the step response, the feedback controller will automatically scale its force output, and the settling time thresholds will also get scaled wider, to generate the same settling time. While the

swing task response matches a classical step response (repositioning the plant state from rest at origin to rest at target state), the posture task involves starting at the origin with an initial velocity and returning to rest at the origin. Instead of calculating both overshoot and settling time on the angle curve, I chose to calculate settling time on the angular velocity curve and overshoot on the angle curve (Fig 4.5). By doing so, the settling time thresholds get scaled based on the size of the initial angular velocity perturbation, but does not change with controller gains. As overshooting the vertical position during a posture correction can also result in loss of balance, I calculated overshoot on the angle curve and constrained it to be zero during the optimization.

Several research groups from the field of engineering control systems have studied the effects of time delays and actuator saturation on feedback control (Cao et al., 2002; Fang and Lin, 2006; Lin and Fang, 2007; Mazenc et al., 2004, 2003; Yakoubi and Chitour, 2007). Rao and Bernstein studied the performance of several controller types including PD controllers in their ability to stabilize control systems with limitations such as saturation limits, mass variation, pole perturbation, feedback time delays, unmodeled dynamics and input nonlinearities (Rao and Bernstein, 2001). They showed that the PD controller worked well compared to other controllers in its ability to stabilize a feedback control system with time delays and saturation limits. Goldfarb and Sirithanapipat studied how actuator saturation affected the tracking performance of a PD controlled servo-motor system (Goldfarb and Sirithanapipat, 1999). For a linear system (without actuator saturation limits) required to track a sinusoidal signal composed of many frequencies, using higher controller gains improves tracking of a reference input, and infinite controller gains provide perfect tracking of all frequencies. The authors showed that for a feedback control system with actuator saturation, there is an optimal set of controller gains that provide the best tracking performance, and these gains command torques that exceed the saturation limits. Using very low gains which prevented actuator saturation caused poor tracking performance, but so did using gains higher than the optimal set. Skogestad provided analytical tuning rules to derive PID controller gains that achieve robust performance in time delayed control systems (Skogestad, 2001). Zhou et al. developed a family of controllers based on low gain feedback methodology derived using the parametric Ricatti equation that can stabilize a double integrator plant with both time delays and actuator saturation (Zhou et al., 2010).

Skogestad, Rao and Bernstein, and Goldfarb and Sirithanapipat show that even though PD control was developed for linear systems, it performs well for control systems with nonlinearities (Goldfarb and Sirithanapipat, 1999; Rao and Bernstein, 2001; Skogestad, 2001). I use the PD controller in this thesis as it is the simplest controller to implement and interpret. I assumed that the synapses at the spinal cord that perform the computations for reflexive control encode simple controller algorithms like PD control, while the supraspinal motor centers handle more complex controller algorithms that could require internal models and memory. In contrast to the engineering application of these studies, I used feedback control systems to model reflexive perturbation responses in animals. Towards this goal, I have optimized the feedback system to produce a very specific response (to achieve fastest settling times without any overshoot), and characterized how the system behaves for changes in time delays and saturation limits.

Animal features that affect feedback control scale at different rates with animal size. For example, in the swing task, limb moment of inertia scales as $2.52\times10^{-4}M^{1.75}$ kg.m^2 while muscle torques scale as $0.54M^{1.19}$ N.m, and sensorimotor delays scale as $31M^{0.21}$ ms (Kilbourne and Hoffman, 2013; More and Donelan, 2018; Thangal and Donelan, 2020). Depending on the relative magnitude of these features to each other, perturbation responses under feedback control in animals of a certain size could be delay-limited or force-limited. This could potentially result in different control choices for perturbation responses in different animal sizes. In the next chapter, I scaled the feedback control system to represent animals of different sizes and also considered gravitational effects, to obtain more realistic estimates for perturbation response times and determine whether terrestrial mammals are delay-limited or force-limited.

Chapter 5. Scaling of response times under feedforward and feedback control with sensorimotor delays in legged animals

5.1. Introduction

Perturbation responses in animals rely on both feedforward and feedback control strategies to generate motor commands (Dickinson et al., 2000; Gordon et al., 2020; Kuo, 2002). As feedforward control produces predefined motor commands which do not rely on sensory feedback, this strategy can be used to rapidly respond to a perturbation. However, since the feedforward controller does not check whether the perturbation response is going as planned, it cannot correct for any unexpected disturbances that occur during its execution. The feedforward controller also relies on previous experience and learned behavior to determine the motor commands, which might not be appropriate in a novel context. On the other hand, feedback controllers determine motor commands using sensory feedback about the plant behavior, and can correct for unexpected disturbances and ensure that the perturbation response proceeds accurately. Feedback controllers have their own disadvantages; they are susceptible to noise and time delays in the signal pathways, and can become unstable under certain conditions. Therefore, by combining both strategies and adapting them to various contexts, animals are able to utilize the advantages of each strategy, while compensating for their drawbacks.

Several groups have studied the neural control of perturbation responses in animals. Daley and colleagues have conducted a comprehensive series of experiments to understand perturbation responses in running guinea fowl. The perturbations included potholes, step up and step down obstacles; these perturbations were significant enough to force the bird to alter its gait, but allowed the bird to continue running and did not cause a fall. They found a consistent set of strategies that the birds used to navigate these perturbations. The birds maintained a constant swing leg angular cycling rate through feedforward control of the proximal leg joints, irrespective of whether they were able to anticipate the perturbation or not. The distal joints then responded preflexively to compensate for the perturbation, acting either as a spring or a damper depending on the leg posture at heelstrike. The

perturbation responses were predominantly under feedforward and preflexive control, and feedback modulation of the leg only occurred towards the very end of the perturbed stance phase (Biewener and Daley, 2007; Daley, 2018; Daley and Biewener, 2011, 2006; Gordon et al., 2020). Farley and colleagues studied human responses to anticipated or unanticipated changes in floor stiffness while hopping and running (Ferris et al., 1999; Moritz and Farley, 2006). They showed that humans adjust the overall limb stiffness under feedforward control and rely on preflexes to dampen out the effects of the perturbation. Similarly, studies on cockroaches have also shown that they rely on feedforward control for navigation (Dudek and Full, 2006; Jindrich and Full, 2002). On the other hand, Welch and Ting studied human postural responses to support surface translation, and showed that a time delayed feedback control model under proportional-derivative-accelerative (PDA) control can reproduce the EMG signals of the postural response (Welch and Ting, 2008), indicating that postural responses have a feedback control component.

Several studies have investigated the effects of sensorimotor delays on neural control, and hypothesized about the compensatory mechanisms that animals could be using to overcome the drawbacks caused by these time delays. The simplest method to deal with time delays in a negative feedback control system is to reduce the controller gains—this slows down the system's performance but prevents instability. Weiland et al. artificially introduced time delays into the reflex loops that control the femur-tibia joint in stick insects, and showed that increasing time delays caused instability in the form of tremors (Weiland et al., 1986). Tuthill et al. proposed that the supraspinal motor centers act to inhibit the activity (reduce the controller gains) in reflex circuits in order to keep them stable despite the sensorimotor delays, as severing supraspinal inputs result in tremors in animals (Dallmann et al., 2021; Tuthill and Azim, 2018). A more computationally intensive method to compensate for delays is to use neural prediction—the nervous system could implement internal models that can estimate the present state of the body from time delayed sensory feedback. Miall et al. suggested that one of the functions of the cerebellum is to act as a Smith predictor, an internal model specifically designed to compensate for time delays in feedback control systems (Miall et al., 1993). Another compensatory method is to use positive feedback control instead of negative feedback control in systems with time delays—studies have shown that the nervous system implements positive force feedback

in the control of rhythmic movements like walking and hopping (Geyer et al., 2003; Hatz et al., 2012; Prochazka et al., 1997a). Besides time delays, the nervous system also has to deal with other drawbacks such as noise, muscle force capacity limits, limited sensory resolution and sensory dead zones. The nervous system could take advantage of the interaction between these drawbacks to simplify control. Milton and colleagues studied posture control in humans, and suggested that act-and-wait control strategies which take advantage of the interplay between the effects of noise and time delays would be effective for neural control (Insperger et al., 2015; Milton et al., 2009; Milton, 2015, 2011). Milton and Insperger also modeled quiet standing in humans using a feedback control system with proportional-derivative (PD) control of an inverted pendulum—and considered time delays, saturation limits on the ankle muscle force capacity, and a sensory deadzone in the sensing of body angle and angular velocity (Milton and Insperger, 2019). While we would expect each of these nonlinearities to detrimentally affect balance, the authors show that together, they improve stability.

As animal size increases, several features that could affect control also change—sensorimotor delays get longer, muscles get proportionally weaker, and body segments get heavier (Alexander et al., 1981; Heglund et al., 1974; Kilbourne and Hoffman, 2013; More and Donelan, 2018; Thangal and Donelan, 2020). But working to the advantage of motor control is that the time available to make a corrective response gets longer—larger animals take longer to fall to the ground when they lose balance, and they have longer stride times when running (Heglund et al., 1974). The detrimental effects of physiological limitations such as time delays and muscle force capacity limits would be most evident when an animal is forced to respond to a perturbation as fast as possible; this will require using the maximum possible muscle forces while ensuring that the response remains accurate and does not go unstable. For a given animal size, feedback control could be delay-limited or force-limited. Feedback control response times could be similar to or slower than feedforward response times. The response times under feedback and feedforward control might exceed available time, especially at fast movement speeds where the available time to prevent a fall after a perturbation is very limited. Depending on these relationships, animals of different sizes could adopt different control strategies: feedback only, feedforward only, or a combination of feedback and feedforward control. As conducting

perturbation studies on animals of varying sizes while they are running at maximum speeds would be difficult, I instead use computational simulations to model their behavior.

My objective is to understand how muscle force capacity limits and sensorimotor delays affect fast perturbation response times in animals of different sizes. Towards this objective, I developed feedforward and feedback control systems that can be scaled to represent the size range of terrestrial mammals, from 1 gram to 10 tons. I parameterized the models with sensorimotor delays, muscle force capacity limits and inertial properties using scaling relationships from literature. I again quantified response times for two perturbation response tasks: a swing leg repositioning task (swing task), and a posture recovery after a balance perturbation task (posture task). I defined response time as the settling time of the control system without overshoot, and determined the controller gains that produced the fastest responses using optimization. From these simulations, I estimated the scaling relationship between response time and animal size for both feedforward and feedback control. I determined whether feedback control of fast perturbation responses in terrestrial mammals is delay-limited or force-limited. By comparing response times under these different types of control to each other, and to available movement times, I quantified the effectiveness of these control strategies across animal size.

5.2. Methods

I developed feedforward and feedback control models that are scaled with animal size and parameterized them with values from literature (Fig 5.1). I created these models using MATLAB (MATLAB R2020a, The MathWorks, Inc., Natick, MA, USA). For the feedforward control models, I used the ode45 (explicit Runge-Kutta algorithm) variable time step solver to numerically integrate the equations of motion. For the feedback control models, which required time-delayed state information, I used the dde23 delay-differential equation solver (explicit Runge-Kutta algorithm with discontinuity tracking) to numerically integrate the equations of motion. For both models, I used a relative tolerance of 10^{-6} and an absolute tolerance of 10^{-9}. I quantified their response times for two perturbation response scenarios in animal locomotion: a swing limb repositioning task and a whole-body posture recovery task. For the swing task, I set the initial conditions for plant

states [θ_0, $\dot{\theta}_0$] to [-15°, 0], and the target state to [15°, 0]. I calculated both settling time and overshoot on the angle vs. time curve. For the posture task, I set the initial conditions to [0, -0.21 dimensionless velocity] and the target state to [0, 0]. I calculated the dimensionless velocity as $\frac{v}{\sqrt{gL}}$, where L is the length of the inverted pendulum. I calculated settling time on the angular velocity curve and the overshoot on the angle curve. I used 2% settling time thresholds to calculate settling time. I defined response time as the fastest settling time of the system without any overshoot, and optimized controller gains to search for this specific response.

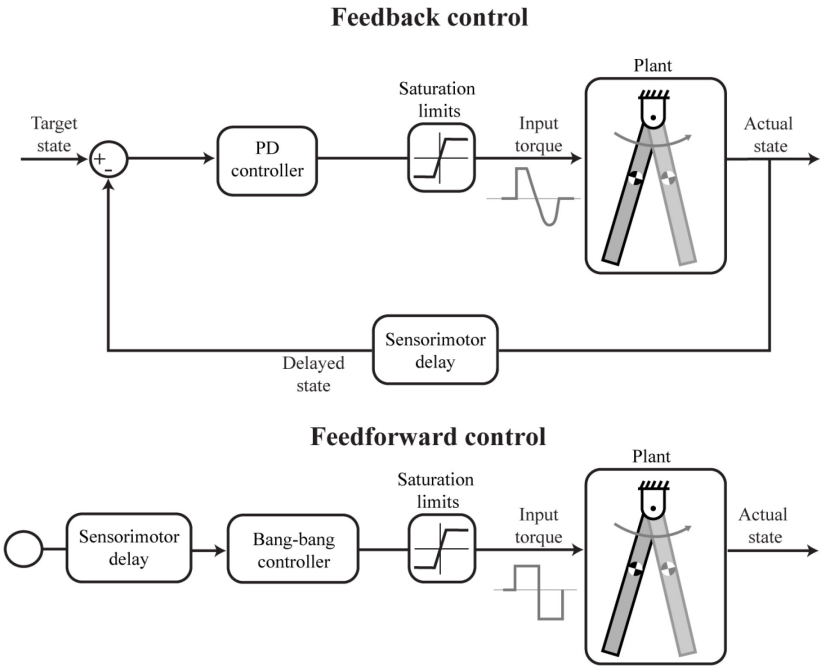

Fig 5.1 Block diagram of the feedback and feedforward control systems.
The feedback system (top) used a PD controller to generate torque based on time delayed state feedback. The feedforward system (bottom) used a bang-bang controller to generate torques.

5.2.1. Swing task

The swing task represented an animal that has encountered a trip of the forelimb during early swing phase, and has to reposition its foot by swinging it forward to avoid a fall (Forssberg, 1979; Rossignol et al., 2006). I modeled the limb as a distributed mass pendulum, and the task required repositioning the foot from rest at an initial clockwise angle to rest at a final counterclockwise angle. The equation of motion is described by:

$$I\ddot{\theta}(t) = \tau_{total} = \tau_{act} + \tau_{gravity} \quad 5.1$$

where τ_{act} is the torque exerted by the muscle, and $\tau_{gravity}$ the torque exerted by gravity. I is the moment of inertia of the pendulum. I set the angle to be zero when the pendulum is pointing vertically downwards and defined the counterclockwise direction to be positive. The torque due to gravity is described by:

$$\tau_{gravity}(t) = M_{limb} g L_{COM} \sin\theta(t) \quad 5.2$$

where M_{limb} is the mass of the pendulum, I is its moment of inertia, and L_{COM} is the distance from the shoulder joint to the limb center of mass. g is the acceleration due to gravity.

Under feedback control, τ_{act} is the torque applied to the plant, and τ_{des} is the PD controller output subject to saturation limits:

$$\tau_{act} = sat(\tau_{des}) = \begin{cases} \tau_{iso} & if\ \tau_{des} > \tau_{iso} \\ \tau_{des} & if\ -\tau_{iso} \leq \tau_{des} \leq \tau_{iso} \\ -\tau_{iso} & if\ \tau_{des} < -\tau_{iso} \end{cases} \quad 5.3$$

τ_{iso} is the saturation limit and is estimated as the maximum torque that can be applied by the triceps muscle about the shoulder joint to reposition the swing limb.

τ_{des} is described by:

$$\tau_{des}(t) = \begin{cases} 0 & if\ 0 < t < t_{SM} \\ K_p[r - \theta(t - t_{SM})] + K_d\left[-\dot{\theta}(t - t_{SM})\right] + \tau_{steadystate} & if\ t \geq t_{SM} \end{cases} \quad 5.4$$

where K_p and K_d are the controller gains, r is the reference, $\tau_{steadystate}$ is the steady state torque required to counter gravity at the final state, and t_{SM} is the sensorimotor delay. For a duration equal to the sensorimotor delay at the beginning of the simulation, the controller did not apply any forces, and the pendulum moved under the influence of gravity. I assumed that the animal had been perturbed during this initial period, but has not had enough time to sense the perturbation, compute a recovery strategy and send the motor

commands to the muscles. Once this deadtime is over, the controller began to exert forces on the pendulum, using historical state information.

As Eqn 5.4 required time delayed state information, I used dde23 to numerically integrate the delay differential equation. I used optimization to solve for the PD controller gains that minimized the settling time, while constraining overshoot to 0.

Under feedforward control, τ_{act} represented the torque produced by the bang-bang controller, with an initial deadtime:

$$\tau_{act}(t) = \begin{cases} 0 & if\ 0 < t < t_{SM} \\ +\tau_{iso} & if\ t_{SM} < t < t_{switch} \\ -\tau_{iso} & if\ t_{switch} < t < t_{end} \end{cases} \quad 5.5$$

As Eqn 5.5 requires only real time state information, I implemented the ode45 solver to integrate the ordinary differential equation. I used the solver's event detection to determine when the pendulum reached zero velocity and stopped the simulation. I used optimization to search for the ideal time to switch the direction of the bang-bang controller torque (t_{switch}), such that it minimized the difference between the reference target and the final position of the pendulum.

I parameterized the models using the same values that I used in my previous work to determine the scaling of inertial delays in chapter 2 and 3 (Thangal and Donelan, 2020). I scaled the sensorimotor delays in the feedback pathway (t_{SM}) as $31M^{0.21}$ ms (More and Donelan, 2018). I scaled the ability of the triceps to generate torque (τ_{iso}) as $0.54M^{1.19}$ Nm, the moment of inertia of the mammalian forelimb (I) as $0.00025M^{1.75}$ kg.m^2, the distance from the shoulder joint to the forelimb center-of-mass (L_{COM}) as $0.056M^{0.36}$ m, and the mass of the forelimb (M_{limb}), as $0.058M^{1}$ kg (Alexander et al., 1981; Kilbourne and Hoffman, 2013; Thangal and Donelan, 2020). I estimated τ_{iso} for each animal size using scaling values for the triceps muscle mass, muscle length and moment arm from Alexander et al. (Alexander et al., 1981). I found muscle volume from mass by assuming a density of 1060 kg/m^3 (Méndez and Keys, 1960), and cross-sectional area by dividing muscle volume by muscle length. I then multiplied cross-sectional area by the isometric stress of muscles, estimated to be 20 N/cm^2 (Close, 1972; Rospars and Meyer-Vernet, 2016), to get muscle

force. τ_{iso} is muscle force multiplied by the moment arm. I assumed that the triceps is the main muscle moving the shoulder joint in quadrupeds, that the antagonistic muscle has similar parameters to the triceps, and that the muscle has constant cross-sectional area, as scaling data on these muscles are limited (Thangal and Donelan, 2020). While feedforward response times increased with the size of the movement, feedback response times did not. The task required swinging the limb from rest at -15° to rest at +15°, for consistency between the feedback and feedforward simulations. I found response times for seven logarithmically spaced animal sizes from 1 gram to 10 tons to cover the size range of terrestrial mammals, and also evaluated sizes of 5 grams and 5 tons to get a more realistic estimates for extant terrestrial mammals (Jürgens, 2002; Larramendi, 2015). I then performed a least squares linear regression on the logarithmically transformed animal mass vs. simulation outputs (controller gains and response times) to extract the coefficient and exponent of the scaling relationship (LaBarbera, 1989). I have tabulated the input and output parameters of the swing task in Table 5.1.

5.2.2. Posture task

The posture task represented an animal recovering its posture after a push forward in the sagittal plane, under the control of its plantarflexors (Winter, 1995; Winter et al., 2001). I used a point mass inverted pendulum to represent the entire body, with a mass M equal to the weight of the whole animal, and length L set to the average length of the forelimb and hindlimb for each animal mass (Kilbourne and Hoffman, 2013). I started the simulation with an initial clockwise angular velocity which I scaled with animal size. The task required rejecting the initial velocity caused by the push, and returning to rest at the vertical position. The equation of motion is described by:

$$I\ddot{\theta}(t) = \tau_{total} = \tau_{act} - \tau_{gravity} \quad 5.6$$

where τ_{act} is the torque exerted by the muscle, and $\tau_{gravity}$ the torque exerted by gravity. I is the moment of inertia of the pendulum, computed as ML^2. I set the angle to be zero when the inverted pendulum is pointing vertically upwards and defined the counterclockwise direction to be positive. The torque due to gravity is described by:

$$\tau_{gravity}(t) = MgL \sin\theta(t) \quad 5.7$$

I determined τ_{act} for feedback and feedforward control in the posture task using the same equations as the swing task, and simulated and optimized my simulations using the same methods. While the swing task had a non-zero final angle and required a steady state torque in the controller to compensate for gravity at the final state, feedback control of the posture task required only proportional-derivative control, as the simulation ends with a vertical final position.

I parameterized the models using the same values that I used in my previous work to determine the scaling of inertial delays in chapter 2 and 3 (Thangal and Donelan, 2020). I scaled τ_{iso} as $3.41M^{1.21}$ Nm, which is four times the maximum torque that can be exerted by the ankle plantarflexors based on Alexander et al. (Alexander et al., 1981). I scaled whole body inertia I as $0.0264M^{1.74}$ kg.m^2, and the length of the pendulum L as $0.162M^{0.37}$ m (Kilbourne and Hoffman, 2013). I started the simulation at the vertical position with an initial forward velocity scaled with a dimensionless velocity of 0.21 Froude number. I again chose this value for consistency between the feedback and feedforward simulations. I have tabulated the input and output parameters of the posture task in Table 5.2.

5.3. Results

5.3.1. Feedback control response time—normalized model predictions vs. simulation results.

Predictions for response time based on the relationship between normalized saturation limits and response time ($\overline{t}_{resp}$ vs. $\overline{\tau}_{iso}$) from chapter 4 compared well to results from the more biologically realistic and scaled model simulations in chapter 5. The normalized models did not incorporate gravitational torques, only torques generated by the PD controller. For the scaled models, I considered gravitational torques. I subjected the PD controller torques to time delays and saturation limits, but did not do so to the gravitational torques. Additionally for the swing task, the scaled models also incorporated a steady state torque to counter gravitational torques at the target state. The predictive equations for the swing task are:

$$\bar{t}_{resp} = f(\bar{\tau}_{iso}) = \begin{cases} 7.09 & \bar{\tau}_{iso} \geq 0.162 \\ 5.56e^{-27.1\bar{\tau}_{iso}} + 8.64e^{-1.29\bar{\tau}_{iso}} & 0.079 \leq \bar{\tau}_{iso} < 0.161 \\ 18.33e^{-73.12\bar{\tau}_{iso}} + 10.12e^{-2.88\bar{\tau}_{iso}} & 0.009 \leq \bar{\tau}_{iso} < 0.078 \end{cases} \quad 4.21$$

Feedback control response times in the realistic simulations for the swing task scaled as 199 $M^{0.21}$ ms. The normalized equations predicted response time from the scaled simulations with an average accuracy of -10.5% (range: -8%, -14%) (Fig 5.2 left).

The predictive equations for the posture task are:

$$\bar{t}_{resp} = f(\bar{\tau}_{iso}) = \begin{cases} 7.39 & \bar{\tau}_{iso} \geq 0.80 \\ 1.61\,\bar{\tau}_{iso}^{\,-1.10} + 5.17 & 0.14 \leq \bar{\tau}_{iso} < 0.80 \end{cases} \quad 4.22$$

Feedback control response times in the realistic simulations for the posture task scaled as 240 $M^{0.22}$ ms. The normalized equations predicted response time from the scaled models with an average accuracy of 5% (range: 2%, 13%) (Fig 5.2 right).

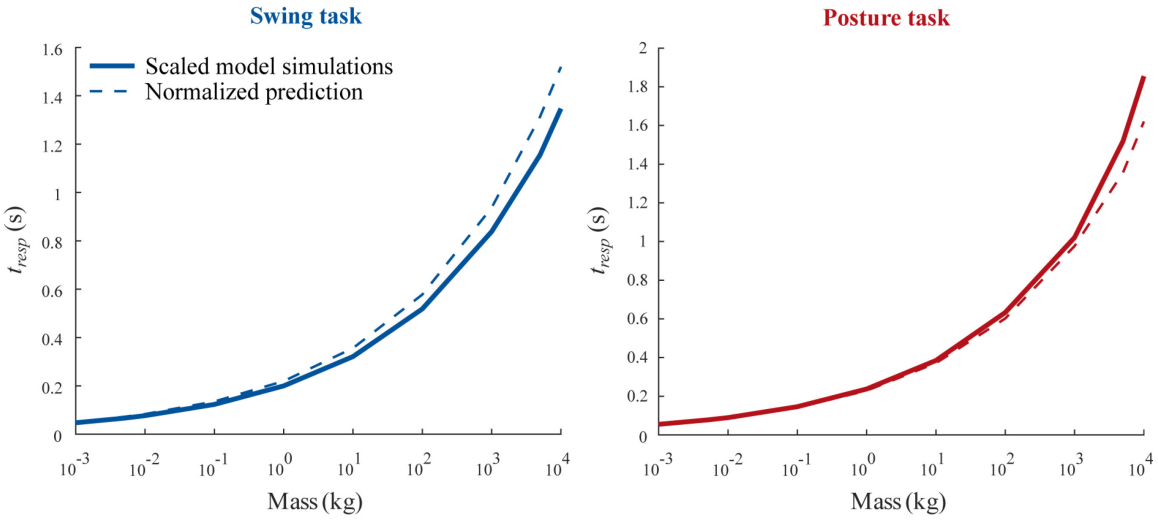

Fig 5.2 Feedback control response time—normalized model predictions vs. simulation results.
Normalized prediction for the swing task (left) and posture task (right) in dotted lines. Scaled feedback control model simulation results in solid lines.

5.3.2. Scaling of control in the swing task

Feedback control performed poorly when compared to feedforward control (Figs 5.3 and 5.4). In the fastest feedforward control responses, the response time depends on the size of the movement–small movements are accomplished quickly, but large movements

take more time. Perhaps non-intuitively, response time is independent of movement size in feedback control–it takes the same amount of time to perform a small movement as a large movement if the controller gains are the same and the torques do not exceed saturation limits. Thus, to compare response times in the two types of control, it is useful to pick a movement size. Here I used a swing leg repositioning from -15° to +15° because sensorimotor delays and inertial delays are equally matched in a one kg animal for this movement size (Thangal and Donelan, 2020). For this movement size, the fastest response times under feedback control scaled as 199 $M^{0.21}$ ms, compared to 62$M^{0.24}$ ms under feedforward control (Fig 5.3c). More generally, feedback control response times ranged from four times longer in smaller animals to two times longer in larger animals, when compared to feedforward control (Fig 5.4b). This is because the feedback controllers were delay-limited, and unable to utilize a significant portion of their muscle torque capacity due to the stability limitations imposed by long sensorimotor delays (Fig 5.4a).

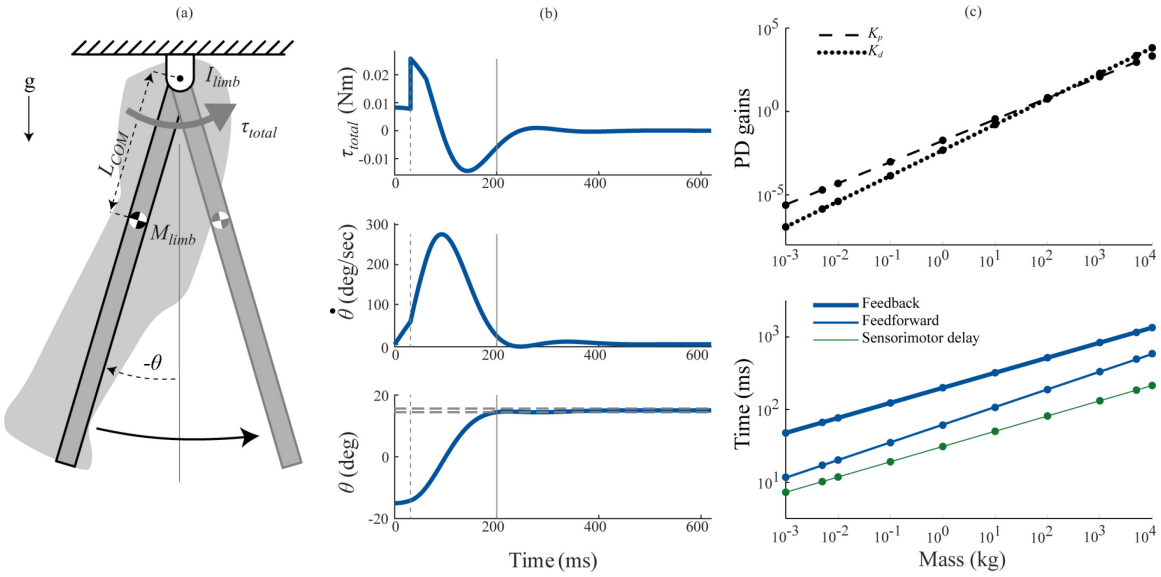

Fig 5.3 Swing task under feedback control.
This model represents repositioning of the swing limb in response to a trip. (a) I modeled the plant as a distributed mass pendulum actuated by torques generated by the PD controller. (b) Torque (τ_{total}), angular velocity ($\dot{\theta}$) and angle (θ) profiles in the swing task for a 1 kg animal and a 30 degree movement under feedback control. The grey dashed line at 31 ms represents the initial sensorimotor delay period and the gray vertical line at 200 ms represents response time, computed as the settling time of the angle curve with a 2% threshold (grey dashed horizontal lines). (c) Log-log plots for the scaling of the controller gains (top) and the response times under feedback control (thick blue line), feedforward control (thin blue line) and sensorimotor delays (thin green line). The dots denote the actual values obtained through optimization, while the lines denote the power law fit.

Larger animals also have slower characteristic movements, giving them longer to complete a perturbation response. I estimated the shortest time available to complete a perturbation response for animals of different sizes, as the swing duration at maximum sprint speed (More and Donelan, 2018; Thangal and Donelan, 2020). Response times under feedback control exceeded swing duration at maximum sprint speed at all animal sizes, while feedforward control did not (Fig 5.4 c).

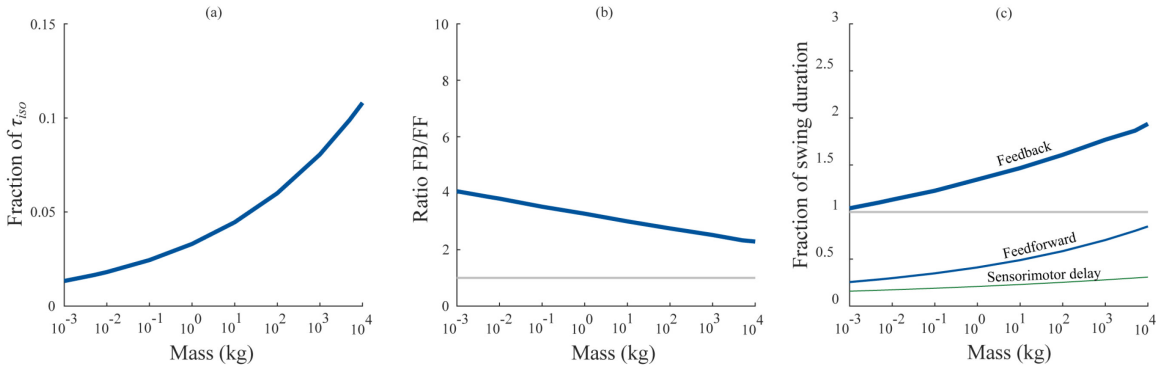

Fig 5.4 Swing task—comparison of feedforward and feedback response times.
(a) The fraction of maximum isometric torque (τ_{iso}) utilized by the feedback controller in the swing task. (b) The ratio of feedback control response times to feedforward control response times. (c) Fraction of swing duration at maximum sprint speed required to perform a corrective movement using feedback control (thick blue line), feedforward control (thin blue line) and sensorimotor delays (thin green line).

In section 5.3.5, I have provided a breakdown of the various contributors to total torque (Fig 5.3b top panel) applied by the feedback controller. Table 5.1 lists the input parameters and the optimized output parameters in the swing task.

Table 5.1 Table of input parameters and results for the swing task.

Parameter	Coefficient (*a*)	Exponent (*b*)
Swing task inputs		
t_{SM}: Sensorimotor delay (ms)	31	0.21
M_{limb}: Forelimb mass (kg)	5.8×10^{-2}	1.00
I: Forelimb inertia (kg.m^2)	2.52×10^{-4}	1.75
L_{COM}: COM length (m)	5.6×10^{-2}	0.36
τ_{iso}: Triceps torque (N.m)	0.54	1.19
Swing task outputs		
Swing duration at max sprint (ms)	147.85	0.17
Feedback control results		
K_p: Proportional gain (N.m/rad)	1.76×10^{-2}	1.28
K_d: Derivative gain (N.m/(rad/s))	4.76×10^{-3}	1.54
Feedback response time (ms)	199.43	0.21
Feedforward control results		
t_{switch}: Switch time (ms)	46.32	0.23
Feedforward response time (ms)	61.90	0.24

5.3.3. Scaling of control in the posture task

While the feedback controllers in the posture task were able to use more of the available torque than in the swing task, it still performed poorly compared to feedforward control (Figs 5.5 and 5.6). In order to compare response times, I chose to perturb the inverted pendulum by a force causing an initial dimensionless velocity of 0.21 Froude number for both the feedforward and feedback control simulations, resulting in larger initial velocities for larger animals (Thangal and Donelan, 2020). Since larger animals have heavier bodies, longer limbs and larger muscles, I scaled the perturbation with size in order to elicit equivalent responses from different sized animals. For this perturbation size, the fastest response times under feedback control scaled as $240\ M^{0.22}$ ms, compared to $95M^{0.28}$ ms under feedforward control (Fig 5.5c). Feedback control response times ranged from four times longer in smaller animals to one and a half times longer in larger animals, when compared to feedforward control (Fig 5.6b). Other than for the largest animals, feedback control in the posture task was also delay-limited (Fig 5.6a).

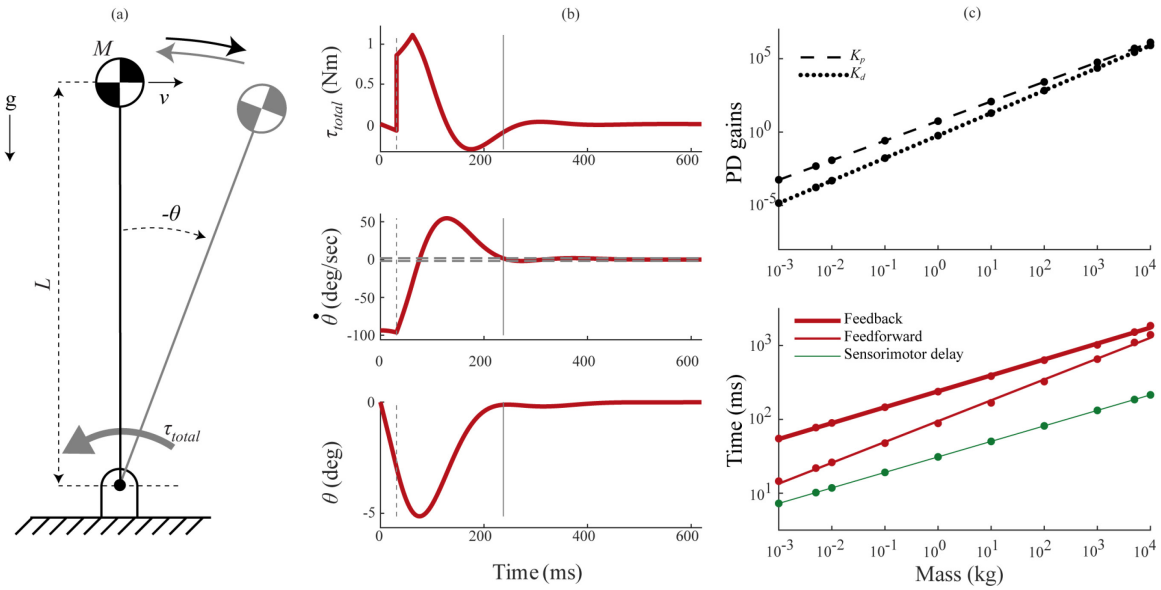

Fig 5.5 Posture task under feedback control.
This model represents whole body posture control after a push forward in the sagittal plane. (a) I modeled the plant as a point mass pendulum actuated by torques generated by the PD controller. (b) Torque (τ_{total}), angular velocity ($\dot{\theta}$) and angle (θ) profiles in the posture task for a 1 kg animal, perturbed by a force causing an initial velocity of 0.21 dimensionless velocity, under feedback control. The grey dashed line at 31 ms represents the initial sensorimotor delay period and the gray vertical line at 238 ms represents response time, computed as the settling time of the angular velocity curve with a 2% threshold (grey horizontal dashed lines). (c) Log-log plots for the scaling of the controller gains (top) and the response times under feedback control (thick red line), feedforward control (thin red line) and sensorimotor delays (thin green line). The dots denote the actual values obtained through optimization, while the lines denote the power law fit.

Feedback control response times in the posture task also exceeded available time for all animal sizes. I estimated time available to complete the perturbation response as the time required to fall under gravity to the ground, from a height equal to the leg length for each animal size, which scaled as $182M^{0.19}$ ms. Feedforward response times for the largest animals also exceeded available time (Fig 5.6c).

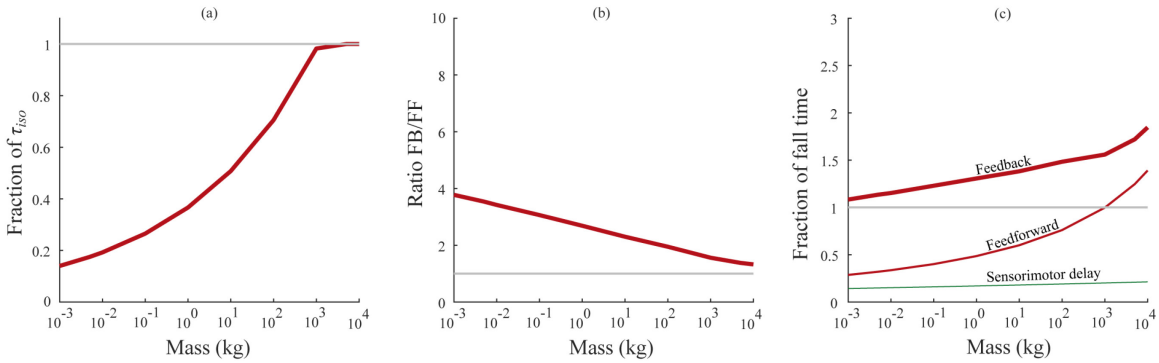

Fig 5.6 Posture task—comparison of feedforward and feedback response times.
(a) The fraction of maximum isometric torque (τ_{iso}) utilized by the feedback controller in the posture task. (b) The ratio of feedback control response times to feedforward control response times. (c) Fraction of time taken to fall to the ground under gravity required to perform a corrective movement using feedback control (thick red line), feedforward control (thin red line) and sensorimotor delays (thin green line).

In section 5.3.5, I have provided a breakdown of the various contributors to total torque (Fig 5.5b top panel) applied by the feedback controller. Table 5.2 lists the input parameters and the optimized output parameters in the posture task.

Table 5.2 Table of input parameters and results for the posture task.

Parameter	Coefficient (*a*)	Exponent (*b*)
Posture task inputs		
$\boldsymbol{t_{SM}}$: Sensorimotor delay (ms)	31	0.21
$\boldsymbol{I}$: Whole body inertia (kg.m^2)	2.64×10^{-2}	1.74
$\boldsymbol{L}$: Center of mass height (m)	1.62×10^{-1}	0.37
$\boldsymbol{\tau_{iso}}$: Plantarflexor torque (N.m)	3.41	1.21
Posture task outputs		
Time to fall leg length (ms)	182.02	0.19
Feedback control results		
$\boldsymbol{K_p}$: Proportional gain (N.m/rad)	5.64	1.34
$\boldsymbol{K_d}$: Derivative gain (N.m/(rad/s))	5.80×10^{-1}	1.53
Feedback response time (ms)	239.96	0.22
Feedforward control results		
$\boldsymbol{t_{switch}}$: Switch time (ms)	72.30	0.28
Feedforward response time (ms)	94.55	0.28

5.3.4. Comparing swing and posture task responses to in-vivo perturbation studies

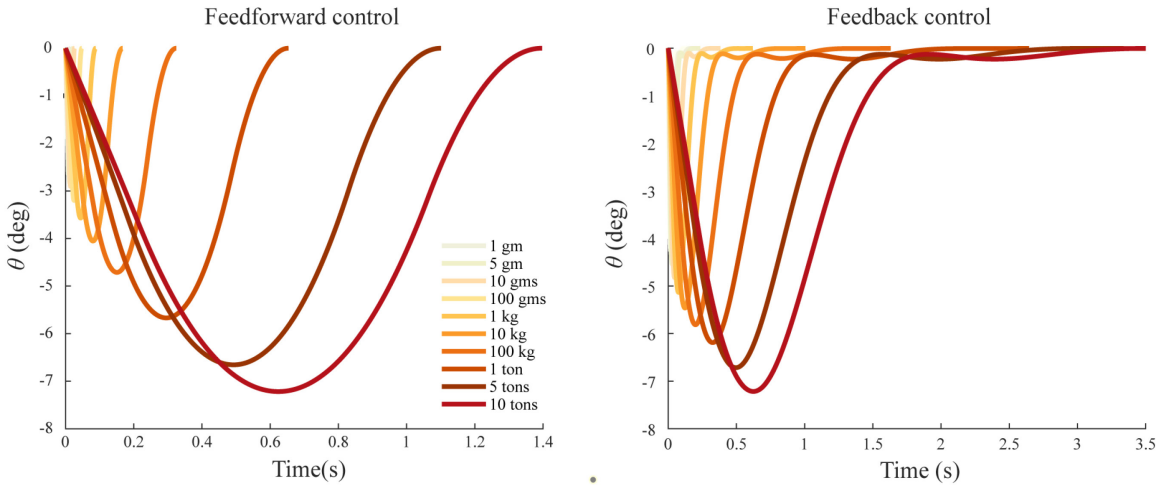

Fig 5.7 Angle profiles for the posture task under feedforward and feedback control.
Angle vs. time profiles from the posture correction response for animal sizes ranging from 1 gram to 10 tons under feedforward control (left) and feedback control (right), for a 0.21 dimensionless velocity perturbation.

The kinematic profiles from my simulations are qualitatively similar to those reported in in-vivo perturbation studies, even though most perturbation studies on animals do not elicit the fastest possible responses. My simulations model the fastest perturbation responses controlled purely through monosynaptic reflex pathways, and I consider feedforward and feedback control separately. Perturbation responses from in-vivo studies are difficult to separate into purely feedforward or feedback strategies, and often involve both the reflexive and supra-spinal motor pathways. Eng et al. studied stumble corrective responses in humans, and reported that an approximately 40° swing leg repositioning response to an early swing phase trip took about 500 ms (Eng et al., 1994). According to my simulations, for a 70 kg human performing a 30° swing leg repositioning, the fastest possible swing task responses would take 172 ms under feedforward control and 487 ms under feedback control. I also compared my posture task simulations to three studies that reported on human and cat postural responses to support-surface translations (Horak and Nashner, 1986; Ting and Macpherson, 2004; Welch and Ting, 2008). Horak and Nashner reported that for a 0.05 dimensionless velocity perturbation, their human subjects took about 600 ms to regain posture, and suffered a maximum lean of 3° (Horak and Nashner, 1986). Welch and Ting reported that for a 0.09 dimensionless velocity perturbation, their

human subjects took about 1000 ms to regain posture, and suffered a maximum lean of 5° (Welch and Ting, 2008). My posture task simulations predict that for a 70 kg human subjected to a 0.21 dimensionless velocity perturbation, recovering balance would take 310 ms under feedforward control and 611 ms under feedback control, and also force them to lean to a maximum angle of about 5°. Ting and Macpherson reported that cats subjected to a 0.09 dimensionless velocity postural perturbation take about 1000 ms to regain posture, and exhibit a 5° lean (Ting and Macpherson, 2004). My posture task simulations predict that for a 4 kg cat subjected to a 0.21 dimensionless velocity perturbation, recovering balance would take 140 ms under feedforward control and 326 ms under feedback control, and force it to lean to a maximum angle of about 3.5°. In Fig 5.7, I have shown the angle vs. time profiles for different sized animals in the posture task under feedforward and feedback control. These profiles match the behavior seen in studies on posture correction in quadrupeds. The maximum lean of the posture task model (about 7° for a 0.21 dimensionless velocity perturbation) would not cause the center of mass to move outside the base of support in quadrupeds. However, I have not considered similar effects in bipeds. Bipeds would be forced to use a stepping strategy, instead of a hip or ankle strategy, if large perturbations cause the center of mass to move beyond the base of support.

5.3.5. Components of total applied torque under feedback control

I calculated the total torque experienced by the pendulum as the sum of the muscle torque (generated by the feedback controller), and gravitational torque. The muscle torque composed of proportional and derivative components in the posture task, and an additional steady state component in the swing task. I capped the muscle torques at a saturation limit, computed as the maximum isometric torque that can be produced by the relevant muscles. Saturation occurred only for animals heavier than one ton in the posture task. During an initial delay period equal to the sensorimotor delay, I did not apply muscle torques and the pendulum moved purely under gravitational torques. I considered this the time required for the animal to sense the perturbation, compute the motor commands and transmit the signals to the muscles. After this deadtime, I turned on the muscle torques, computed based on time delayed state feedback. Fig 5.8 depicts the contribution of each component to the applied torque for a 1 kg animal in the swing task and posture task.

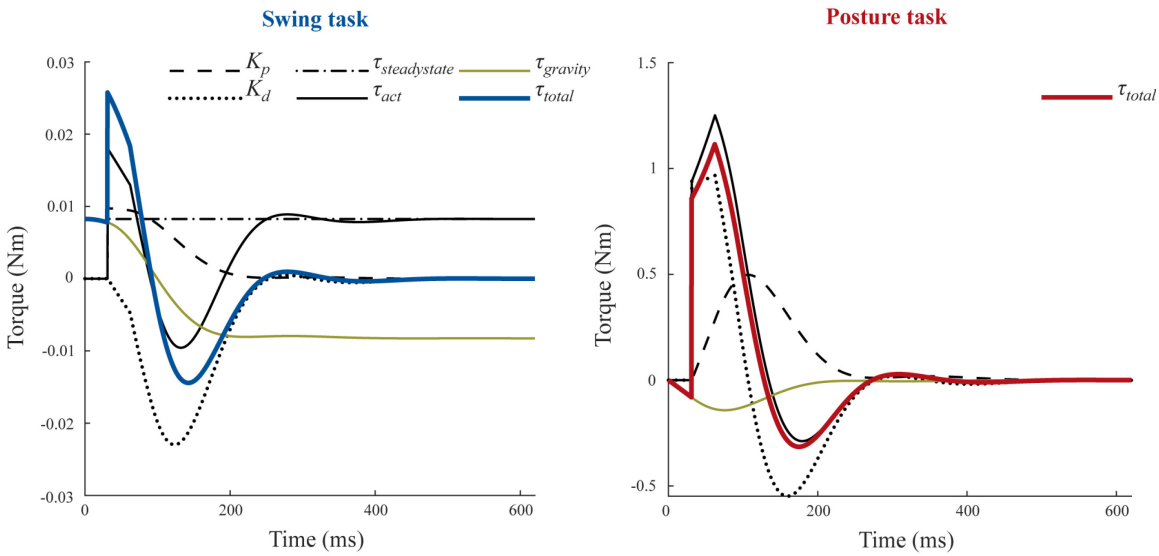

Fig 5.8 Components of total torque.
For the swing task on the left, the controller torque consisted of a proportional component (K_p—black dashed line), a derivative component (K_d—black dotted line), and a steady state component ($\tau_{steadystate}$—black dash dot line). These three components made up the muscle torque (τ_{act}—solid black line). The total torque (τ_{total}—thick blue line) is the sum of τ_{act} and gravitational torque ($\tau_{gravity}$—yellow green line). For the posture task on the right, I show the total torque in red. The posture task does not have a steady state torque component. The values shown here are for a 1 kg animal in the swing task and posture task.

5.4. Discussion

Using neuromechanical models representing fast perturbation responses, I quantified the scaling of response times under feedforward and feedback control, subject to muscle force capacity limits and sensorimotor delays. Previous work in my lab had quantified the scaling of sensorimotor delays (signal transmission and processing time delays in the mono-synaptic stretch reflex) (More and Donelan, 2018), and I quantified inertial delays (movement time required to physically reposition body segments as part of the response to a perturbation) in Chapter 2 and 3 of this thesis (Thangal and Donelan, 2020). In this chapter, I evaluated how the type of control used (feedforward vs. feedback control) further affected response times. In general terms, feedforward control is fast but inaccurate, feedback control is slow but ensures accuracy. In this study, I have only considered the speed of the response, I have ensured perfect accuracy under both types of control. Response times under feedforward and feedback control depended on several factors such as the force generation capacity of muscles, the moment of inertia of the body segments and the sensorimotor delays in the reflex pathways. If sensorimotor delays were

short relative to the other factors, feedback control could have produced comparable response times to feedforward control. I could also have found different results for small and large animals—feedback control could have performed comparably to feedforward control in larger animals, but worse in smaller animals. However, I found that while feedforward control can fully activate muscles and produce fast responses, long sensorimotor delays required feedback control to use low gains to ensure stability, allowing only a fraction of the muscles' force capabilities to be utilized. That is, the effectiveness of feedback control within the size range of terrestrial mammals is delay-limited rather than force-limited. Responses under feedback control were at least two times longer than feedforward control across animal size, for both the swing task and posture task. Feedback control response times exceeded available movement time for all animal sizes, while feedforward response times did so only for the largest animals in the posture task (Figs 5.4c and 5.6c). Feedback control does not seem effective for fast perturbation responses in animals of all sizes.

In chapter 4, I had proposed a method to normalize the feedback control system using three constant parameters which also represent characteristic features of a perturbation response—the sensorimotor delays in the control pathways (t_d), the moment of inertia of the body segment being moved (I), and the size of the corrective movement (θ_r). The normalized feedback control model illustrated how perturbation responses in animals could either be delay-limited or force-limited. Using curve fitting, I obtained equations for the relationship between normalized response time and saturation limits ($\overline{t}_{resp}$ vs. $\overline{\tau}_{iso}$). Predictions from these equations compared well to results from the more biologically realistic simulations in chapter 5 that were scaled with animal size (-10.5% accuracy in the swing task and 5% accuracy in the posture task). Because my results from chapter 4 based on fundamental principles held up when I increased the complexity of my simulations, I gain confidence that my predictions and trends in this study are correct, and will be relevant in in-vivo studies.

While my simulations determined that feedback control is delay-limited, I have not considered realistic muscle dynamics in my simulations, and I did not limit the available torque depending on the velocity of the movement. In real life, an animal performing fast

perturbation responses will not be able to generate high torques at high muscle contraction velocities due to force-velocity properties of muscle. Therefore, perturbation responses involving large corrective movements and high velocities might still be force-limited instead of delay-limited. Due to insufficient literature to accurately model the muscle tendon architecture across the size range of terrestrial mammals, I did not incorporate Hill type muscles in my simulations. Perhaps, more biologically realistic multi-segmented and muscled neuro-musculoskeletal models that represent the response of a single species, and which can be fully parameterized based on literature, will be more appropriate to understanding the effects of incorporating realistic muscle dynamics.

To reach these conclusions, I had to make several assumptions and simplifications. I have carried over assumptions made in the estimation of parameters in previous publications, such as for the scaling of sensorimotor delays (More and Donelan, 2018) and the inertial delays (Thangal and Donelan, 2020). For example, for the scaling of sensorimotor delay, More et al. had assumed sensing delay, synaptic delay and neuro-muscular junction delay are constant across animal size based on limited information in the literature. In calculating isometric torque limits, I assumed that the triceps (swing task) and the ankle extensors (posture task) are the dominant muscles involved in moving their respective joints, that their antagonistic muscles scale similarly, and that the isometric stress produced by mammalian muscle is constant at 20 N/cm^2 (Rospars and Meyer-Vernet, 2016). Although animal limbs are actually multi jointed and muscled, I used pendular models to represent body segments, and a single pair of opposing muscles to actuate them (Alexander et al., 1981; Böhmer et al., 2020). I have also not considered several animal features that have been shown to change with animal size such as posture, limb stiffness, joint damping, and sensor accuracy; evaluating the effects of these features would require more complete neuromusculoskeletal models (Biewener, 2005; Garcia et al., 2000; More et al., 2010). I used a PD feedback controller as it is simple to implement, simple to interpret, and has been successfully used in the literature to model control of locomotion (Donelan and Pearson, 2004; Geyer et al., 2003; Hatz et al., 2012; Prochazka et al., 1997b; Welch and Ting, 2008). However, the actual control strategy implemented within the spinal reflex pathways is undoubtedly more complex, involving several control pathways with varying time delays and control strategies, and remains a topic of research (Nishikawa et

al., 2007; Prochazka et al., 1997c; Yakovenko et al., 2004; Zehr and Stein, 1999). In engineering control systems, there are advanced feedback controller types such as Model Predictive Control (MPC), or Smith-predictors, which can compensate for time delays and also generate bang-bang control. Here, I assumed that the spinal level synapses that represent the feedback controller do not encode these complex algorithms and use the simpler and more straightforward PD control instead. Here I have tried to estimate the limits of this neural control system by considering sensorimotor delays from the longest reflex pathways (transmitted twice the animal's leg length), which uses the least neural computation (a single synapse), and compared response times to the shortest available movement times (swing duration at maximum sprint speed). Using these highly simplified models and evaluating the limits of their performance as a function of animal size, I gain insight into the complex processes of animal locomotor control (Full et al., 1999). Given these assumptions, as well as the nature of any purely modeling approach, these results are estimates that need to be tested experimentally. One candidate experimental approach would be in-vivo experiments where the delays in sensory feedback or transmission of motor commands can be systematically manipulated while studying the response of the nervous system (Weiland et al., 1986).

While I find that time delays are detrimental to the control of fast perturbation responses, other studies have pointed out that the nervous system could use time delays to its benefit in certain control situations. Prochazka et al. studied how delayed positive feedback can help stabilize reflexive control pathways (Prochazka et al., 1997c). Nishikawa et al. show that time delays increase gains at the resonant frequency of a control system, which could assist in the control of rhythmic movements (Nishikawa et al., 2007). Milton et al. suggested that the nervous system could be implementing adaptive act-and-wait control strategies which use the interplay between noise and delays to simplify control (Milton et al., 2009; Milton, 2011). However, during my simulations, delays did not provide any benefits. For example, if an animal trips during early swing while running at high speed, it would want to react immediately, fully activating its muscles to rapidly and accurately place its foot forward to regain stability. Irrespective of the control strategy, the animal would lose the time required to sense the perturbation and transmit action potentials to the spinal cord. Under feedback control, the animal is further limited as it has to use low

gains in order to ensure a stable response, while the corrective movement might not be quick enough to prevent a fall. Under this scenario, and others like it, delays appear to only negatively affect the control of movement.

One implication of my findings is that the compensatory mechanisms used by animals to overcome the disadvantages caused by long sensorimotor delays will likely vary with animal size. Previous studies in small animals such as guinea fowl (Biewener and Daley, 2007; Daley and Biewener, 2006) and cockroaches (Dudek and Full, 2006; Garcia et al., 2000; Jindrich and Full, 2002) have shown that smaller animals rely more on feedforward control than feedback control for fast locomotion, and utilize the inherent mechanical properties of their musculoskeletal system (preflexes) to compensate for perturbations encountered during movement (Brown and Loeb, 2000). Garcia et al. showed that as animal size decreases, the damping ratio of their limbs increases—making small animals overdamped and larger animals underdamped (Garcia et al., 2000). Muscle forces applied to an overdamped limb will rapidly reposition itself and come to rest—the damping will prevent overshoot or oscillations. Therefore, smaller animals would prefer to use feedforward control, which can produce faster responses than feedback control while still ensuring stability. Muscle forces applied to an underdamped limb will cause it to accelerate quickly, which could result in overshoot and oscillations. Therefore, larger animals would prefer to use feedback control which can ensure accuracy and stability. My results further add to these studies, by showing that uncompensated feedback control is up to four times slower than feedforward control in the smallest animals, but only about two to one and a half times slower in the largest animals. If larger animals could compensate for sensorimotor delays and reduce feedback control response times to be shorter than available movement time, feedback control could perform comparably to feedforward control. Larger animals do not have highly damped joints, but synaptic delays make up a smaller proportion of overall response time (More and Donelan, 2018). These relatively shorter synaptic delays might allow larger animals to rely on more computationally expensive control strategies that combine feedback control with internal models that compensate for delays (Smith predictors) (Miall et al., 1993). My results show that as animal size increases, delayed feedback control is able to use more of the available muscle force capacity, narrowing the performance advantage that feedforward control has over

feedback control. Effective feedback control, when combined with the computational options available when synaptic delays are relatively short, may be a more viable control strategy for larger animals.

Chapter 6. Conclusion

While it is generally accepted that delays detrimentally affect biological control systems, there is a lack of literature quantifying these delays and their impact on the neural control of locomotion. In this thesis, I have used computational models to investigate the effect of delays on the neural control of fast perturbation responses as a function of animal size. I built on previous electrophysiological studies from my lab which quantified the sensorimotor delays that constitute the time required to transmit neural signals and process the motor commands required to respond to a perturbation (More and Donelan, 2018). In order to get a complete picture of response time, I had to quantify inertial delays—the time required to overcome inertia and reposition body segments as part of the perturbation response. In chapter 2, I studied a simple model of a rotor being repositioned under muscle torques, and used it to analytically derive estimates for inertial delays. I developed two different tasks designed to represent perturbation scenarios commonly encountered during animal locomotion: a swing leg repositioning task, and a posture recovery task. I showed that if muscle forces scaled with dynamic similarity, inertial delays would scale at the same rate as the time available to make a perturbation response. Therefore, larger animals would not be disproportionately burdened by inertial delays when compared to smaller animals. Instead, if muscle forces only scale with geometric similarity, inertial delays scale faster than the available time, making inertial delays a bigger problem for neural control in larger animals. Next, I used more biologically realistic models with anatomical, muscular and inertial properties parameterized with scaling values from literature, and numerically simulated them to get better estimates for inertial delays. My results showed that inertial delays depended both on movement task and movement size, and the results fell in between analytical predictions based on the scaling of muscle force with dynamic similarity vs. geometric similarity. As movement magnitude increased, inertial delays exceeded sensorimotor delays, and this occurred for smaller movements in larger animals. My results indicate that if small animals were trying to improve their response times by compensating for delays, they would benefit more from compensating for sensorimotor delays, as they are the larger source of delay. On the other hand, larger animals would benefit more from

reducing inertial delays, which could be achieved through postural changes or neural prediction.

In chapters 4 and 5, I compared feedback and feedforward control in their ability to perform fast perturbation responses. I first developed a normalized model of feedback control to understand how two factors affect response times: the ability of muscles to generate force and time delays in the feedback pathways. I showed that feedback control could be force-limited or delay-limited, and developed predictive equations for the relationship between normalized torque limits and response time. Next, I determined whether feedback control in animals of different sizes is force-limited or delay-limited, using more elaborate models scaled with animal size. My results showed that feedback control in animals of all sizes is delay-limited rather than force-limited. Feedback control response times also exceeded available movement times in animals of all sizes, while feedforward control did so only for the largest animals. Feedback control was about four times slower than feedforward control in the smallest animals, but only around two times slower in the largest animals. Thus, smaller animals are more likely to use feedforward control and preflexes to remain stable against perturbations. Larger animals would also depend predominantly on feedforward control, but could rely on feedback control with internal models that can compensate for delays and allow higher gains resulting in faster responses.

This research has both fundamental and applied importance. By studying which aspects of neural control are preserved and which ones are modified with animal size, I added to our understanding of the fundamental principles of the nervous system (More and Donelan, 2018). My results help understand the role of control in determining the limits of animal performance, such as top speed and agility. Developing algorithms that allow legged robots to independently maintain stability and locomotion has been challenging. Studying how evolution has tackled these control challenges gives us a better understanding of the variety of control methods which might have applications in legged locomotion.

6.1. Future work

Lack of sufficient data for several parameters limited the fidelity of my models, and new studies to quantify the scaling of these features will help build more accurate models for neural control in legged animals. Based on limited data from More et al., I assumed that the sensing delay, synaptic delay and neuromuscular junction delay components of sensorimotor delay are constant and do not change with size (More and Donelan, 2018). I could find only one publication which reported on the scaling of cross-sectional area and moment arm features of muscles in terrestrial mammals necessary to estimate the torque generated by them (Alexander et al., 1981). A recent publication by Bishop and colleagues reported on the scaling of limb muscle features in terrestrial mammals (Bishop et al., 2021). They grouped together muscles into proximal muscles (muscles with majority of their bulk above the elbow or knee) and distal muscles (muscles with most of their bulk below the elbow or knee), and reported values for the forelimb and hindlimb. They found that for proximal forelimb muscles, the muscle mass, muscle length, physiological cross-sectional area and force generation capacity scaled with $M^{1.01}$, $M^{0.27}$, $M^{0.73}$ and $M^{0.72}$, respectively. For the swing task, I used values of $M^{1.11}$, $M^{0.33}$, $M^{0.78}$ and $M^{0.78}$ respectively—based on values for the triceps reported by Alexander et al. Bishop and colleagues found that for distal hindlimb muscles, the muscle mass, muscle length, physiological cross-sectional area and force generation capacity scaled with $M^{0.90}$, $M^{0.20}$, $M^{0.78}$ and $M^{0.72}$, respectively. For the posture task, I used values of $M^{0.97}$, $M^{0.14}$, $M^{0.83}$ and $M^{0.83}$, respectively—based on values for the ankle extensors reported by Alexander et al. While the exponents reported by the two studies are generally similar, the differences could be due to Alexander et al. considering only individual muscles, whereas Bishop et al. considered all the proximal or distal muscles together. However, Bishop et al. do not report values for muscle moment arms, necessary to calculate muscle torques in my models. Publications that quantify the scaling of features of prime mover muscles of limbs in terrestrial mammals are needed, along similar lines to Dick and Clemente, who have compiled the scaling of muscle features in Verano lizards (Dick and Clemente, 2016). I have also not considered joint stiffness and damping in my simulations, as I could not find publications that have quantified the scaling of these features in terrestrial mammals. In my studies on both inertial delays and

perturbation response times, predictions and trends from simple models matched well with more biologically realistic simulations. This gives me confidence that my predictions will continue to be relevant in even more elaborate and morphologically accurate multi-jointed and multi-muscled models. These future studies can check if my assumptions and simplifications hold true, and shed light on how factors that I have not considered affect my results.

Perturbation studies involving the manipulation of sensorimotor delays in-vivo can shed light on the control strategies used by the nervous system. Several studies have investigated the effects of removing sensory feedback on locomotor behavior in animal models (Donelan and Pearson, 2004; Gordon et al., 2020; Rossignol et al., 2006; Stapley et al., 2002). Instead of removing sensory feedback, we could decrease the nerve conduction velocity using cooling techniques to increase the sensorimotor delays in the reflex (Herrera et al., 2010; Todnem et al., 1989). Such experiments would have to devise ways to cool only the nerves while minimizing changes to the muscle, perhaps by using nerve cuffs (Haugland and Hoffer, 1994). Animals use a combination of feedforward control and feedback control, with feedback control dominating the response for slower movements, and feedforward control dominating at faster movements (Daley, 2018; Dickinson et al., 2000; Gordon et al., 2020). I hypothesize that increasing sensorimotor delays would detrimentally affect feedback control more than feedforward control, causing feedforward control to dominate the response at slower movement speeds. We can design perturbation studies that elicit stumble corrective responses or posture recovery responses, and analyse the EMG signals to differentiate the feedforward and feedback contributions to the response (Eng et al., 1994; Gordon et al., 2020; Welch and Ting, 2008). We should also study how the control strategies scale with perturbation size, with the largest perturbations resulting in a fall, as this will elicit the fastest possible responses. Such studies would help validate my predictions, and improve our understanding of how the nervous system deals with time delays.

I have also used torque actuation in my simulations and have not incorporated Hill-type muscle models. In my simulations, I have considered electromechanical delay (after the motor signal has crossed the neuromuscular junction, time required for action potentials

to travel over the muscle, release Ca^{2+} ions from the sarcoplasmic reticulum, and start cross bridge cycling) and force generation delay (time from detection of force in the muscle to peak twitch force) (Section 1.4.1). These two components are the dominant contributors to sensorimotor delay time across animal size (More and Donelan, 2018). These constant time delays approximate the activation-deactivation dynamics and the gradual increase in forces seen in real muscle. I could remove these constant delays and incorporate Hill-type muscle models. However, I would require parameters to characterize the activation-deactivation dynamics, force-length relationship, force-velocity relationship, pennation angle, parallel elastic element properties and series elastic element properties—for the shoulder flexor and extensor muscles (swing task), and the ankle dorsiflexor and plantarflexor muscles (posture task). For my simulations, I used the muscle mass, muscle length and moment arm data for the triceps and ankle plantarflexor muscles from Alexander et al. to determine the maximum isometric force (F_{musc}), assuming muscle density of 1060 kg/m^3 (Méndez and Keys, 1960), and maximum isometric stress to be 20 N/cm^2 (Close, 1972; Rospars and Meyer-Vernet, 2016). I could use these same values to parametrize scaled Hill-type muscle models (Zajac, 1989). I could parameterize the force-length curve by setting the peak of the force-length curve to F_{musc}, and the optimal fiber length and force-length relationship width to equal muscle length. I can similarly characterize the force-velocity curve, setting the force intercept to F_{musc}, the velocity intercept to be 10 muscle lengths/sec, and eccentric contraction force to be $1.5F_{musc}$. I could also assume that the muscles acting at F_{musc} produce a stress of 32 Mpa in the tendon causing a strain of 3.3 %, to calculate series elastic element stiffness. However, scaling studies have reported that several of these parameters that Zajac assumes are constant do change with animal size, such as fiber type distribution and maximum shortening velocity (Marx et al., 2006; Medler, 2002). Shadwick and Pollock provide scaling equations for gastrocnemius tendon elastic modulus, cross-sectional area and slack length, which I can use to calculate tendon stiffness (Pollock and Shadwick, 1994a, 1994b). However, I have not been able to find similar series elastic element parameters for the shoulder muscles, and the parallel elastic element properties for either set of muscles. While adding Hill type muscle models will make my simulations more biologically realistic, this would also reduce the fidelity of my models due to the

increased number of parameters and the variability in the reported values of these parameters in the literature.

Certain features of muscle behavior that are not captured by Hill-type muscle models—such as short-range stiffness, history dependent effects and muscle internal mass effects—can also influence perturbation responses. Muscles exhibit short-range stiffness, a large increase in force beyond what is predicted by the force-length curve, for a short range at the beginning of a muscle stretch movement (Rack and Westbury, 1974). De Groote et al. have shown that short-range stiffness has to be considered to accurately simulate the preflexive part of the response to a support surface translation perturbation in standing humans (De Groote et al., 2017). Muscles also exhibit history dependent effects which can be important for perturbation responses. The forces generated by a muscle depend not just on its present activation, length, and velocity—but also on the movement preceding the present state (Lin, 2009). Lin and Rymer conducted postural response experiments with mass loads—and showed that the initial short-range stiffness after a perturbation acted as a spring to return the body to its original posture, while the subsequent reduction in muscle forces prevented oscillations that could arise from the spring-like initial response (Lin and Rymer, 2000). Ross et al. have shown that the internal mass of the muscle also affects its maximum contraction velocity and force production, indicating that Hill-type muscle models might overestimate the perturbation rejection capabilities in larger animals (Ross et al., 2018b; Ross and Wakeling, 2016). New muscle models which can emulate these features of muscle behavior, such as cross-bridge models, titin-clutch models and mass enhanced Hill-type models, can improve simulations of perturbation responses (Campbell, 2009; Nishikawa, 2020; Ross et al., 2018a).

While this thesis focusses on the effect of delays on the response time to a perturbation, we can use similar modeling approaches to evaluate the effect of delays on stability against perturbation responses. We could implement the simplest models of rhythmic limit-cycle locomotion such as walking or hopping gait with time-delayed neural control and realistic muscle dynamics (Blickhan, 1989; Geyer et al., 2003; Seyfarth et al., 2003)—and quantify stability using stability measures such as the Lyapunov exponent or Gait Sensitivity Norm (Bruijn et al., 2011; Dingwell and Cusamano, 2000; Hobbelen and

Wisse, 2007; Lockhart and Liu, 2008; Thangal et al., 2013). Several muscle features such as their force-length and force-velocity properties, short range stiffness and history dependent behavior have been shown to be important to the stability of limit-cycle gaits (Gerritsen et al., 1998; Lin, 2009). The collision of the foot with the ground during rhythmic locomotion is also important for stability (Daley, 2018; Wong and Donelan, 2017). Future studies should explore how time-delayed control, rhythmic locomotion and realistic muscle models interact, and how this affects stability of locomotion.

Research suggests that animals use state estimation and internal models to compensate for sensorimotor delays, and animals of different sizes could require different levels of complexity in their internal models for effective locomotion (Miall et al., 1993; Wolpert and Ghahramani, 2000; Wolpert and Kawato, 1998). While the sensorimotor delays experienced by an animal are fixed, inertial delays vary with movement size and movement task. My results indicate that sensorimotor delays would be the dominant contributor to response time in smaller animals, while inertial delays would be the dominant contributor in larger animals (Section 3.3.3). To the best of my knowledge, synaptic delay (the time required for an action potential to cross a single synapse) is about 0.7 ms and does not change significantly with animal size (More and Donelan, 2018), while movement times do scale steeply with animal size (Heglund et al., 1974; Heglund and Taylor, 1988). Larger animals could use the increased computation time available to them to employ more complex and accurate internal models to compensate for the longer delays faced by them, and we could test this idea using simulations. Synaptic delay can also represent the time required for the multi-synaptic neuronal computations associated with state estimation. Since synaptic delay takes up a smaller fraction of the available movement time as animal size increases, this could promote the use of more computational resources for state estimation in larger animals. Alternatively, we could find that increased internal model complexity is not needed—simple internal models could prove effective in compensating for delays and producing effective motor control in animals of all sizes. A candidate internal model is the Smith Predictor, which is specifically designed to compensate for time delays (Miall et al., 1993; Nise, 2011). The Smith Predictor adds two more loops with internal models to the original feedback control system; these additional feedback loops predict the time delayed feedback from the original feedback system and

cancel out the time delayed feedback. Theoretically, this allows the feedback controller to use high gains without the risk of instability. The effectiveness of using state estimation depends on the accuracy of the internal models, and we have to vary the accuracy of the internal models in the simulation. We could use artificial neural networks with increasing layers to simulate increased complexity. If larger animals require more layers to accurately compensate for delays, this would support the idea that different sized animals require different levels of complexity in their internal models for effective locomotion.

Recent findings have challenged the assumption that neural computations occur only at the synapse, and that complex computations require multi-synaptic circuits (Gidon et al., 2020). In this thesis, I have assumed that control of the perturbation responses that I have modeled are mediated through mono-synaptic reflexes—hence, it can only encode simple control algorithms. Gidon et al. showed that the dendrites within the body of a single human layer 2/3 cortical neuron can perform XOR computations, previously thought to require at least two layers of neural synapses (Gidon et al., 2020). This study indicates that we underestimate the computational power of neurons. A monosynaptic reflex itself could potentially encode complex controllers which could compensate for noise and time delays, and produce faster control than predicted by my simulations.

References

Alexander, R.M., 2003. Principles of animal locomotion, 1st ed. Princeton University Press, Princeton, New Jersey.

Alexander, R.M., 2002. Stability and manoeuvrability of terrestrial vertebrates. Integr Comp Biol 42, 158–164. https://doi.org/10.1093/icb/42.1.158

Alexander, R.M., Jayes, A.S., 1983. A dynamic similarity hypothesis for the gait of quadruped mammals. J. Zool. 201, 135–152.

Alexander, R.M., Jayes, A.S., Maloiy, G.M.O., Wathuta, E.M., 1981. Allometry of the leg muscles of mammals. J. Zool. 194, 539–552. https://doi.org/10.1111/j.1469-7998.1981.tb04600.x

Åström, K.J., Murray, R.M., 2008. Feedback systems: an introduction for scientists and engineers, Princeton University Press. Princeton University Press, Princeton, New Jersey.

Bechhoefer, J., 2021. Control Theory for Physicists. Cambridge University Press, Cambridge, GB.

Biewener, A.A., 2005. Biomechanical consequences of scaling. J. Exp. Biol. 208, 1665–1676. https://doi.org/10.1242/jeb.01520

Biewener, A.A., 1990. Biomechanics of mammalian terrestrial locomotion. Science 250, 1097–1103. https://doi.org/10.1126/science.2251499

Biewener, A.A., 1989a. Scaling body support in mammals: limb posture and muscle mechanics. Science 245, 45–48.

Biewener, A.A., 1989b. Scaling body support in mammals: limb posture and muscle mechanics. Science 245, 45–48. https://doi.org/10.1126/science.2740914

Biewener, A.A., 1983. Allometry of quadrupedal locomotion: the scaling of duty factor, bone curvature and limb orientation to body size. J. Exp. Biol. 105, 147–171.

Biewener, A.A., Daley, M.A., 2007. Unsteady locomotion: integrating muscle function with whole body dynamics and neuromuscular control. J. Exp. Biol. 210, 2949–2960. https://doi.org/10.1242/jeb.005801

Bishop, P.J., Wright, M.A., Pierce, S.E., 2021. Whole-limb scaling of muscle mass and force-generating capacity in amniotes. PeerJ 9, e12574.

Blickhan, R., 1989. The spring-mass model for running and hopping. J. Biomech. 22, 1217–1227. https://doi.org/10.1016/0021-9290(89)90224-8

Böhmer, C., Theil, J.-C., Fabre, A.-C., Herrel, A., 2020. Atlas of Terrestrial Mammal Limbs. CRC Press, Boca Raton.

Bonner, J.T., 2011. Why size matters. Princeton University Press, Princeton, New Jersey.

Brown, I., Loeb, G., 2000. A reductionist approach to creating and using neuromusculoskeletal models. Biomech. neural Control posture Mov. 148–163. https://doi.org/10.1007/978-1-4612-2104-3_10

Bruijn, S.M., Bregman, D.J.J., Meijer, O.G., Beek, P.J., van Dieën, J.H., 2011. Maximum Lyapunov exponents as predictors of global gait stability: A modelling approach. Med. Eng. Phys. 34, 428–436. https://doi.org/10.1016/j.medengphy.2011.07.024

Buchanan, T.S., 1995. Evidence that maximum muscle stress is not a constant: differences in specific tension in elbow flexors and extensors. Med. Eng. Phys. 17, 529–536. https://doi.org/10.1016/1350-4533(95)00005-8

Buckland, S.T., 1984. Monte Carlo Confidence Intervals. Biometrics 40, 811–817. https://doi.org/10.2307/2530926

Burke, R.E., Levine, D.N., Tsairis, P., Zajac, F.E., 1973. Physiological types and histochemical profiles in motor units of the cat gastrocnemius. J. Physiol. 234, 723–748.

Campbell, K.S., 2009. Interactions between connected half-sarcomeres produce emergent mechanical behavior in a mathematical model of muscle. PLoS Comput. Biol. 5, e1000560.

Cao, Y.-Y., Lin, Z., Hu, T., 2002. Stability analysis of linear time-delay systems subject to input saturation. IEEE Trans. Circuits Syst. I Fundam. Theory Appl. 49, 233–240.

Close, R.I., 1972. Dynamic properties of mammalian skeletal muscles. Physiol. Rev. 52, 129–197. https://doi.org/10.1152/physrev.1972.52.1.129

Cowan, N.J., Ankarali, M.M., Dyhr, J.P., Madhav, M.S., Roth, E., Sefati, S., Sponberg, S., Stamper, S.A., Fortune, E.S., Daniel, T.L., 2014. Feedback control as a framework for understanding tradeoffs in biology, in: Integrative and Comparative Biology. pp. 223–237. https://doi.org/10.1093/icb/icu050

Daley, M.A., 2018. Understanding the agility of running birds: sensorimotor and mechanical factors in avian bipedal locomotion. Integr. Comp. Biol. 58, 884–893.

Daley, M.A., Biewener, A.A., 2011. Leg muscles that mediate stability: mechanics and control of two distal extensor muscles during obstacle negotiation in the guinea fowl. Philos. Trans. R. Soc. B Biol. Sci. 366, 1580–1591.

Daley, M.A., Biewener, A.A., 2006. Running over rough terrain reveals limb control for intrinsic stability. Proc. Natl. Acad. Sci. 103, 15681–15686. https://doi.org/10.1073/pnas.0601473103

Daley, M.A., Voloshina, A., Biewener, A.A., 2009. The role of intrinsic muscle mechanics in the neuromuscular control of stable running in the guinea fowl. J. Physiol. 587, 2693–2707.

Dallmann, C.J., Karashchuk, P., Brunton, B.W., Tuthill, J.C., 2021. A leg to stand on: Computational models of proprioception. Curr. Opin. Physiol. 22, 100426.

De Groote, F., Allen, J.L., Ting, L.H., 2017. Contribution of muscle short-range stiffness to initial changes in joint kinetics and kinematics during perturbations to standing balance: A simulation study. J. Biomech. 55, 71–77.

Delp, S.L., Anderson, F.C., Arnold, A.S., Loan, P., Habib, A., John, C.T., Guendelman, E., Thelen, D.G., 2007. OpenSim: Open-source software to create and analyze dynamic simulations of movement. IEEE Trans. Biomed. Eng. 54, 1940–1950. https://doi.org/10.1109/TBME.2007.901024

Dick, T.J.M., Clemente, C.J., 2016. How to build your dragon: scaling of muscle architecture from the world's smallest to the world's largest monitor lizard. Front. Zool. 13, 1–17.

Dickinson, M.H., Farley, C.T., Full, R.J., Koehl, M.A.R., Kram, R., Lehman, S., 2000. How Animals Move: An Integrative View. Science 288, 100–106. https://doi.org/10.1126/science.288.5463.100

Dingwell, J.B., Cusamano, J., 2000. Nonlinear time series analysis of normal and pathological human walking. Chaos 10, 848–863.

Donelan, J.M., Pearson, K.G., 2004. Contribution of Force Feedback to Ankle Extensor Activity in Decerebrate Walking Cats. J. Neurophysiol. 92, 2093–2104. https://doi.org/10.1152/jn.00325.2004

Dudek, D.M., Full, R.J., 2006. Passive mechanical properties of legs from running insects. J. Exp. Biol. 209, 1502–15. https://doi.org/10.1242/jeb.02146

Economos, A.C., 1981. The largest land mammal. J. Theor. Biol. 89, 211–214.

Eng, J.J., Winter, D.A., Patla, A.E., 1994. Strategies for recovery from a trip in early and

late swing during human walking. Exp. Brain Res. 102, 339–349. https://doi.org/10.1007/BF00227520

Fang, H., Lin, Z., 2006. A further result on global stabilization of oscillators with bounded delayed input. IEEE Trans. Automat. Contr. 51, 121–128.

Ferris, D.P., Liang, K., Farley, C.T., 1999. Runners adjust leg stiffness for their first step on a new running surface. J. Biomech. 32, 787–794.

Forssberg, H., 1979. Stumbling corrective reaction: a phase-dependent compensatory reaction during locomotion. J. Neurophysiol. 42, 936–953.

Full, R.J., Koditschek, D.E., Full, R.J., 1999. Templates and anchors: neuromechanical hypotheses of legged locomotion on land. J. Exp. Biol. 2, 3–125.

Garcia, M.S., Kuo, A.D., Peattie, A., Wang, P., Full, R.J., 2000. Damping And Size: Insights And Biological Inspiration, in: International Symposium on Adaptive Motion of Animals and Machines.

Gerritsen, K.G., van den Bogert, a J., Hulliger, M., Zernicke, R.F., 1998. Intrinsic muscle properties facilitate locomotor control - a computer simulation study. Motor Control 2, 206–220. https://doi.org/10.1123/mcj.2.3.206

Geyer, H., Seyfarth, A., Blickhan, R., 2003. Positive force feedback in bouncing gaits? Proc. R. Soc. London. Ser. B Biol. Sci. 270, 2173–2183.

Gidon, A., Zolnik, T.A., Fidzinski, P., Bolduan, F., Papoutsi, A., Poirazi, P., Holtkamp, M., Vida, I., Larkum, M.E., 2020. Dendritic action potentials and computation in human layer 2/3 cortical neurons. Science 367, 83–87.

Goldfarb, M., Sirithanapipat, T., 1999. Effect of actuator saturation on the performance of PD-controlled servo systems. Mechatronics 9, 497–511. https://doi.org/10.1016/S0957-4158(99)00013-6

Gordon, J.C., Holt, N.C., Biewener, A., Daley, M.A., 2020. Tuning of feedforward control enables stable muscle force-length dynamics after loss of autogenic proprioceptive feedback. Elife 9, e53908. https://doi.org/10.7554/eLife.53908

Grillner, S., 1972. The Role of Muscle Stiffness in Meeting the Changing Postural and Locomotor Requirements for Force Development by the Ankle Extensors. Acta Physiol. Scand. 86, 92–108. https://doi.org/10.1111/j.1748-1716.1972.tb00227.x

Halliday, D., Resnick, R., Walker, J., 2010. Fundamentals of Physics, 9th ed. John Wiley & Sons, New York, NY.

Hatz, K., Mombaur, K., Donelan, J.M., 2012. Control of ankle extensor muscle activity in walking cats. J. Neurophysiol. 108, 2785–2793. https://doi.org/10.1152/jn.00944.2011

Haugland, M.K., Hoffer, J.A., 1994. Slip information provided by nerve cuff signals: application in closed-loop control of functional electrical stimulation. IEEE Trans. Rehabil. Eng. 2, 29–36.

Heglund, N.C., Taylor, C.R., 1988. Speed, stride frequency and energy cost per stride: how do they change with body size and gait? J. Exp. Biol. 138, 301–318.

Heglund, N.C., Taylor, C.R., McMahon, T.A., 1974. Scaling Stride Frequency and Gait to Animal Size: Mice to Horses. Science 186, 1112–1113. https://doi.org/10.1126/science.186.4169.1112

Herrera, E., Sandoval, M.C., Camargo, D.M., Salvini, T.F., 2010. Motor and sensory nerve conduction are affected differently by ice pack, ice massage, and cold water immersion. Phys. Ther. 90, 581–591.

Herzfeld, D.J., Shadmehr, R., 2014. Cerebellum estimates the sensory state of the body. Trends Cogn. Sci. https://doi.org/10.1016/j.tics.2013.10.015

Hobbelen, D.G.E., Wisse, M., 2007. A Disturbance Rejection Measure for Limit Cycle Walkers: The Gait Sensitivity Norm. IEEE Trans. Robot. 23, 1213–1224.

Hof, A.L., 1996. Scaling gait data to body size. Gait Posture 3, 222–223. https://doi.org/10.1016/0966-6362(95)01057-2

Hooper, S.L., 2012. Body size and the neural control of movement. Curr. Biol. 22, R318–R322. https://doi.org/10.1016/j.cub.2012.02.048

Hooper, S.L., Guschlbauer, C., Blümel, M., Rosenbaum, P., Gruhn, M., Akay, T., Büschges, A., Blumel, M., Rosenbaum, P., Gruhn, M., Akay, T., Buschges, A., 2009. Neural control of unloaded leg posture and of leg swing in stick insect, cockroach, and mouse differs from that in larger animals. J. Neurosci. 29, 4109–4119. https://doi.org/10.1523/JNEUROSCI.5510-08.2009

Horak, F.B., Nashner, L.M., 1986. Central programming of postural movements: adaptation to altered support-surface configurations. J. Neurophysiol. 55, 1369–1381. https://doi.org/10.1152/jn.1986.55.6.1369

Hutchinson, J.R., Garcia, M., 2002. Tyrannosaurus was not a fast runner. Nature 415, 1018–1021. https://doi.org/10.1038/4151018a

Insperger, T., Milton, J., Stepan, G., 2015. Semi-discretization and the time-delayed PDA

feedback control of human balance, in: IFAC-PapersOnLine. pp. 93–98. https://doi.org/10.1016/j.ifacol.2015.09.360

Insperger, T.T., 2006. Act-and-wait concept for continuous-time control systems with feedback delay. IEEE Trans. Control Syst. Technol. 14, 974–977. https://doi.org/10.1109/TCST.2006.876938

Jindrich, D.L., Full, R.J., 2002. Dynamic stabilization of rapid hexapedal locomotion. J. Exp. Biol. 205, 2803–2822.

Jürgens, K.D., 2002. Etruscan shrew muscle: the consequences of being small. J. Exp. Biol. 205, 2161–2166.

Kilbourne, B.M., Hoffman, L.C., 2013. Scale effects between body size and limb design in quadrupedal mammals. PLoS One 8, e78392.

Kuo, A.D., 2002. The relative roles of feedforward and feedback in the control of rhythmic movements. Motor Control 6, 129–145. https://doi.org/10.1123/mcj.6.2.129

Kuo, A.D., 1999. Stabilization of Lateral Motion in Passive Dynamic Walking. Int. J. Rob. Res. 18, 917–930. https://doi.org/10.1177/02783649922066655

LaBarbera, M., 1989. Analyzing Body Size as a Factor in Ecology and Evolution. Annu. Rev. Ecol. Syst. 20, 97–117. https://doi.org/10.1146/annurev.es.20.110189.000525

Larramendi, A., 2015. Shoulder height, body mass, and shape of proboscideans. Acta Palaeontol. Pol. 61, 537–574.

Libby, T., Johnson, A.M., Chang-Siu, E., Full, R.J., Koditschek, D.E., 2016. Comparative Design, Scaling, and Control of Appendages for Inertial Reorientation. IEEE Trans. Robot. PP. https://doi.org/10.1109/TRO.2016.2597316

Lin, D.C., 2009. History-Dependent Properties of Skeletal Muscle BT - Encyclopedia of Neuroscience, in: Binder, M.D., Hirokawa, N., Windhorst, U. (Eds.), Encyclopedia of Neuroscience. Springer Berlin Heidelberg, Berlin, Heidelberg, pp. 1856–1859. https://doi.org/10.1007/978-3-540-29678-2_2223

Lin, D.C., Rymer, W.Z., 2000. Damping actions of the neuromuscular system with inertial loads: soleus muscle of the decerebrate cat. J. Neurophysiol. 83, 652–658.

Lin, Z., Fang, H., 2007. On asymptotic stabilizability of linear systems with delayed input. IEEE Trans. Automat. Contr. 52, 998–1013.

Lloyd, D.P.C., 1943. Conduction and synaptic transmission of the reflex response to stretch in spinal cats. J. Neurophysiol. 6, 317–326. https://doi.org/10.1152/jn.1943.6.4.317

Lockhart, T.E., Liu, J., 2008. Differentiating healthy and fall-prone adults using local dynamic stability. Ergonomics 51, 1860–1872.

Loeb, G.E., Pratt, C.A., Chanaud, C.M., Richmond, F.J.R., 1987. Distribution and innervation of short, interdigitated muscle fibers in parallel-fibered muscles of the cat hindlimb. J. Morphol. 191, 1–15. https://doi.org/10.1002/jmor.1051910102

Madhav, M.S., Cowan, N.J., 2020. The synergy between neuroscience and control theory: the nervous system as inspiration for hard control challenges. Annu. Rev. Control. Robot. Auton. Syst. 3, 243–267.

Marx, J.O., Olsson, M.C., Larsson, L., 2006. Scaling of skeletal muscle shortening velocity in mammals representing a 100,000-fold difference in body size. Pflügers Arch. J Physiol 452, 222–230.

Matthews, P.B., 1964. Muscle spindles and their motor control. Physiol. Rev. 44, 219–288. https://doi.org/10.1152/physrev.1964.44.2.219

Mazenc, F., Mondié, S., Niculescu, S.-I., 2004. Global stabilization of oscillators with bounded delayed input. Syst. Control Lett. 53, 415–422.

Mazenc, F., Mondié, S., Niculescu, S.-I., 2003. Global asymptotic stabilization for chains of integrators with a delay in the input. IEEE Trans. Automat. Contr. 48, 57–63.

Mcgeer, T., 1990. Passive Bipedal Running. Proc. R. Soc. Ser. B-Biological Sci. 240, 107–134.

McMahon, T.A., 1975. Using body size to understand the structural design of animals: quadrupedal locomotion. J. Appl. Physiol. 39, 619–627.

McMahon, T.A., Bonner, J.T., 1983. On size and life. Scientific American Library.

Medler, S., 2002. Comparative trends in shortening velocity and force production in skeletal muscles. Am. J. Physiol. Integr. Comp. Physiol. 283, R368–R378. https://doi.org/10.1152/ajpregu.00689.2001

Méndez, J., Keys, A., 1960. Density and composition of mammalian muscle. Metab. Exp. 9, 184–188.

Miall, R.C., Weir, D.J., Wolpert, D.M., Stein, J.F., 1993. Is the cerebellum a smith predictor? J. Mot. Behav. 25, 203–216.

Milton, J., Cabrera, J.L., Ohira, T., Tajima, S., Tonosaki, Y., Eurich, C.W., Campbell, S.A., 2009. The time-delayed inverted pendulum: Implications for human balance control. Chaos 19. https://doi.org/10.1063/1.3141429

Milton, J., Insperger, T., 2019. Acting together, destabilizing influences can stabilize human balance. Philos. Trans. R. Soc. A 377, 20180126.

Milton, J.G., 2015. Time delays and the control of biological systems : An overview, in: Proceedings of IFAC TDS 2015.

Milton, J.G., 2011. The delayed and noisy nervous system: Implications for neural control. J. Neural Eng. 8, 065005. https://doi.org/10.1088/1741-2560/8/6/065005

Mochon, S., McMahon, T.A., 1980. Ballistic Walking. J. Biomech. 13, 49–57.

More, H.L., 2013. Scaling of sensorimotor control in terrestrial mammals. Simon Fraser Univ. Simon Fraser University, Burnaby, B.C., Canada.

More, H.L., Chen, J., Gibson, E., Donelan, J.M., Beg, M.F., 2011. A semi-automated method for identifying and measuring myelinated nerve fibers in scanning electron microscope images. J. Neurosci. Methods 201, 149–158.

More, H.L., Donelan, J.M., 2018. Scaling of sensorimotor delays in terrestrial mammals. Proc. R. Soc. B Biol. Sci. 285, 20180613.

More, H.L., Hutchinson, J.R., Collins, D.F., Weber, D.J., Aung, S.K.H., Donelan, J.M., 2010. Scaling of sensorimotor control in terrestrial mammals. Proc. R. Soc. B Biol. Sci. 277, 3563–3568.

More, H.L., O'Connor, S.M., Brøndum, E., Wang, T., Bertelsen, M.F., Grøndahl, C., Kastberg, K., Hørlyck, A., Funder, J., Donelan, J.M., 2013. Sensorimotor responsiveness and resolution in the giraffe. J. Exp. Biol. 216, 1003–1011.

Moritz, C.T., Farley, C.T., 2006. Human hoppers compensate for simultaneous changes in surface compression and damping. J. Biomech. 39, 1030–1038. https://doi.org/10.1016/j.jbiomech.2005.02.011

Mörl, F., Siebert, T., Schmitt, S., Blickhan, R., Günther, M., 2012. Electro-mechanical delay in hill-type muscle models. J. Mech. Med. Biol. 12, 1250085. https://doi.org/10.1142/S0219519412500856

Nise, N.S., 2011. Control Systems Engineering, 6th ed. John Wiley & Sons Inc.

Nishikawa, K., 2020. Titin: A Tunable Spring in Active Muscle. Physiology 35, 209–217. https://doi.org/10.1152/physiol.00036.2019

Nishikawa, K., Biewener, A.A., Aerts, P., Ahn, A.N., Chiel, H.J., Daley, M.A., Daniel, T.L., Full, R.J., Hale, M.E., Hedrick, T.L., Lappin, A.K., Nichols, T.R., Quinn, R.D., Satterlie, R.A., Szymik, B., 2007. Neuromechanics: An integrative approach for

understanding motor control. Integr. Comp. Biol. 47, 16–54. https://doi.org/10.1093/icb/icm024

Norberg, R.Å., Aldrin, B.S.W., 2010. Scaling for stress similarity and distorted-shape similarity in bending and torsion under maximal muscle forces concurs with geometric similarity among different-sized animals. J. Exp. Biol. 213, 2873–88. https://doi.org/10.1242/jeb.044180

Pearson, K., Gordon, J., 2000. Spinal Reflexes, in: Principles of Neural Science. pp. 713–736.

Pollock, C.M., Shadwick, R.E., 1994a. Allometry of muscle, tendon, and elastic energy storage capacity in mammals. Am. J. Physiol. 266, R1022–R1031.

Pollock, C.M., Shadwick, R.E., 1994b. Relationship between body mass and biomechanical properties of limb tendons in adult mammals. Am. J. Physiol. 266, R1016–R1021.

Powell, M.J.D., 1968. A FORTRAN subroutine for solving systems of nonlinear algebraic equations., Atomic Energy Research Establishment. Harwell (England).

Preacher, K.J., Selig, J.P., 2012. Advantages of Monte Carlo Confidence Intervals for Indirect Effects. Commun. Methods Meas. 6, 77–98. https://doi.org/10.1080/19312458.2012.679848

Prochazka, A., Gillard, D., Bennett, D.J., 1997a. Implications of positive feedback in the control of movement. J. Neurophysiol. https://doi.org/10.1152/jn.1997.77.6.3237

Prochazka, A., Gillard, D., Bennett, D.J., 1997b. Positive force feedback control of muscles. J. Neurophysiol. 77, 3226–3236.

Prochazka, A., Gillard, D., Bennett, D.J., 1997c. Implications of positive feedback in the control of movement. J. Neurophysiol. 77, 3237–3251. https://doi.org/10.1152/jn.1997.77.6.3237

Rack, P.M.H., Westbury, D.R., 1974. The short range stiffness of active mammalian muscle and its effect on mechanical properties. J. Physiol. 240, 331–350.

Rajagopal, A., Dembia, C.L., DeMers, M.S., Delp, D.D., Hicks, J.L., Delp, S.L., 2016. Full body musculoskeletal model for muscle- driven simulation of human gait. IEEE Trans. Biomed. Eng. 63, 2068–2079. https://doi.org/10.1109/TBME.2016.2586891

Rao, V.G., Bernstein, D.S., 2001. Naive control of the double integrator. IEEE Control Syst. Mag. 21, 86–97. https://doi.org/10.1109/37.954521

Rios, E., Pizarro, G., Stefani, E., 1992. Charge movement and the nature of signal transduction in skeletal muscle excitation-contraction coupling. Annu. Rev. Physiol. 54, 109–133.

Rospars, J.-P., Meyer-Vernet, N., 2016. Force per cross-sectional area from molecules to muscles: a general property of biological motors. R. Soc. open Sci. 3, 160313.

Ross, S.A., Nigam, N., Wakeling, J.M., 2018a. A modelling approach for exploring muscle dynamics during cyclic contractions. PLoS Comput Biol 14. https://doi.org/10.1371/journal.pcbi.1006123

Ross, S.A., Ryan, D.S., Dominguez, S., Nigam, N., Wakeling, J.M., 2018b. Size, history-dependent, activation and three-dimensional effects on the work and power produced during cyclic muscle contractions. Integr. Comp. Biol. 58, 232–250.

Ross, S.A., Wakeling, J.M., 2016. Muscle shortening velocity depends on tissue inertia and level of activation during submaximal contractions. Biol. Lett. 12, 20151041. https://doi.org/10.1098/rsbl.2015.1041

Rossignol, S., Dubuc, R., Gossard, J.-P.P., 2006. Dynamic Sensorimotor Interactions in Locomotion. Physiol. Rev. 86, 89–154.

Ruina, A., Pratap, R., 2015. Introduction to Statics and Dynamics. Oxford University Press, Inc. (Preprint).

Rushmer, D.S., Russell, C.J., Macpherson, J., Phillips, J.O., Dunbar, D.C., 1983. Automatic postural responses in the cat: responses to headward and tailward translation. Exp. brain Res. 50, 45–61. https://doi.org/10.1007/BF00238231

Ryu, H.X., Kuo, A.D., 2021. An optimality principle for locomotor central pattern generators. Sci. Rep. 11, 1–18.

Seyfarth, A., Geyer, H., Herr, H., 2003. Swing-leg retraction: a simple control model for stable running. J. Exp. Biol. 206, 2547–2555. https://doi.org/10.1242/jeb.00463

Skogestad, S., 2001. Probably the best simple PID tuning rules in the world, in: AIChE Annual Meeting, Reno, Nevada.

Srinivasan, M., 2010. Fifteen observations on the structure of energy-minimizing gaits in many simple biped models. J. R. Soc. Interface 8, 74–98. https://doi.org/10.1098/rsif.2009.0544

Stapley, P.J., Ting, L.H., Hulliger, M., Macpherson, J.M., 2002. Automatic postural responses are delayed by pyridoxine-induced somatosensory loss. J. Neurosci. 22, 5803–5807.

Taga, G., 1995a. A model of the neuro-musculo-skeletal system for human locomotion - II. Real-time adaptability under various constraints. Biol. Cybern. 73, 113–121. https://doi.org/10.1007/BF00204049

Taga, G., 1995b. A model of the neuro-musculo-skeletal system for human locomotion - I. Emergence of basic gait. Biol. Cybern. 73, 97–111. https://doi.org/10.1007/BF00204048

Thangal, S.N.M., Donelan, J.M., 2020. Scaling of inertial delays in terrestrial mammals. PLoS One 15, e0217188. https://doi.org/10.1371/journal.pone.0217188

Thangal, S.N.M., Talaty, M., Balasubramanian, S., 2013. Assessment of gait sensitivity norm as a predictor of risk of falling during walking in a neuromusculoskeletal model. Med. Eng. Phys. 35, 1483–1489.

Ting, L.H., Macpherson, J.M., 2004. Ratio of Shear to Load Ground-Reaction Force May Underlie the Directional Tuning of the Automatic Postural Response to Rotation and Translation. J. Neurophysiol. 92, 808–823. https://doi.org/10.1152/jn.00773.2003

Todnem, K., Knudsen, G., Riise, T., Nyland, H., Aarli, J.A., 1989. The non-linear relationship between nerve conduction velocity and skin temperature. J. Neurol. Neurosurg. Psychiatry 52, 497–501. https://doi.org/10.1136/jnnp.52.4.497

Todorov, E., 2004. Optimality principles in sensorimotor control. Nat. Neurosci. https://doi.org/10.1038/nn1309

Todorov, E., Jordan, M.I., 2002. Optimal feedback control as a theory of motor coordination. Nat. Neurosci. 5, 1226–1235. https://doi.org/10.1038/nn963

Tuthill, J.C., Azim, E., 2018. Proprioception. Curr. Biol. 28, R194–R203. https://doi.org/10.1016/j.cub.2018.01.064

Weiland, G., Bässler, U., Brunner, M., 1986. A biological feedback control system with electronic input: the artificially closed femur-tibia control system of stick insects. J. Exp. Biol. 120, 369–385.

Welch, T.D.J., Ting, L.H., 2008. A feedback model reproduces muscle activity during human postural responses to support-surface translations. J. Neurophysiol. https://doi.org/10.1152/jn.01110.2007

Winter, D.A., 1995. Human balance and posture control during standing and walking. Gait Posture 3, 193–214.

Winter, D.A., Patla, A.E., Rietdyk, S., Ishac, M.G., 2001. Ankle muscle stiffness in the control of balance during quiet standing. J. Neurophysiol. 85, 2630.

Wolpert, D.M., Ghahramani, Z., 2000. Computational principles of movement neuroscience. Nat. Neurosci. 3, 1212–1217.

Wolpert, D.M., Kawato, M., 1998. Multiple paired forward and inverse models for motor control. Neural Networks. https://doi.org/10.1016/S0893-6080(98)00066-5

Wolpert, D.M., Miall, R.C., Kawato, M., 1998. Internal models in the cerebellum. Trends Cogn. Sci. 2, 338–347. https://doi.org/10.1016/S1364-6613(98)01221-2

Wong, J.D., Donelan, J.M., 2017. Principles of energetics and stability in human locomotion, in: Goswami, A., Vadakkepat, P. (Eds.), Humanoid Robotics: A Reference. Springer, Dordrecht.

Yakoubi, K., Chitour, Y., 2007. Linear systems subject to input saturation and time delay: Global asymptotic stabilization. IEEE Trans. Automat. Contr. 52, 874–879.

Yakovenko, S., Gritsenko, V., Prochazka, A., 2004. Contribution of stretch reflexes to locomotor control: A modeling study. Biol. Cybern. 90, 146–155. https://doi.org/10.1007/s00422-003-0449-z

Zajac, F.E., 1989. Muscle and tendon: properties, models,scaling, and application to biomechanics and motor control. Crit Rev Biomed Engin 17, 359–411.

Zehr, E.P., Stein, R.B., 1999. What functions do reflexes serve during human locomotion? Prog. Neurobiol. 58, 185–205. https://doi.org/10.1016/S0301-0082(98)00081-1

Zhou, B., Duan, G., Lin, Z., 2010. Global stabilization of the double integrator system with saturation and delay in the input. IEEE Trans. Circuits Syst. I Regul. Pap. 57, 1371–1383. https://doi.org/10.1109/TCSI.2009.2028645

Zuur, A.T., Lundbye-Jensen, J., Leukel, C., Taube, W., Grey, M.J., Gollhofer, A., Nielsen, J.B., Gruber, M., 2010. Contribution of afferent feedback and descending drive to human hopping. J. Physiol. 588, 799–807. https://doi.org/10.1113/jphysiol.2009.182709